General Disclaimer

One or more of the Following Statements may affect this Document

- This document has been reproduced from the best copy furnished by the organizational source. It is being released in the interest of making available as much information as possible.

- This document may contain data, which exceeds the sheet parameters. It was furnished in this condition by the organizational source and is the best copy available.

- This document may contain tone-on-tone or color graphs, charts and/or pictures, which have been reproduced in black and white.

- This document is paginated as submitted by the original source.

- Portions of this document are not fully legible due to the historical nature of some of the material. However, it is the best reproduction available from the original submission.

Produced by the NASA Center for Aerospace Information (CASI)

LASER DOPPLER VELOCIMETER SYSTEM SIMULATION FOR

SENSING AIRCRAFT WAKE VORTICES

PART II:

PROCESSING AND ANALYSIS OF LDV DATA
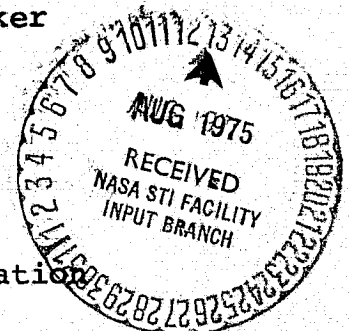## (FOR RUNS 1023 AND 2023)

J.C.S. Meng and J.A.L. Thomson

REPORT DOCUMENTATION PAGE		READ INSTRUCTIONS BEFORE COMPLETING FORM
1. REPORT NUMBER	2. GOVT ACCESSION NO.	3. RECIPIENT'S CATALOG NUMBER
4. TITLE (and Subtitle) LASER DOPPLER VELOCIMETER SYSTEM SIMULATION FOR SENSING AIRCRAFT WAKE VORTICES. PART II: PROCESSING AND ANALYSIS OF LDV DATA (FOR RUNS 1023 AND 2023)		5. TYPE OF REPORT & PERIOD COVERED Final Report
		6. PERFORMING ORG. REPORT NUMBER PD-75-077
7. AUTHOR(s) J.C.S. Meng and J.A.L. Thomson		8. CONTRACT OR GRANT NUMBER(s) NAS8-28984
9. PERFORMING ORGANIZATION NAME AND ADDRESS Physical Dynamics, Inc. P. O. Box 1069 Berkeley, Ca. 94701		10. PROGRAM ELEMENT, PROJECT, TASK AREA & WORK UNIT NUMBERS
11. CONTROLLING OFFICE NAME AND ADDRESS George C. Marshall Space Flight Center Natl. Aeronautics and Space Admin. Marshall Space Flight Center, Ala. 35812		12. REPORT DATE February 1975
		13. NUMBER OF PAGES 78
14. MONITORING AGENCY NAME & ADDRESS(if different from Controlling Office)		15. SECURITY CLASS. (of this report) Unclassified
		15a. DECLASSIFICATION/DOWNGRADING SCHEDULE

16. DISTRIBUTION STATEMENT (of this Report)

17. DISTRIBUTION STATEMENT (of the abstract entered in Block 20, if different from Report)

Approved for public release; distribution unlimited.

18. SUPPLEMENTARY NOTES

19. KEY WORDS (Continue on reverse side if necessary and identify by block number)

aircraft trailing vortex
laser doppler velocimeter
data analysis
wind shear
location algorithms

20. ABSTRACT (Continue on reverse side if necessary and identify by block number)

A data analysis program has been constructed to assess LDV system performance, to validate the simulation model, and to test various vortex location algorithms. It takes either real or simulated doppler spectra versus range and elevation, calculates the spatial distributions of various spectral moments (mean velocity, variance, skewness, kurtosis) or other spectral characteristics (V_{peak}, V_{width}, V_{max}, I_{peak}, I_{sum}) and presents these in a 3-D display (co-

DD FORM 1473   EDITION OF 1 NOV 65 IS OBSOLETE   UNCLASSIFIED

Abstract (cont'd)

ordinate range and angle) so that spatial correlations and patterns can be identified. The format of these displays is identical to that used for the simulation output. These data (either real or simulated) are then subjected to various processing procedures designed to enhance the patterns and determine vortex locations. Each of the real or simulated scans can be processed by one of three different procedures: simple frequency or wavenumber filtering, matched filtering, and deconvolution filtering. The final output is displayed as contour plots in an x-y coordinate system, as well as in the form of vortex tracks deduced from the maxima of the processed data.

In order that two LDV systems may be compared, data from either system is first converted to a common Cartesian coordinate system. This is done for each of the spectral moments in turn. Vortex tracks can either be obtained by cross correlation of data from both systems or by a triangulation method. A detailed analysis of run number 1023 and run number 2023 is presented to demonstrate the data analysis procedure. Vortex tracks and system range resolutions are compared with theoretical predictions.

ACKNOWLEDGMENT

TABLE OF CONTENTS

LIST OF FIGURES

iii

LIST OF FIGURES (cont'd)

I. SUMMARY

A data analysis program has been constructed to assess the SLDV (Scanning Laser Doppler Velocimeter) system performance, to validate the simulation model, and to test various vortex location algorithms. The program takes either real or simulated doppler spectra versus range and elevation, calculates the spatial distributions of various spectral moments (mean velocity, variance, skewness, kurtosis) or other spectral characteristics (V_{peak}, V_{max}, V_{width}, I_{peak}, I_{sum}) and presents these in a 3-D display (coordinate range and angle) so that spatial correlations and patterns can be identified. The format of these displays is identical to that used for the simulation output. These data (either real or simulated) are then subjected to various processing procedures designed to enhance the patterns and determine vortex locations.

Each of the real or simulated scans can be processed by one of three different procedures: simple frequency or wavenumber filtering, matched filtering, and deconvolution filtering. The final output is displayed as contour plots in an x-y coordinate system, as well as in the form of vortex tracks deduced from the maxima of the processed data.

In order that two LDV systems may be compared, data from either system is first converted to a common Cartesian

coordinate system. This is done for each of the spectral moments in turn. Vortex tracks can either be obtained by cross correlation of data from both systems or by a triangulation method.

A detailed analysis of run number 1023 and run number 2023 is presented to demonstrate the data analysis procedure. Vortex tracks and system range resolutions are compared with theoretical predictions.

II. INTRODUCTION

The objectives of the data analysis study are:

1) to identify the parameters affecting the detection capabilities of the LDV system, and

2) to define and optimize vortex location algorithms.

Analyses of a particular flight test (Runs 1023 and 2023, flyby of a B737) have been carried out. A detailed presentation of the results is given in this report. The format has been chosen to match that of the simulation code to facilitate detailed comparisons. Since vortex location is a prime objective, emphasis is placed upon the spectral distribution of the return signal and the effects of thresholding (both of intensity and velocity) upon it. Vortex location algorithms using data from either one or two LDV systems are tested against the simulation results.

The LDV return signal is in the form of a spectrum (intensity versus velocity) at a large number of points in space. The positions of these points are given in terms of range R and elevation angle θ for each system. Values of the following derived variables are computed for each spectrum:

1)   average velocity, $\overline{V}$

2)   variance, σ

3)   skewness, β

4) kurtosis, κ

5) velocity (above threshold) at which the intensity (above threshold) is maximum, V_{max}

6) maximum recorded velocity, V_{peak}

7) difference between maximum and minimum non-zero velocity after thresholding, V_{width}

8) sum of the intensity in all velocity channels, I_{sum}

9) maximum intensity, I_{peak}

These variables are plotted both as functions of range at constant elevation angle and as contour plots in Cartesian coordinates. The R-θ plot shows range-angle correlations, while the contour plot shows the spatial variation in the scan plane.

The effects of applying intensity and velocity thresholds to the spectra have been examined. The optimal intensity threshold I_{th} is found by successive approximation, increasing I_{th} until a clear contrast is achieved between the localized vortex return and the distributed background return. The results of this process can be summarized as follows:

1) A low intensity threshold results in a noisy "vortex" signature broadly distributed in space for all of the variables derived from the spectrum, except higher order moments of velocity which show localized signatures.

2) Medium intensity thresholds result in I_{sum} (and also I_{peak}, for non-zero velocity thresholds) being localized near the vortex core. Other variables are noisy and broadly distributed.

3) High intensity thresholds result in localized distributions for all variables; I_{sum} is most localized.

Only two velocity thresholds V_{th} (3.815 and 20.165 m/sec) have been examined, and no systematic investigations of the effects of the value of V_{th} have been carried out. All variables (and especially I_{peak}) are affected by V_{th}.

The sensitivity of the results to the values of the thresholds is reduced by averaging the spectra. The averaging process redistributes the signal intensity in a given channel to its nearest neighbors according to a prescribed distribution formula. Averaging was found to be helpful in removing noise from either atmospheric turbulence or the LDV system itself. Three filtering procedures (simple frequency, matched filter, and deconvolution filtering) can also be used to enhance the maxima of the contour plots and to reduce the effects of noise.

The simulation studies show that the core location is that of the maxima of $\overline{V}$, σ, β, and κ. Applying this criterion to the contour plots from the data tape gives the vortex core location for the flyby case. The vortex

5

track obtained by plotting the positions of the maxima in I_{sum} derived from the data tape versus time can be analyzed to yield values of descent rate, vortex separation, and circulation. These values agree well with predicted values.

Simultaneously obtained data from two LDV systems can also be used to determine the vortex track. Two different procedures have been examined. In the first, the vortex location is prescribed as that of the maximum in the product of a derived variable for one system with that of the same variable for the second system (e.g., $\overline{V}_1 \overline{V}_2$). In the second, the vortex system is located by triangulation using the values of V_{peak} from both systems. The way in which V_{peak} information is used depends upon range. At long range, the elevation angle of the vortex core was shown by the simulation studies to coincide with that of the maximum in V_{peak}. At short range (≤ 70 m), V_{peak} is a minimum at the vortex core, and maximum to either side in elevation angle. These criteria define a vortex core elevation angle for each system, and the core position is at the intersection of lines drawn from each system at the determined angle.

III. DATA REDUCTION AND ANALYSIS

• <u>Smoothing Procedure for the Signal Intensity Spectrum</u>:

A typical spectrum is shown below: the abscissa is the velocity or channel numbers (the channel width is equal to .545 m/sec) and the ordinate is signal intensity. The high velocity channels have little signals, the low velocity channels contain wind information, and all channels contain fluctuations. Even after thresholds are applied, there remain fluctuations which make it difficult to identify the vortex location.

We have implemented a smoothing scheme which redistributes the intensity level $I(n_o)$ of the original data to its neighboring channels according to the relation

$$I(n) = \sum_{|n-n_o| \leq 5} \left[\frac{I(n_o)-I_{th}}{1+n^2} \middle/ \sum_{m=-5}^{5} \frac{1}{1+m^2} \right]$$

The signals at channels below zero velocity are reflected back to channels above zero velocity. The result is a much smoother spectrum and contours obtained are also smoother. The horizontal line represents the intensity threshold I_{th}. The left figure shows the original spectrum, while the right figure shows the same spectrum after smoothing.

The variation is much smoother and gradual than the
original spectrum. All variables derived from this
smoothed spectrum should also exhibit similar smoothness.
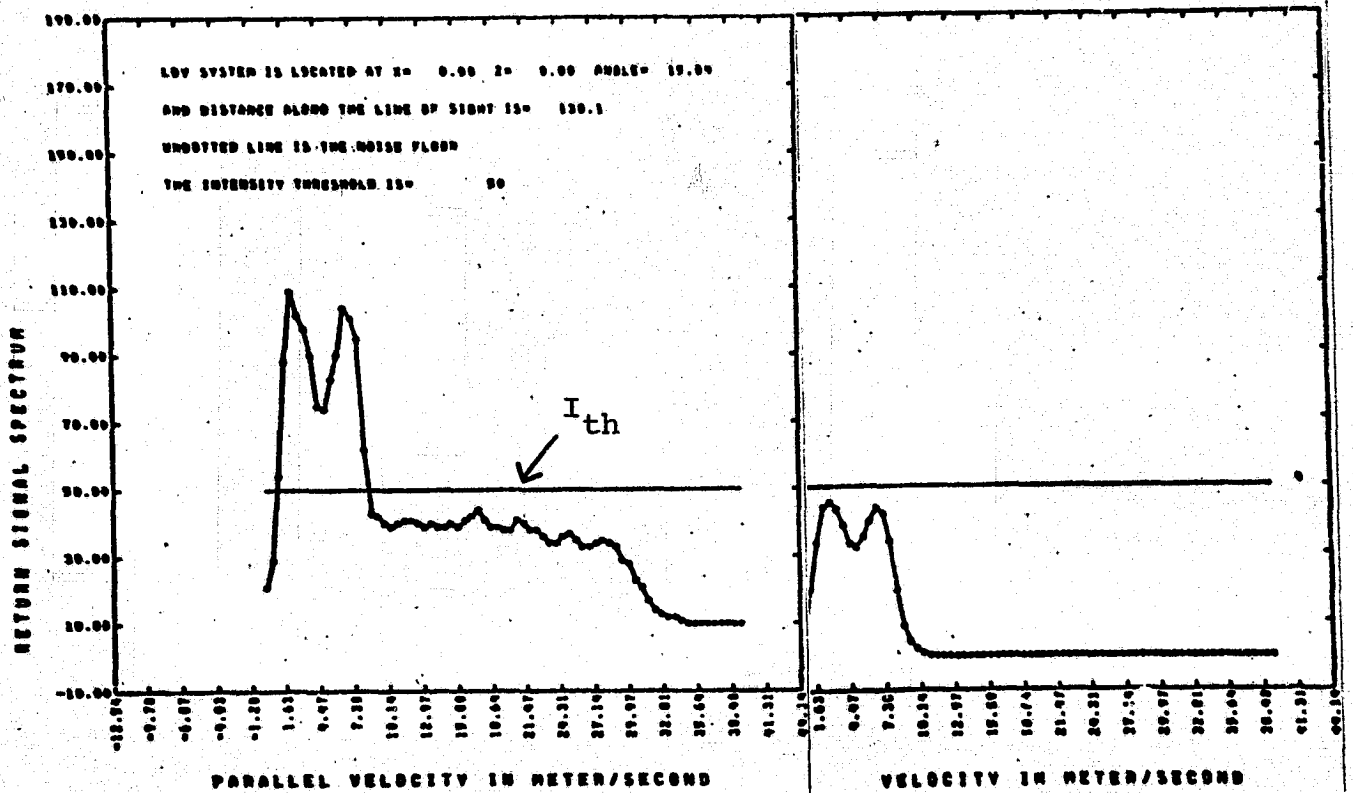
• Determination of Intensity Thresholds

Since both the LDV system mechanisms and the atmospheric turbulence generate a certain amount of noise, the output from raw data without applications of intensity thresholds appear irregular and bear no similarity to the simulation results. It is therefore important to determine the noise level from the data. The noise level in general is a function of both channel number and time t. In principle, one could block the laser beam window and obtain the system noise spectrum as a function of channel number at a given time and use this in reducing the data for a subsequent scan. In practice, this is not done; a constant noise level is specified for all channels. Applying this noise level to the data is straightforward. However, if the noise level is set too high, valuable signals will be lost, and if too low, the desired signature can still be indistinguishable from the background noise. A second method we have adopted is to look through the entire scan frame and select the lowest signal intensity for each channel as the noise level.

Different intensity threshold levels can be then applied above the noise level determined by either method to study the effects.

• <u>Construction of the Contour Plots</u>:

Since data are only available at the focal points depicted by the fan beam configuration, it is convenient to redistribute the data on a rectangular mesh to obtain the contour plots. The separation between data points is large near the long range end of the fan, and it is desirable to find a way which can fill up the void space between each range scan smoothly.

The procedure we have implemented here is to distribute the quantity carried by the focal point P (see sketch) onto a square having the same dimensions as that of the desired mesh. Then a weighted value (proportional to the shaded overlapping area) of that quantity is assigned to each of the neighboring cells A, B, C and D. The mesh dimension should be comparable or smaller than the largest separation between points in the fan beam. The void space outside the fan was assigned a value equal to the minimum of the quantity to be contour-plotted. This was found effective in removing the large number of contours which would otherwise appear near the edge of the fan.
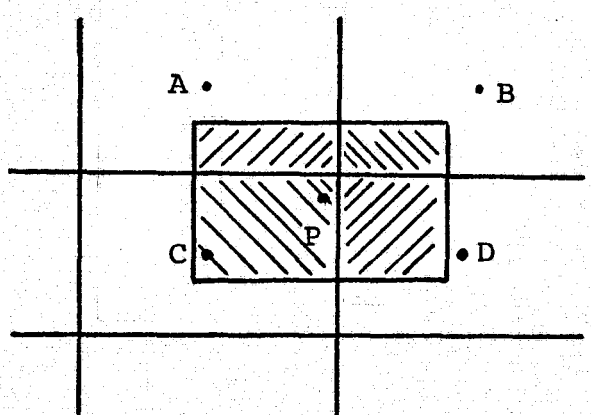
• <u>Filtering Procedures</u>:

Techniques commonly used in the analysis of radar data to maximize the signal-to-noise ratio can also be applied to the LDV returns. Detailed descriptions are given by Skolnik (1970).

The return signal $s(\vec{x})$ can be considered as consisting of two parts, $f(\vec{x})$ which is due to the vortex at the unknown location $\vec{x}_o$ (which is to be determined) and $n(\vec{x})$ which is due to noise. Then

$$s(\vec{x}) = cf(\vec{x}-\vec{x}_o) + n(\vec{x})$$

where c is an arbitrary constant. The Fourier transform of this equation is

$$s_{\vec{k}} = cf_{\vec{k}}\, e^{i\vec{k}\cdot\vec{x}_o} + n_{\vec{k}} \quad .$$

Dividing both sides by $f_{\vec{k}}$, we have

$$P_{\vec{k}} = \frac{s_{\vec{k}}}{f_{\vec{k}}} = ce^{i\vec{k}\cdot\vec{x}_o} + \frac{n_{\vec{k}}}{f_{\vec{k}}} \quad .$$

In general, filtering involves applying a weighting function $w_{\vec{k}}$ to the Fourier components $p_{\vec{k}}$ and then retransforming to the physical plane,

11

$$F^{-1}(p_{\vec{k}}w_{\vec{k}}) = c\int_{-\infty}^{\infty} w_k \, e^{i\vec{k}\cdot\vec{x}_0} \, e^{-i\vec{k}\cdot\vec{x}} \, d\vec{k} + F^{-1}\left(\frac{n_{\vec{k}}w_{\vec{k}}}{f_{\vec{k}}}\right) \quad .$$

The object of the filtering procedure is to enhance the first term with respect to the second. Different forms of the weighting or filter function $w_{\vec{k}}$ produce transformed signals with different properties.

Deconvolution filter: Here we set $w_{\vec{k}} \equiv 1$, so that

$$F^{-1}(p_{\vec{k}}w_{\vec{k}}) = c\int_{-\infty}^{\infty} e^{i\vec{k}\cdot(\vec{x}_0-\vec{x})} \, d\vec{k} + F^{-1}(n_{\vec{k}}/f_{\vec{k}})$$

$$= c\delta(\vec{x}-\vec{x}_0) + G(\vec{x}) \quad .$$

In the absence of noise, this filter produces a delta function at $\vec{x}_0$. When substantial noise is present, $G(\vec{x})$ can be appreciable at some values of $\vec{x}$, and it becomes difficult to identify the delta function.

Matched filter: This is the optimum filter when the signal is observed in the presence of white noise ($n_{\vec{k}}$ independent of $\vec{k}$). The weight function is $w_{\vec{k}} = |f_{\vec{k}}|^2$, and

12

$$F^{-1}(p_{\vec{k}}w_{\vec{k}}) = c \int_{-\infty}^{\infty} f_{\vec{k}} f_{\vec{k}}^* \, e^{i\vec{k}\cdot\vec{x}_o} \, e^{-i\vec{k}\cdot\vec{x}} \, d\vec{k} + F^{-1}(n_{\vec{k}}f_{\vec{k}}^*)$$

$$= c \int_{-\infty}^{\infty} e^{-i\vec{k}\cdot x} \underbrace{\int_{-\infty}^{\infty} f(\vec{x}) f^*(\vec{x}-\vec{x}_o) \, e^{i\vec{k}\cdot\vec{x}} \, d\vec{x}}_{} \, d\vec{k}$$

$$+ F^{-1}(n_{\vec{k}}f_{\vec{k}}^*) \quad .$$

The underlined integral is a correlation and can be shown to have a maximum at $\vec{x}_o$. Then the inverse transform $F^{-1}(p_{\vec{k}}w_{\vec{k}})$ will also be a maximum at x_o.

Simple frequency filter: In this case, the weight function is $w_{\vec{k}} = \exp(-|\vec{k}|^2)$. This filter only smooths out the noise.

The filters described above have been incorporated in the LDVDA code. The usefulness of filtering procedures has not been explored to any great extent and deserves further study.

• Data Reduction Procedures:

The basic set-up is described in the Appendix. The data tapes from NASA/MSFC are first converted into 60-bit binary word tapes to be analyzed on the CDC 7600 computer. The data reduction program LDVDA is then applied to study these tapes.

13

In general, each range scan is composed of approximately 50 points, and about 25 lines of sight for a complete angle scan so that there are approximately 1250 range points in each frame. Assuming each focal point is separated by .008 seconds in time, one complete scan will cover about 5 seconds. Each tape covers about 50 seconds of data so that there should be 12,500 data points altogether. For each focal point in space, there are six numbers to record its frame sequential number, x,y coordinates, range r, angle θ and the clock time plus one number to record the signal intensity for each of the 104 velocity channels. The computer cannot store all this information in the memory core at once, and therefore only 1295 data points are read and stored in the large memory core (LCM) at any one time. Since the recording of the data does not always start at the range maximum or minimum, portions of the 1295 data points are discarded before the beginning of the range scan is found. If the total number of data points in one complete scan frame to be read exceeds what is left in the LCM, the subroutine PUSHUP will discard data points which have already been used and will read another 1295 points into the LCM. The noise level is found, and various intensity and velocity thresholds are applied to calculate $\bar{V}$, V_{peak}, V_{max}, V_{width}, σ, β, κ, I_{sum}, and I_{peak}.

IV. RESULTS AND DISCUSSION

The data reduction program is capable of analyzing both flight and simulation data tapes. The first output of both data tapes is the fan beam configurations. These are shown in Figures 1a and 1b, where Figure 1a is the Run 1023 data and Figure 1b is the simulation data. Both horizontal and vertical coordinates are of the same scale in meters. The caption near the top of the fan describes the lowest and the highest elevation angles, as well as the initial and final clock times in seconds. The jittering of the angle and range scan of the LDV system can be assessed from this plot. The simulation data (Figure 1b) uses a fan of lines-of-sight separated by a constant angle of 1.5° and is extended from the aperture all the way to the outer boundaries of the computation mesh. The higher density of range points near the vortex locations is a result of finer integration steps to resolve the higher velocity gradient there.

Due to the large volume of output for each data tape and the large number of data tapes processed, we will concentrate on discussion of only the best representative cases, i.e., Runs 1023 and 2023, throughout this report.

Run 1023 (run 2023 represents output from the second LDV system) was conducted at MSFC/NASA on July 20, 1974, at
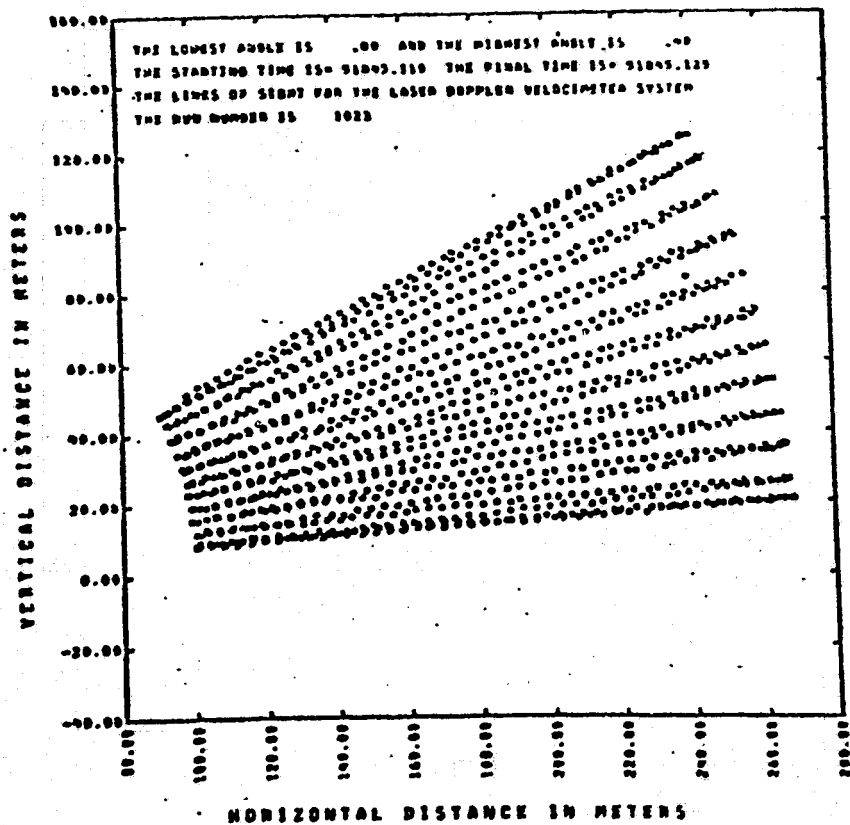
15

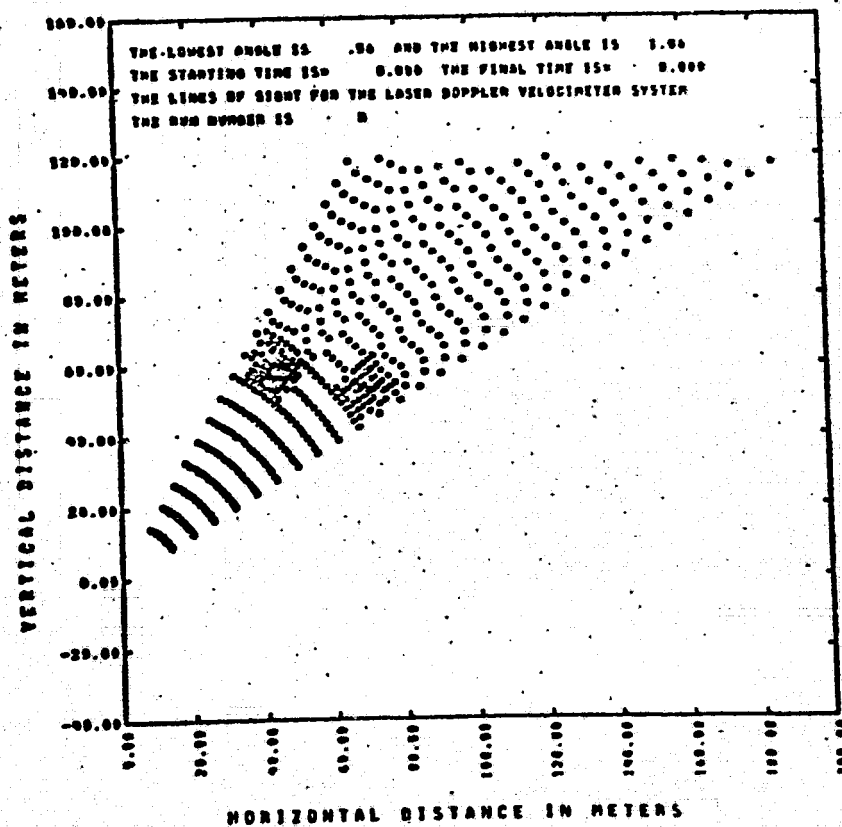FIGURE 1A. FAN BEAM CONFIGURATION FOR RUN 1023

FIGURE 1B. FAN BEAM CONFIGURATION FOR SIMULATION DATA

the Redstone Arsenal airstrip. A B737 was flown from north to south. The first LDV system was located at 61.11 meters to the west, and the second system was at 240 meters to the east.

Figure 2 shows four typical spectra. Figure 2a is a spectrum of the ambient wind; Figure 2b is that of the vortex. Notice the peak intensity is shifted toward higher velocity channels. When there is no noise, defining the noise as the minimum intensity in each channel should yield "noise" which is identically zero. Since there is no noise generated in the simulation data, this procedure did produce a zero noise level. Figure 2c shows a real spectrum due to ambient wind, and Figure 2d shows a spectrum due to the vortex, which brings V_{max} nearly to 7 m/sec from the ambient wind of 1.63 m/sec.

Figure 3 shows the applications of the noise threshold schemes to the real data spectra. The abscissa is the velocity in m/sec or is equivalent to the filter channel numbers. The ordinate is the intensity level. Figures 3a and 3b show the first intensity threshold scheme being applied to two typical vortex signatures, and Figure 3c and 3d show the second noise threshold scheme as applied to the same spectra. The dotted lines are the recorded spectra; the undotted lines are the noise. From Figure 3b, it is expected that the constant intensity threshold of 51 is too low due to the spurious spike
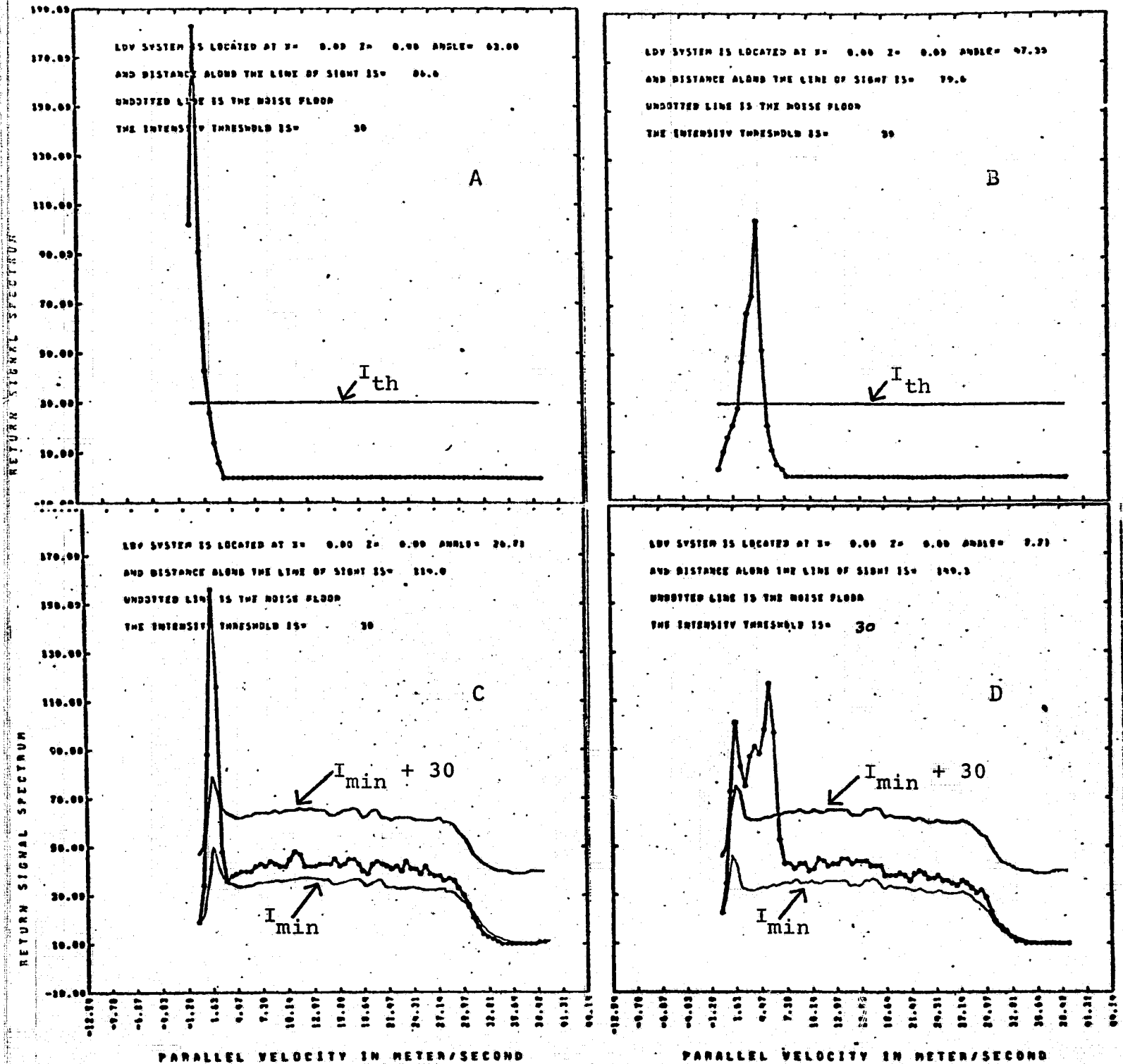
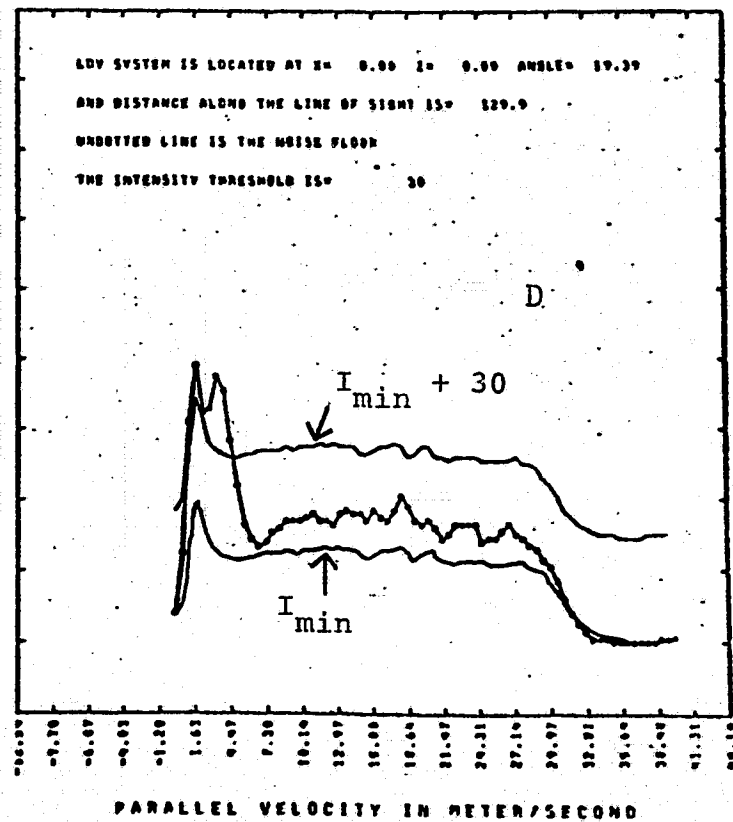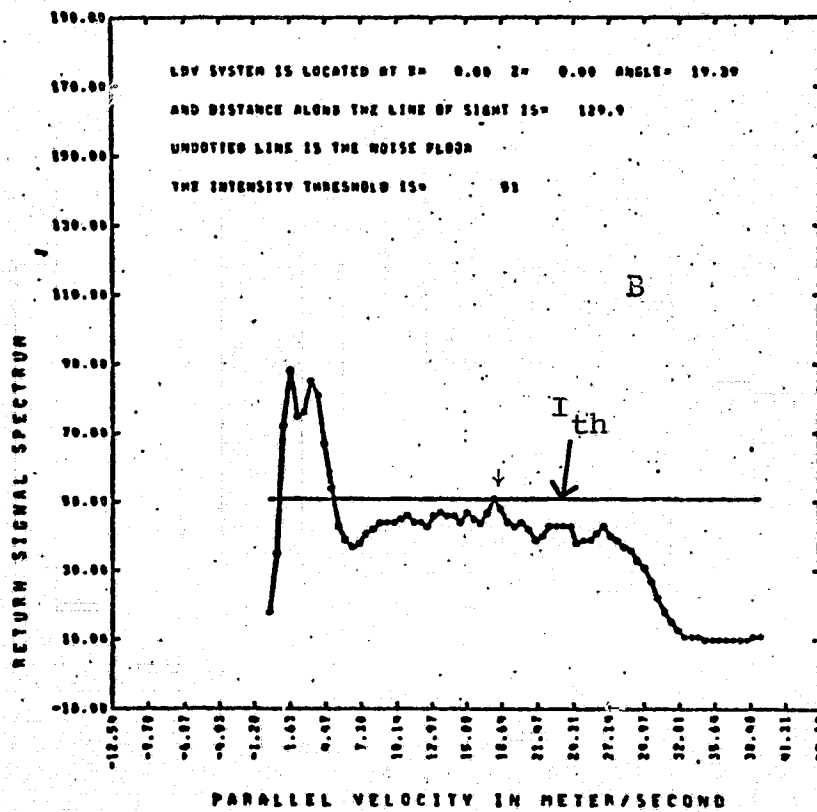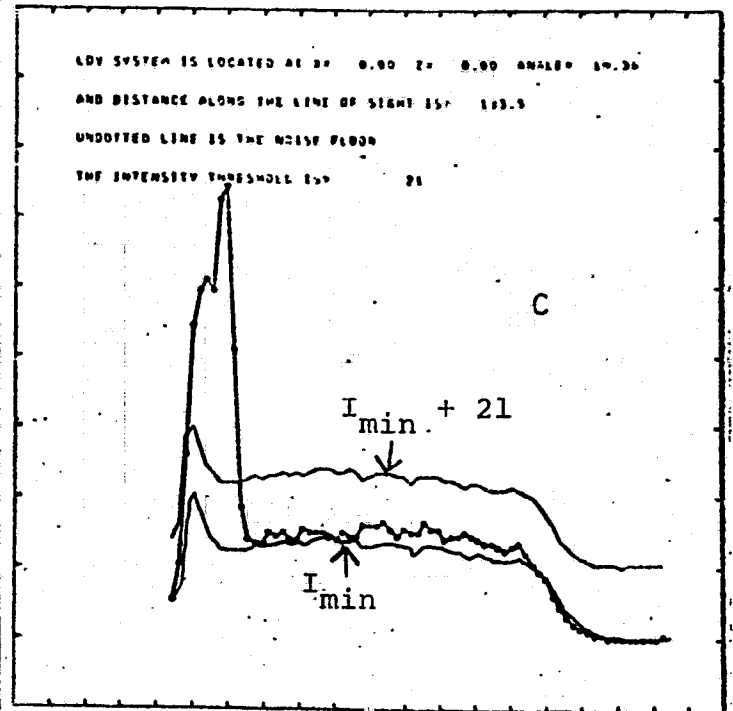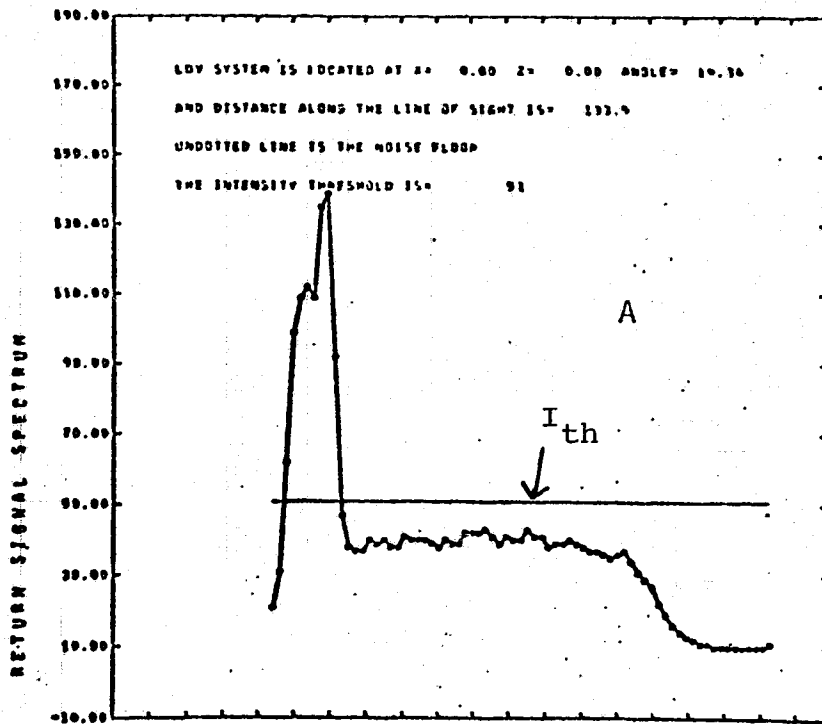FIGURE 2. COMPARISONS OF THE SIMULATED AND REAL SIGNAL SPECTRA

FIGURE 3. COMPARISONS OF THRESHOLD SCHEMES TO TWO TYPICAL
SIGNAL SPECTRA

at a velocity equal to 18.64 m/sec. From Figures 3c and 3d,

it can be seen that the second scheme should subtract out

the ambient wind signature and leave the vortex signature

intact. One might conclude that the second scheme should

be a better scheme to achieve maximum clarity for the vortex

signature. However, as it will be shown later, if the

threshold of the first scheme is high enough, the results

are very close to that of the second scheme at lower inten-

sity thresholds.

Figure 4 shows the results of applying two different

constant intensity thresholds to a set of spectra. Figure 4a

shows a typical spectrum and a threshold level of 51. The

values of $\bar{V}$ and V_{width} which result are shown for all R and

θ in Figure 4b and 4c (left column). In the right column,

Figures 4d, 4e, and 4f, the threshold is set at 60. The

abscissa of each plot is range along the line-of-sight in

meters. The ordinates are indicated by the captions; all

have units of m/sec. Each curve represents the variable

versus the range, and each is displaced vertically by a

constant distance proportional to the difference in elevation

angle. The location of the LDV system, the lowest and high-

est angle and the clock time recorded for the beginning and

end of the frame are written on the plot. The minimum and

maximum values of the variable appearing in the frame are also

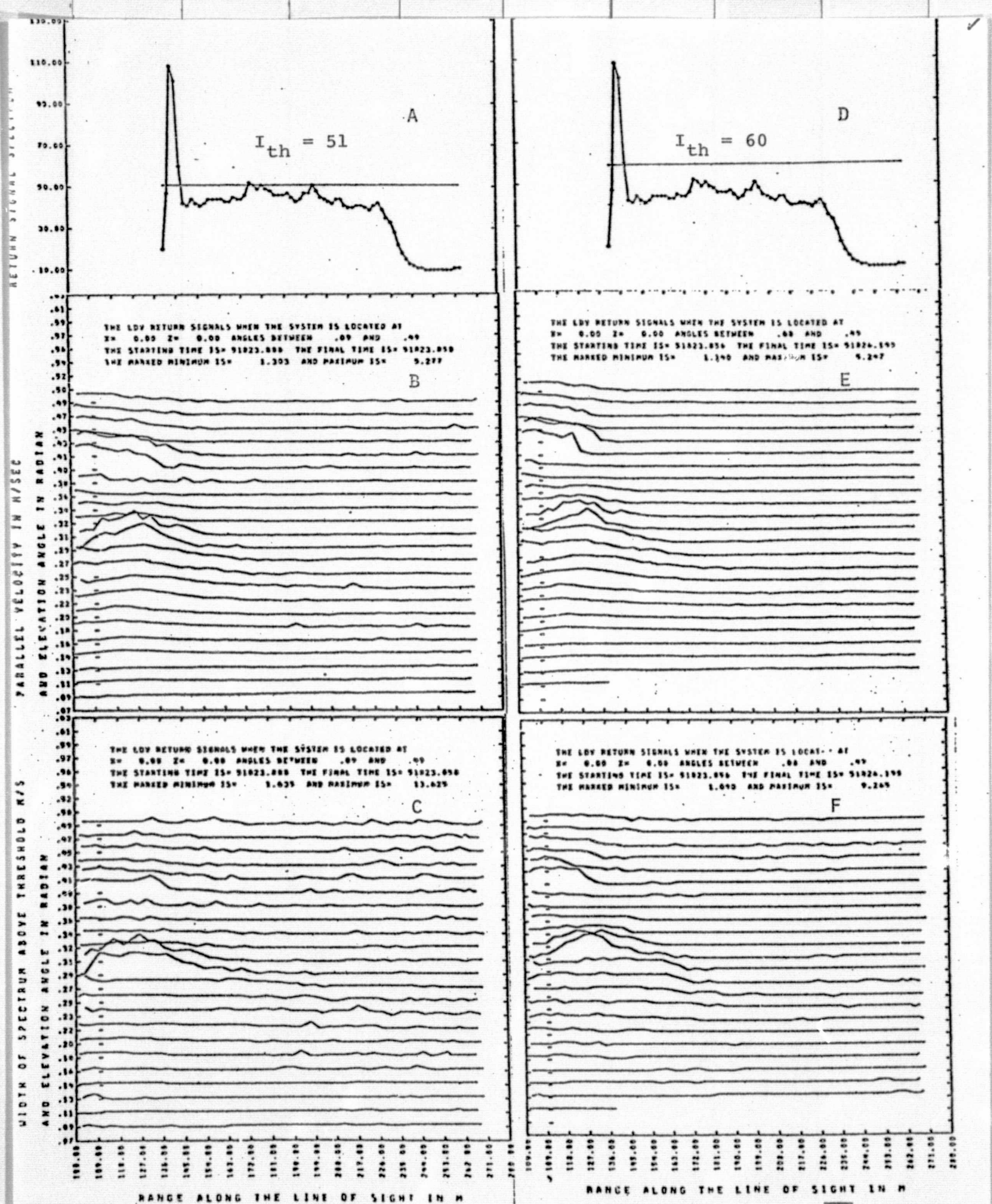indicated. Vertical spacing between each curve represents

FIGURE 4. EFFECTS OF DIFFERENT CONSTANT INTENSITY THRESHOLDS ON $\overline{V}$ AND V_{WIDTH}

half of the difference between the maximum and minimum of the variable plotted. Due to the appearance of several spikes at higher velocity channels in Figure 4a, it is expected that the $\bar{V}$ and V_{width} in the left column will be less smooth than those in the right column. This is found when one compares Figure 4b to 4e and Figure 4c to 4f. Figures 4e and 4f show the localized bumps at elevation angles of .43 and .32 radian and at ranges near 109 meters and 127 meters, respectively.

Figure 5 shows the effects of the same pair of thresholds on V_{peak}, V_{max}, and variance. The V_{peak} shown in Figure 5a is very noisy, while Figure 5d shows well localized vortex signatures. This indicates that V_{peak} is very sensitive to the intensity thresholds. On the other hand, V_{max} (Figures 5b and 5e) shows no dependence upon the intensity thresholds, as is expected. Therefore, we believe V_{max} should be a better quantity to work with than V_{peak} as far as the sensitivity to the intensity thresholds is concerned. Figures 5c and 5f show the effects of different thresholds upon the variance σ in $(m/sec)^2$. They show the same trend as appeared in V_{peak}, but the degree of sensitivity is lessened. Figure 5f shows well localized patterns at angles of .43 and .31 radians and at ranges near 136 meters. From the simulation outputs which were discussed by Thomson and Meng (1974), it is known that if the line-of-sight passes
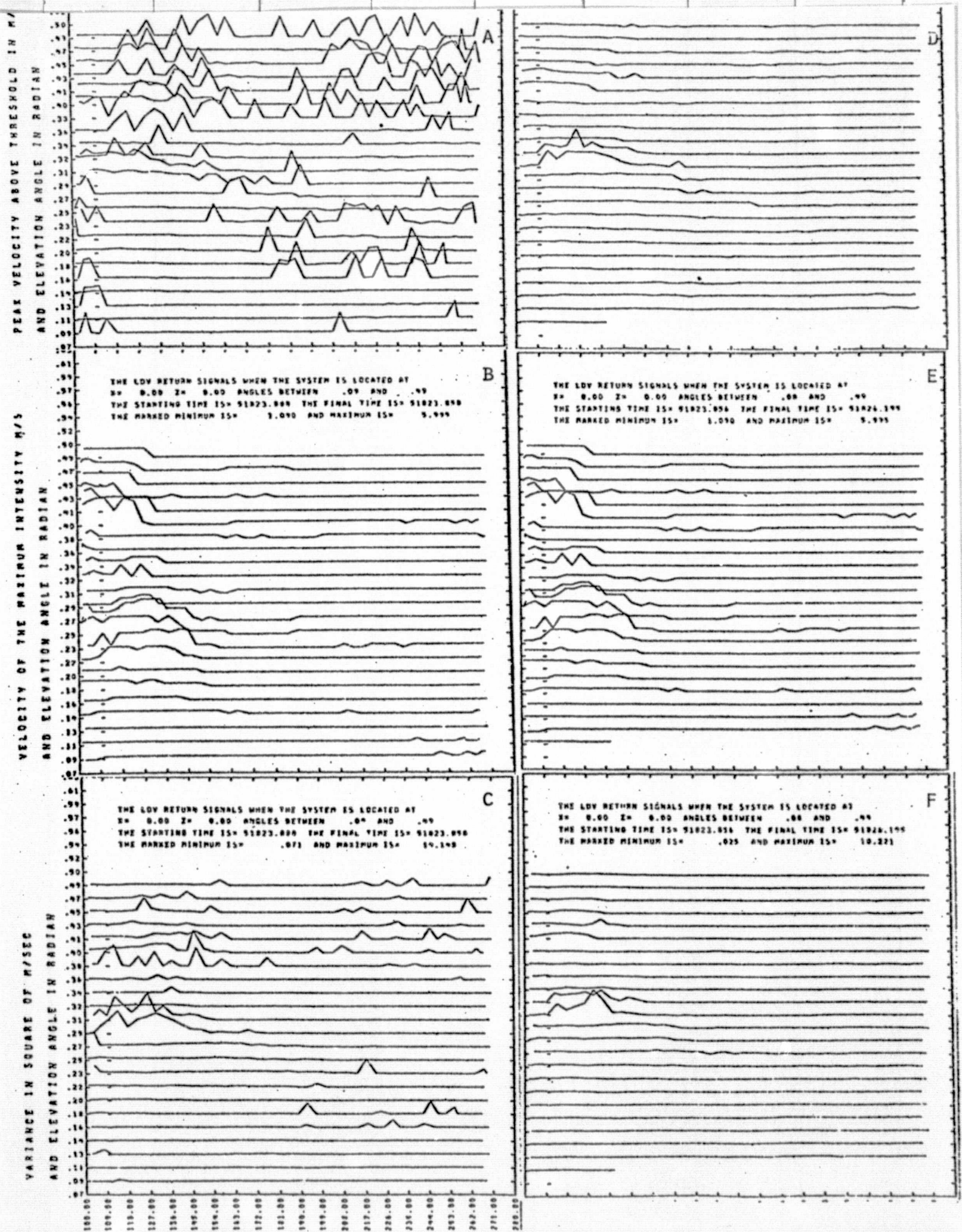
FIGURE 5. EFFECTS OF DIFFERENT CONSTANT INTENSITY THRESHOLDS ON V_{PEAK}, V_{MAX},

directly through the vortex core there is no signal. One may ask whether the signatures in Figure 5f are due to one or two vortices. The separation between bumps at angles of .43 and .31 can be calculated to be approximately 13.6 meters and the horizontal separation distance is 12.7 meters, which is shorter than the initial vortex separation ($\sim$18 meters) predicted for the B737, but longer than the predicted vortex core diameter of four meters. Figures 6a and 6b show the skewness (in $(m/sec)^3$) and kurtosis (in $(m/sec)^4$) at an intensity threshold of 51. They appear quite noisy. Figures 6d and 6e show the skewness and kurtosis for $I_{th} = 60$. Both show well-localized maxima at an angle of .31 radians and have sharper angle resolution than that of the variance in Figure 5f. Figures 6c and 6f show almost identical results of the I_{sum}, which is virtually independent of the value of the intensity threshold. I_{sum} has maxima near the vortices and varies smoothly with both angle and range.

Figures 7a and 7b show I_{peak}. This is not a good indicator for vortex location when there is no velocity threshold but, as will be shown later, it is a good indicator if a velocity threshold is applied. Figures 7c and 7d show the maximum V_{peak} in m/sec for each line-of-sight (that is, the highest V_{peak} for one complete range scan) versus the elevation angle in radians. Because of the low intensity threshold, the maximum V_{peak} in Figure 7c is as high as
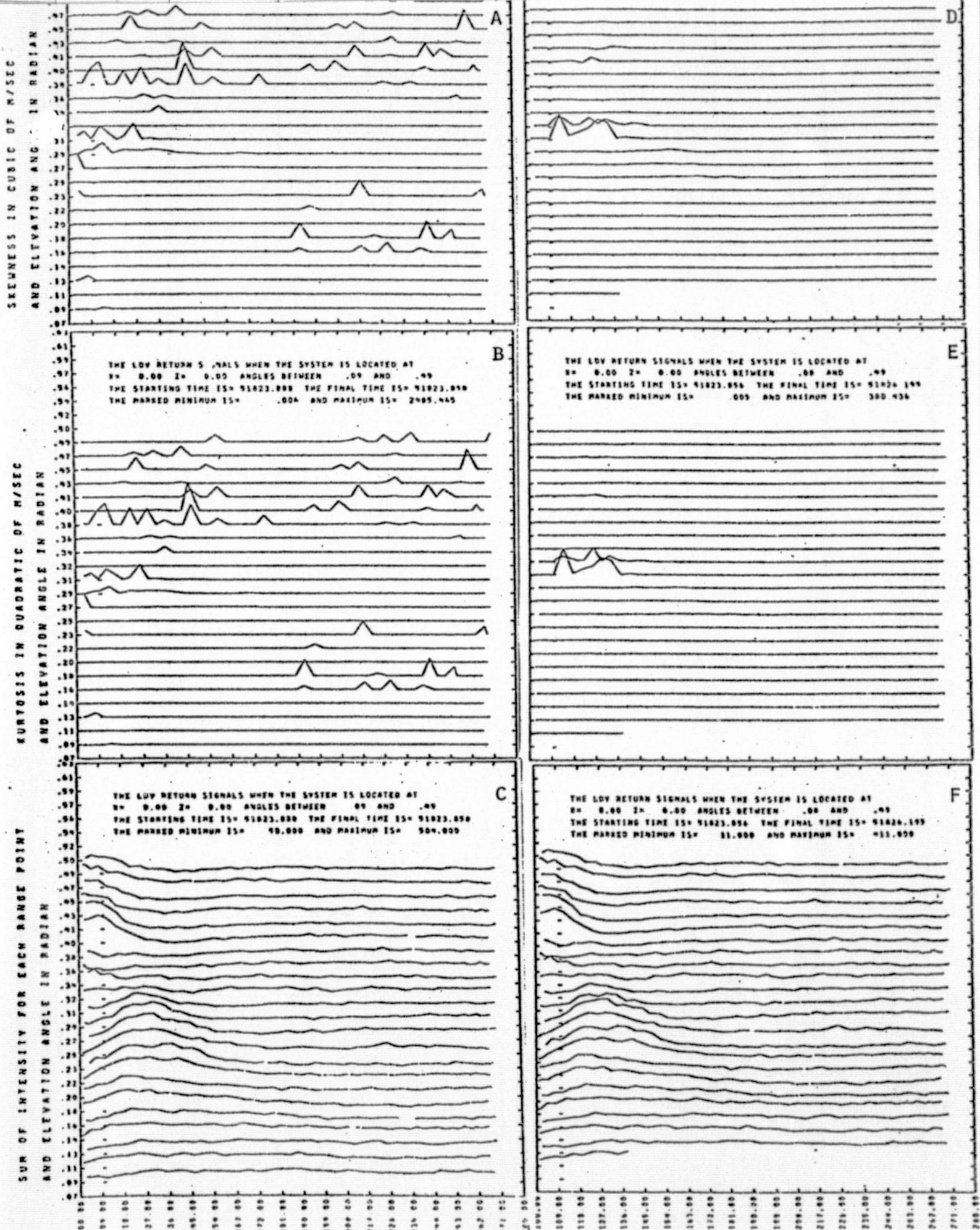
SKEWNESS IN CUBIC OF M/SEC AND ELEVATION ANG . IN RADIAN

KURTOSIS IN QUADRATIC OF M/SEC AND ELEVATION ANGLE IN RADIAN

SUM OF INTENSITY FOR EACH RANGE POINT AND ELEVATION ANGLE IN RADIAN

A

D

B

THE LOV RETURN S .NALS WHEN THE SYSTEM IS LOCATED AT
X= 0.00 Z= 0.00 ANGLES BETWEEN .09 AND .49
THE STARTING TIME IS= 91023.830 THE FINAL TIME IS= 91023.850
THE MARKED MINIMUM IS= .006 AND MAXIMUM IS= 2405.445

E

THE LOV RETURN SIGNALS WHEN THE SYSTEM IS LOCATED AT
X= 0.00 Z= 0.00 ANGLES BETWEEN .09 AND .49
THE STARTING TIME IS= 91023.856 THE FINAL TIME IS= 91026.199
THE MARKED MINIMUM IS= .005 AND MAXIMUM IS= 300.936

C

THE LOV RETURN SIGNALS WHEN THE SYSTEM IS LOCATED AT
X= 0.00 Z= 0.00 ANGLES BETWEEN .09 AND .49
THE STARTING TIME IS= 91023.830 THE FINAL TIME IS= 91023.850
THE MARKED MINIMUM IS= 50.000 AND MAXIMUM IS= 504.000

F

THE LOV RETURN SIGNALS WHEN THE SYSTEM IS LOCATED AT
X= 0.00 Z= 0.00 ANGLES BETWEEN .09 AND .49
THE STARTING TIME IS= 91023.856 THE FINAL TIME IS= 91026.199
THE MARKED MINIMUM IS= 11.000 AND MAXIMUM IS= 411.000

FIGURE 6. EFFECTS OF DIFFERENT CONSTANT INTENSITY THRESHOLDS ON β, κ, I_{SUM}
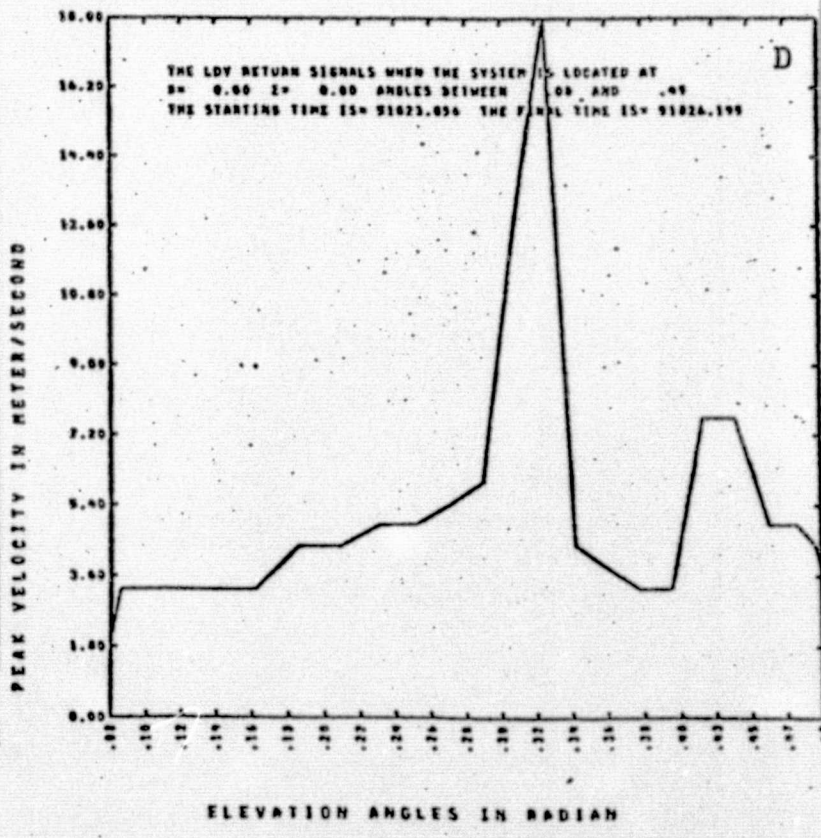
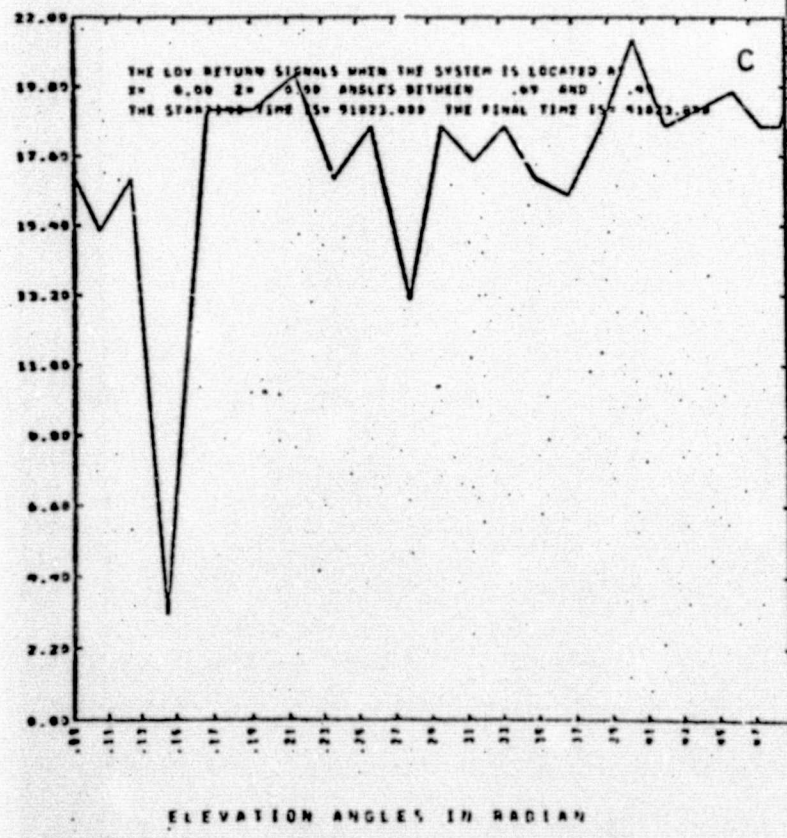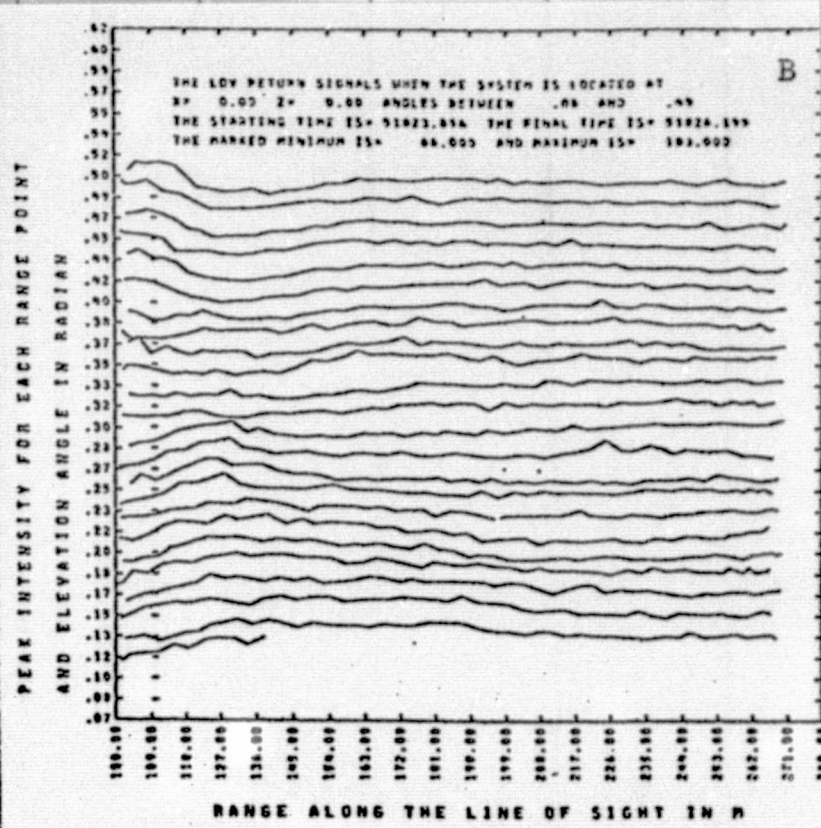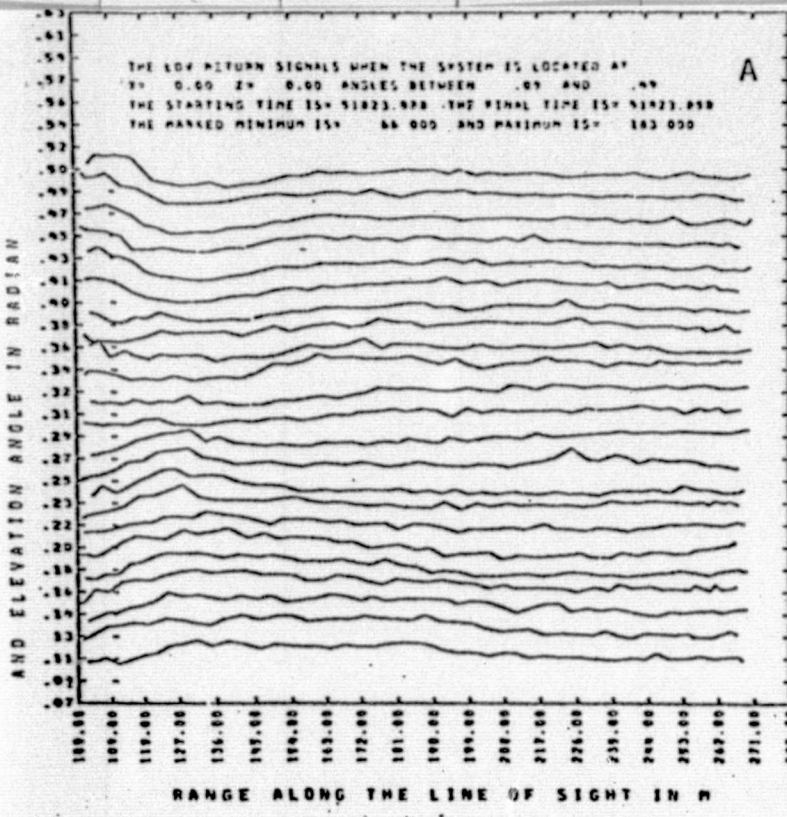FIGURE 7. EFFECTS OF DIFFERENT CONSTANT INTENSITY THRESHOLDS ON I_{PEAK} AND MAXIMUM V_{PEAK} VS. ANGLE

26

21 m/sec and the curve does not reveal the vortex location.
Figure 7d shows two well localized peaks at angles of .32
and .43 radians. These angles are consistent with all
previous plots.

No velocity threshold is applied on the spectrum
shown in Figure 8a. The vertical line indicates the zero
velocity channel, the lower undotted line represents the
I_{min} level determined by the second scheme, and the higher
undotted line represents an intensity threshold of three
added onto the I_{min} level. Figure 8b shows the same spectrum
with velocity threshold at 7.63 m/sec. The 'a' series of
Figure 9 through Figure 17 are the results for "no velocity
threshold" cases, and the 'b' series are those for the
"velocity threshold" cases.

Figure 9a shows $\bar{V}$ is broadly distributed. It becomes
a minimum at vortex locations, while Figure 9b, in which $\bar{V}$
is more localized, shows the same trend. Figure 10a shows
that V_{max} is well localized without a velocity threshold,
and Figure 10b indicates that at this low intensity threshold
level, velocity threshold produces a very noisy plot of V_{max}.
Figures 11a and 11b are identical, since at low intensity
thresholds V_{peak} will not depend upon the velocity thres-
hold. V_{width} in Figures 12a and 12b is almost identical,
and both figures show the same trend observed in $\bar{V}$
(Figure 9). Figures 13a and 13b show slightly improved
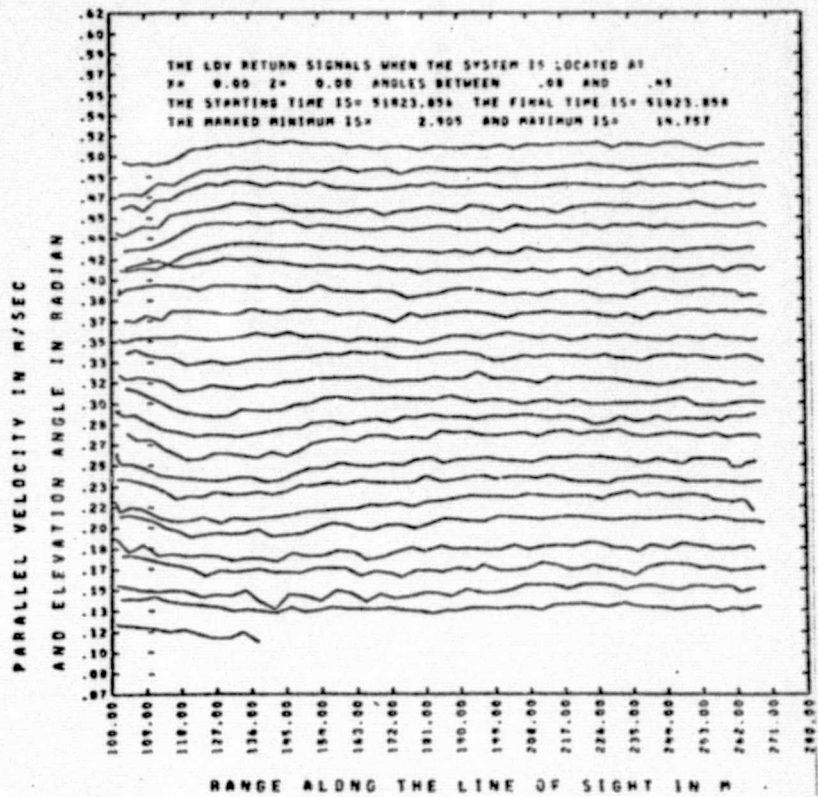localization for $\sqrt{\sigma}$ over that shown in Figure 9. The same
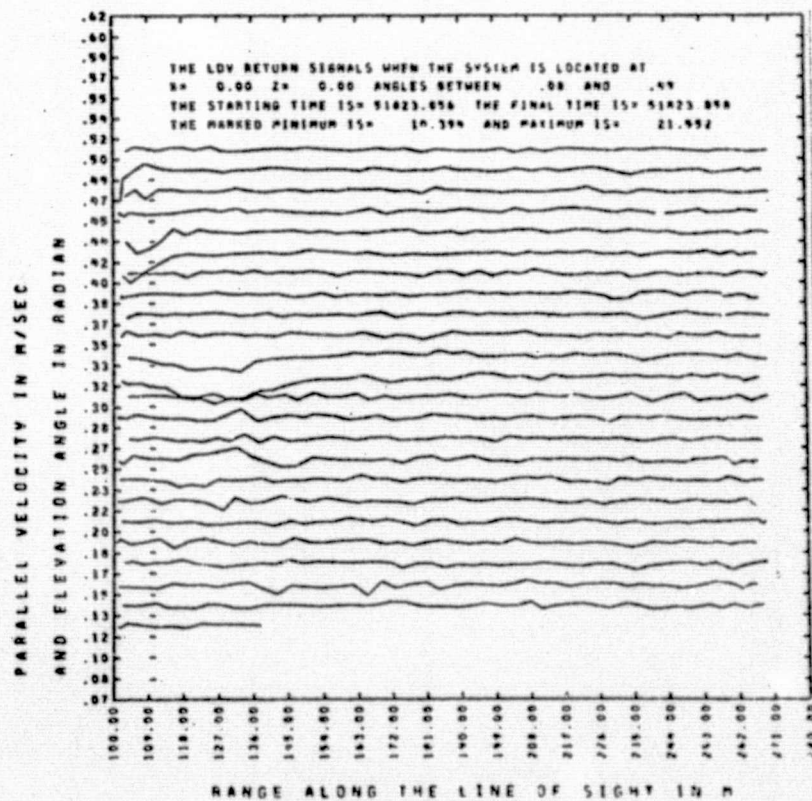
27
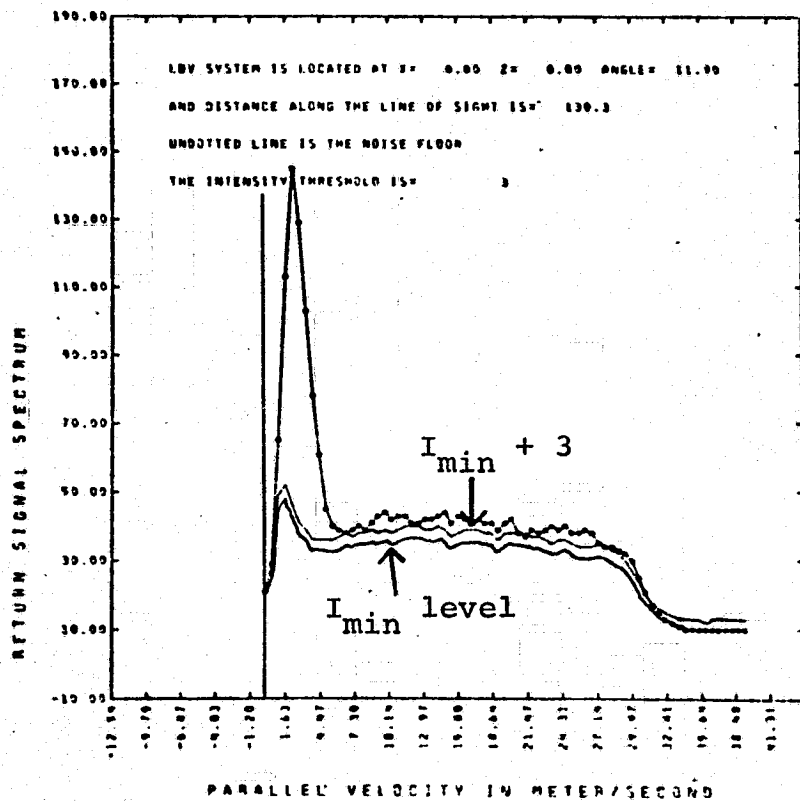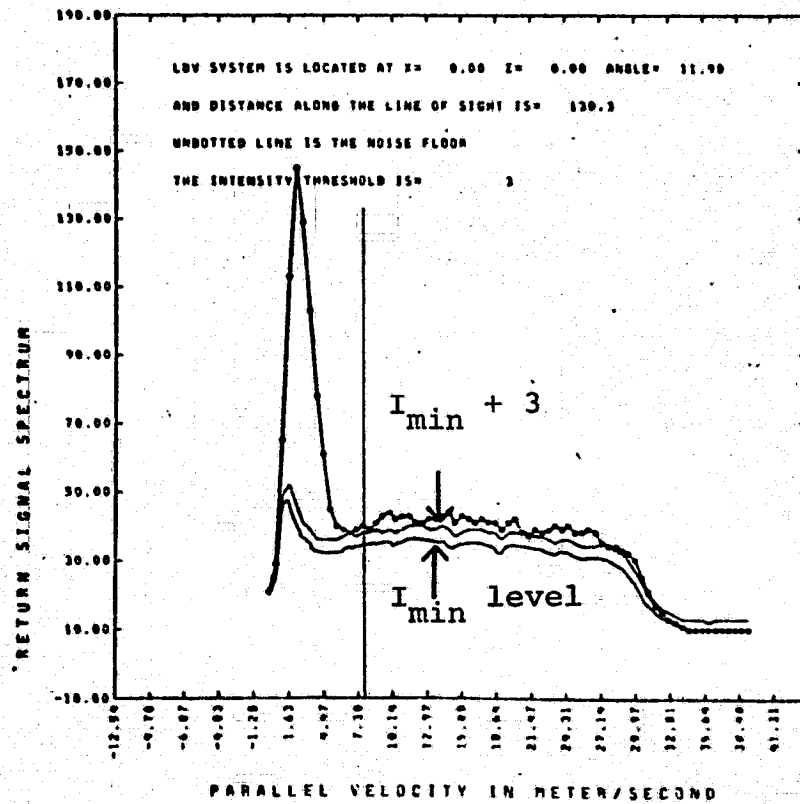
FIGURE 8. SPECTRA SHOWING LOW INTENSITY THRESHOLDS AND
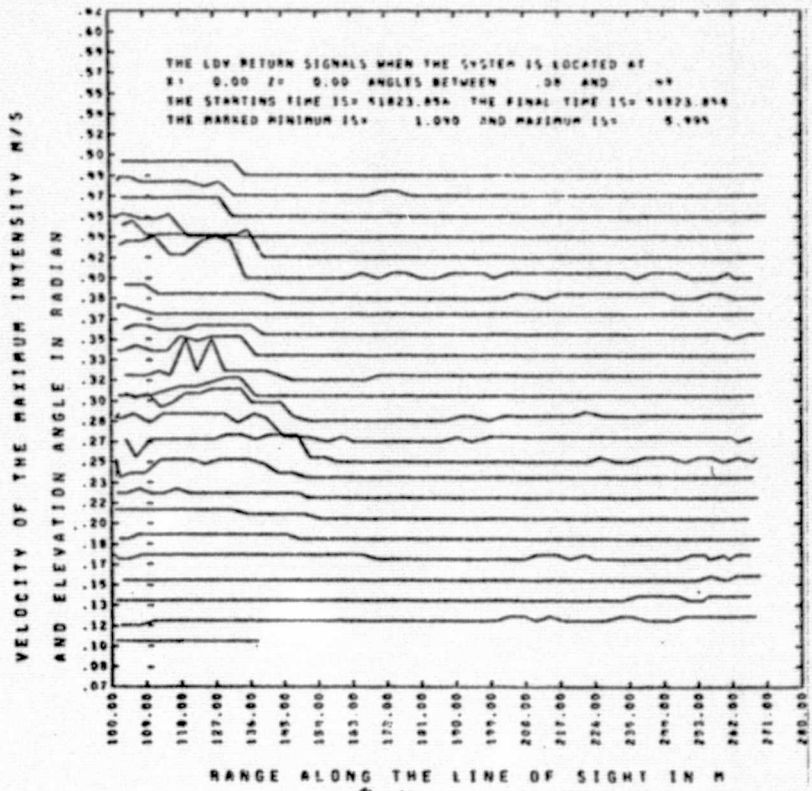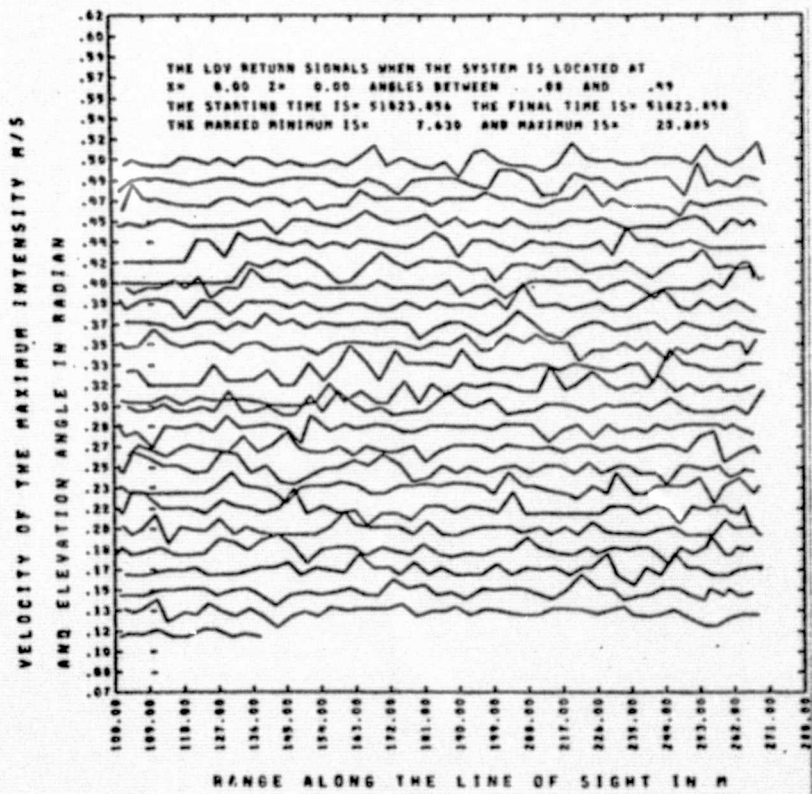VELOCITY THRESHOLD AT 7.53 M/SEC

FIGURE 9. EFFECTS OF VELOCITY THRESHOLD ON $\bar{V}$ AT LOW INTENSITY THRESHOLD

29

FIGURE 10. EFFECT OF VELOCITY THRESHOLD ON V_{MAX} AT LOW
INTENSITY THRESHOLD

30

A

B

FIGURE 11. EFFECT OF VELOCITY THRESHOLD ON V_{PEAK} AT LOW
INTENSITY THRESHOLD

31

A

B

FIGURE 12. EFFECT OF VELOCITY THRESHOLD ON V$_{WIDTH}$ AT LOW
INTENSITY THRESHOLD

32

FIGURE 13. EFFECT OF VELOCITY THRESHOLD ON $\sqrt{\text{VARIANCE}}$ AT LOW INTENSITY THRESHOLD

33

A

B

FIGURE 14. EFFECT OF VELOCITY THRESHOLD ON COEFFICIENT OF
SKEWNESS AT LOW INTENSITY THRESHOLD

34

FIGURE 15. EFFECT OF VELOCITY THRESHOLD ON COEFFICIENT OF KURTOSIS AT LOW INTENSITY THRESHOLD
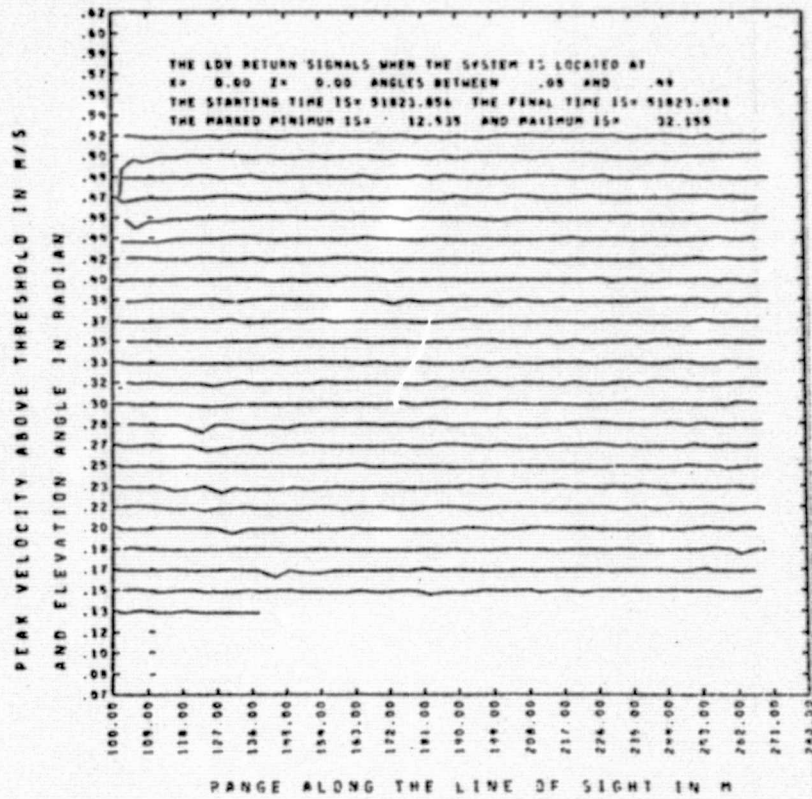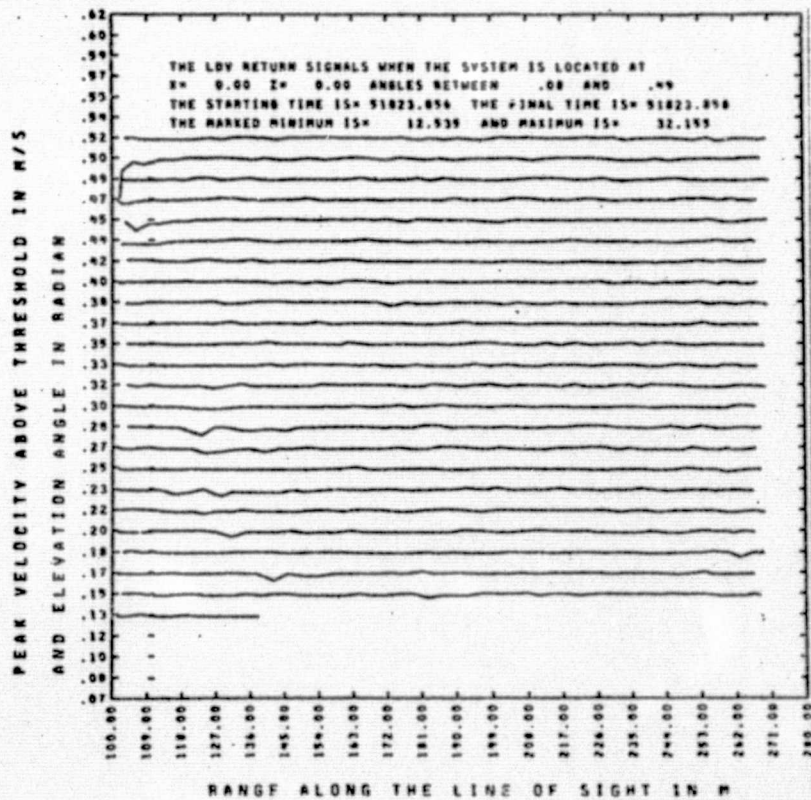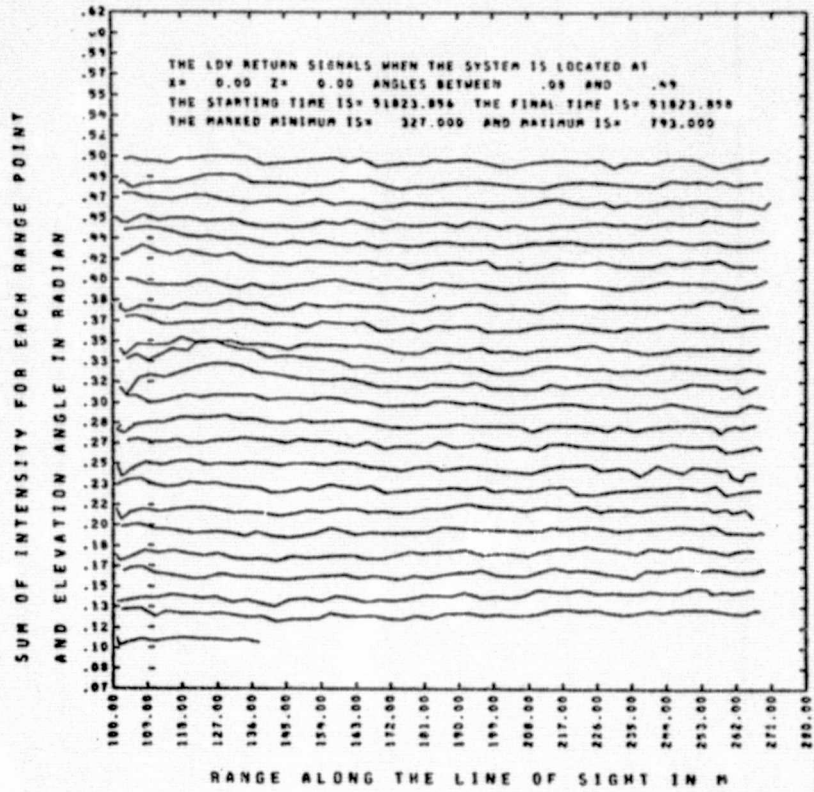
A
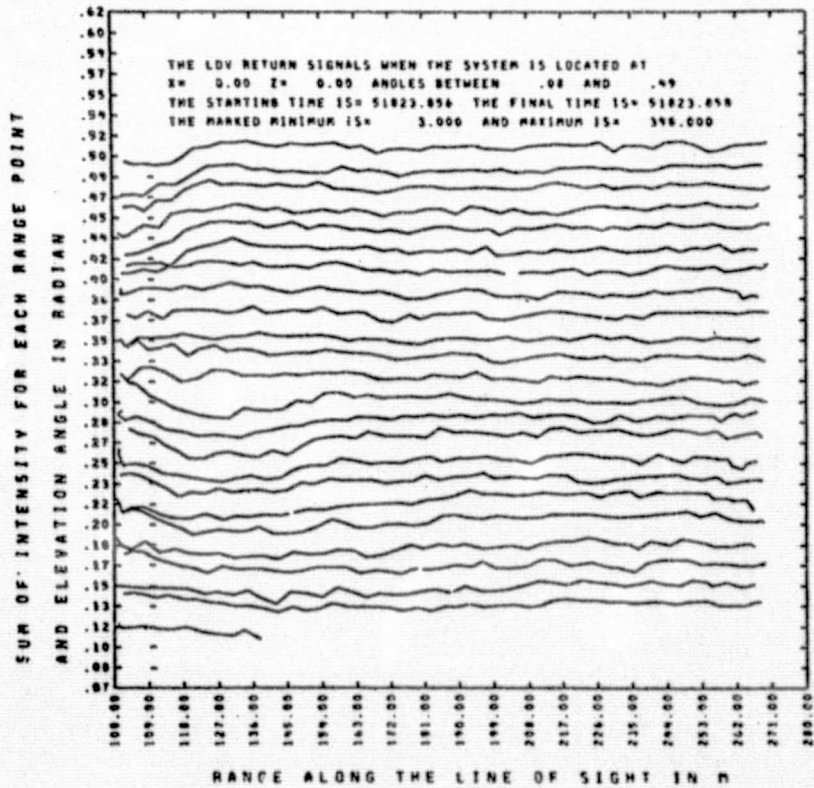
B

FIGURE 16. EFFECT OF VELOCITY THRESHOLD ON I_{SUM} AT LOW
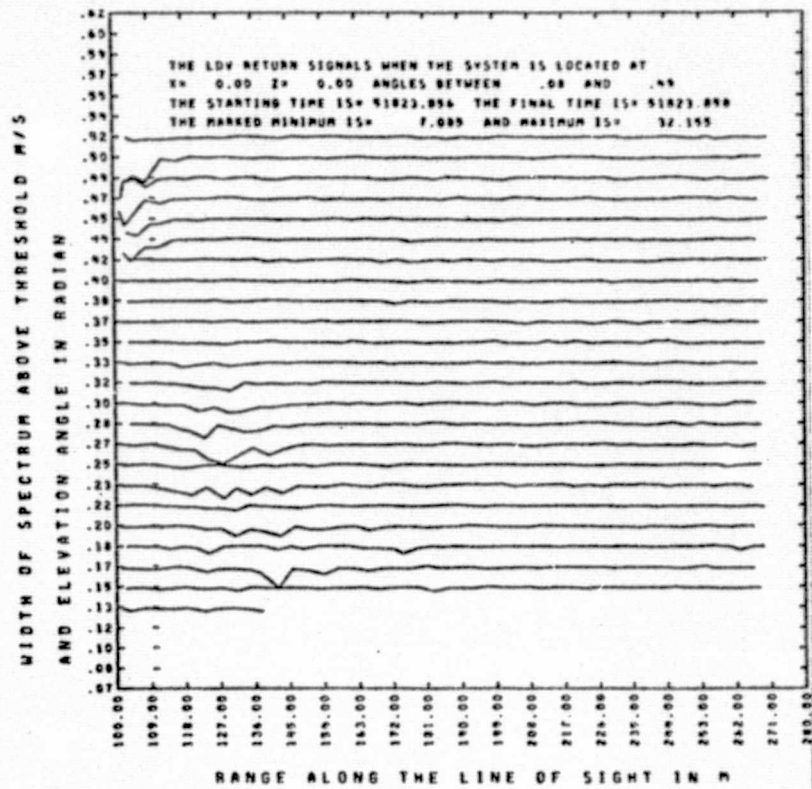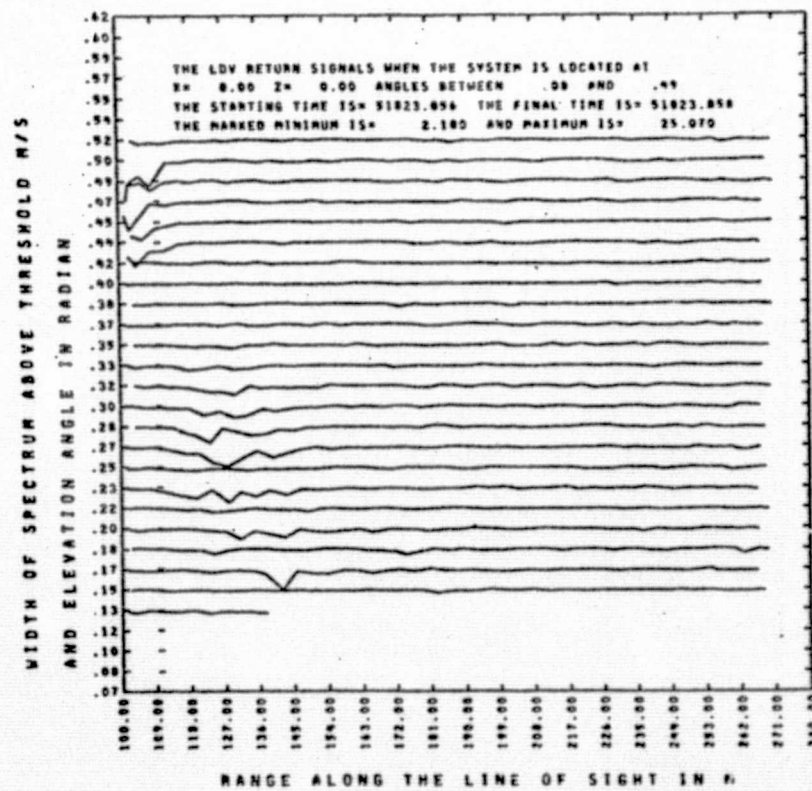INTENSITY THRESHOLD

36
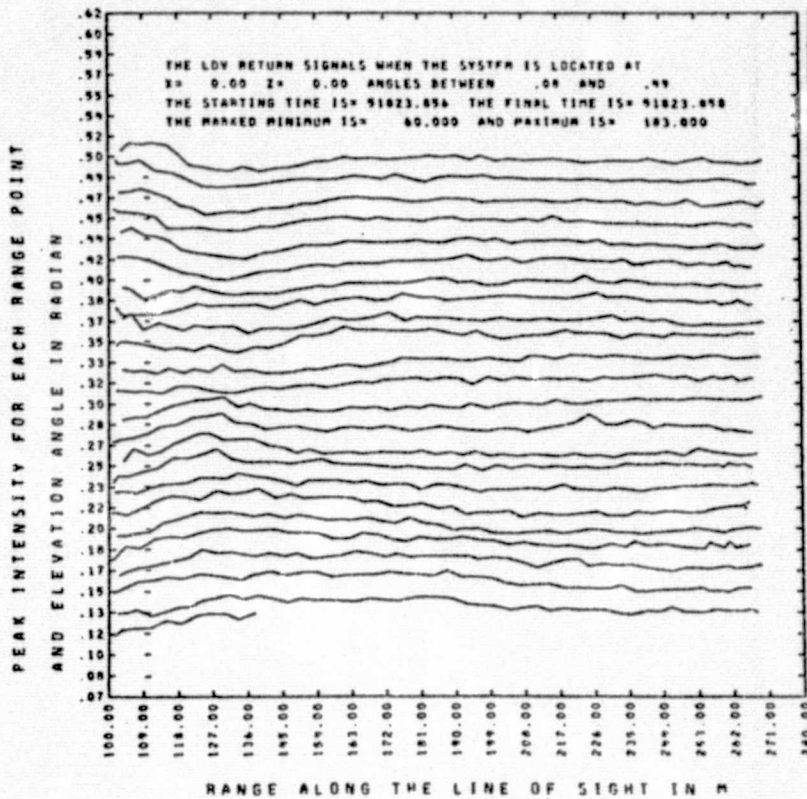
A
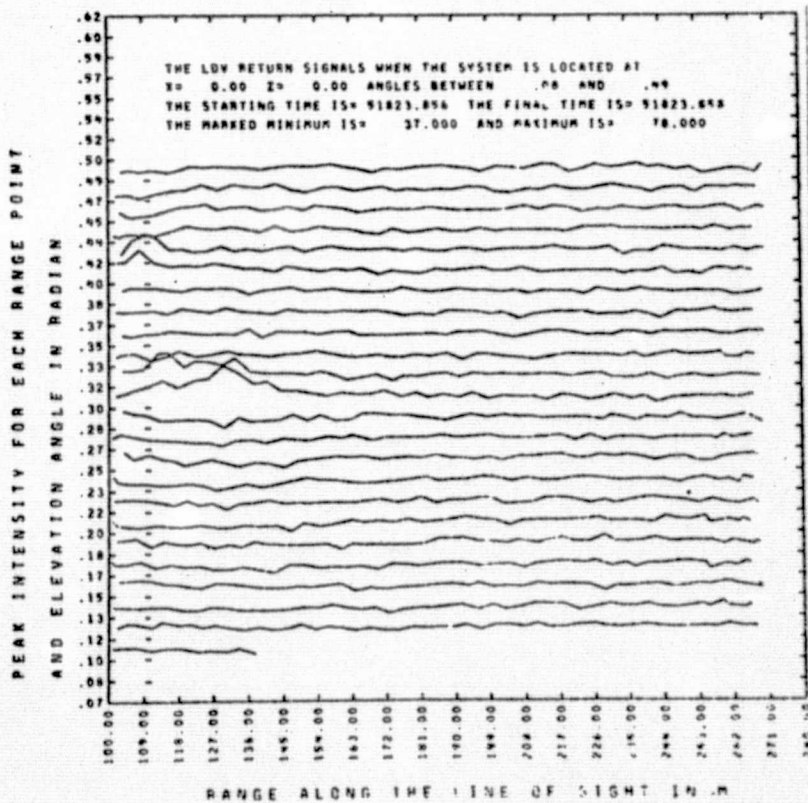
B

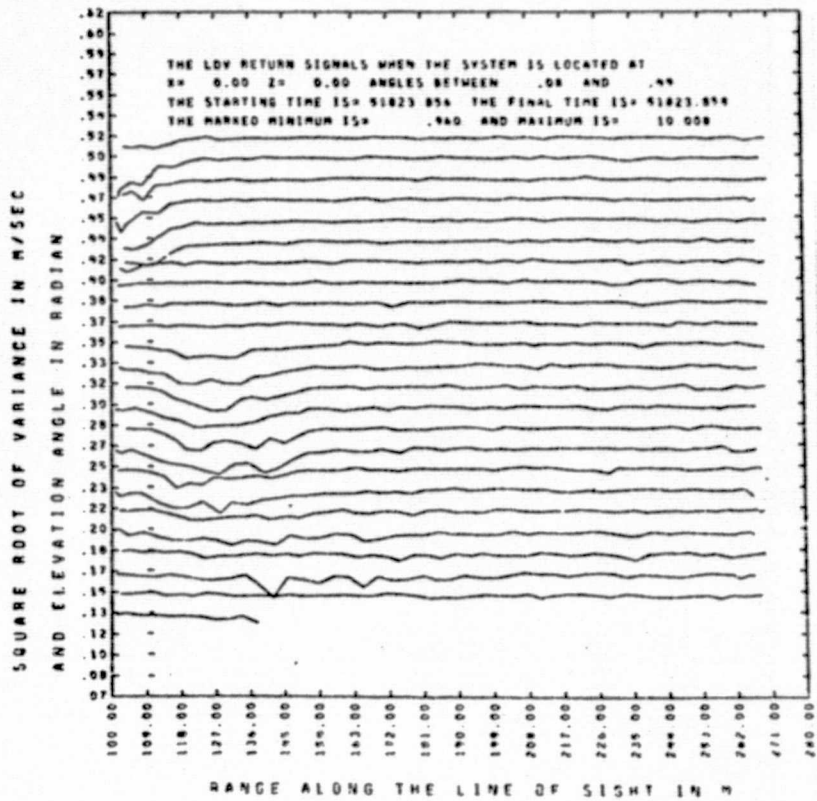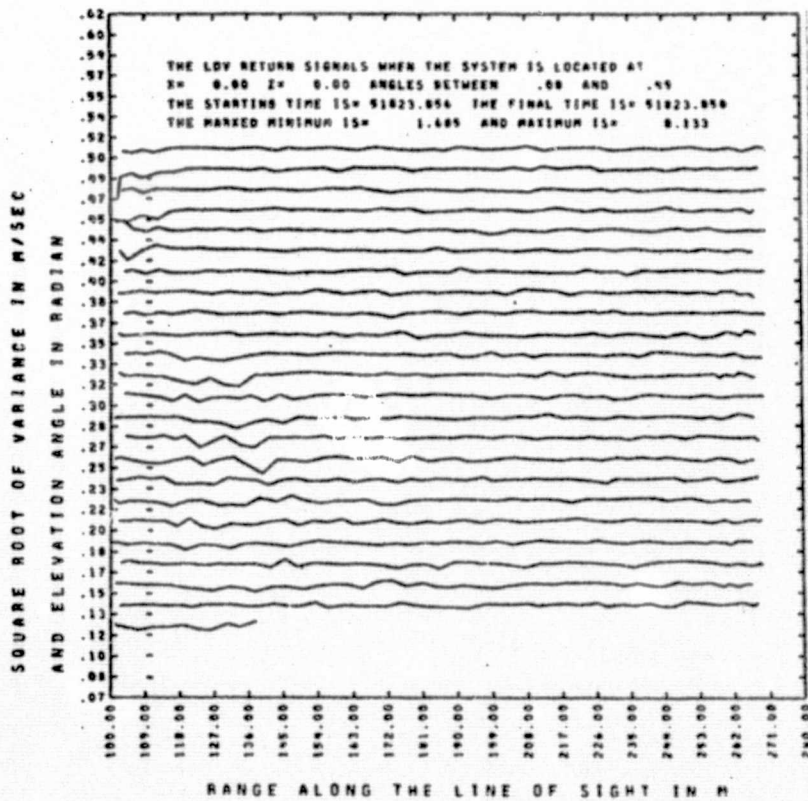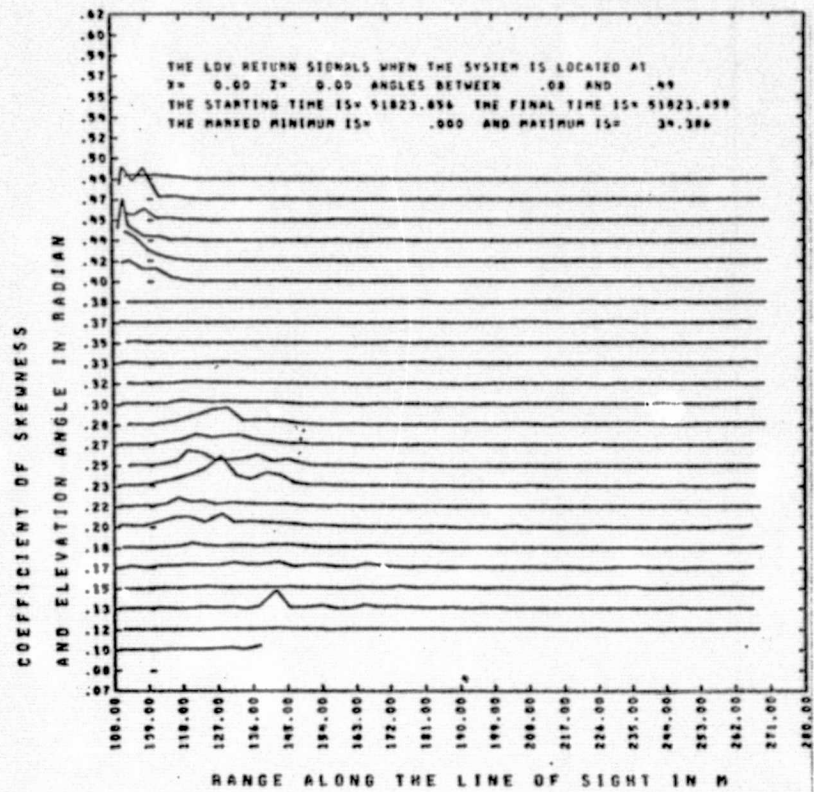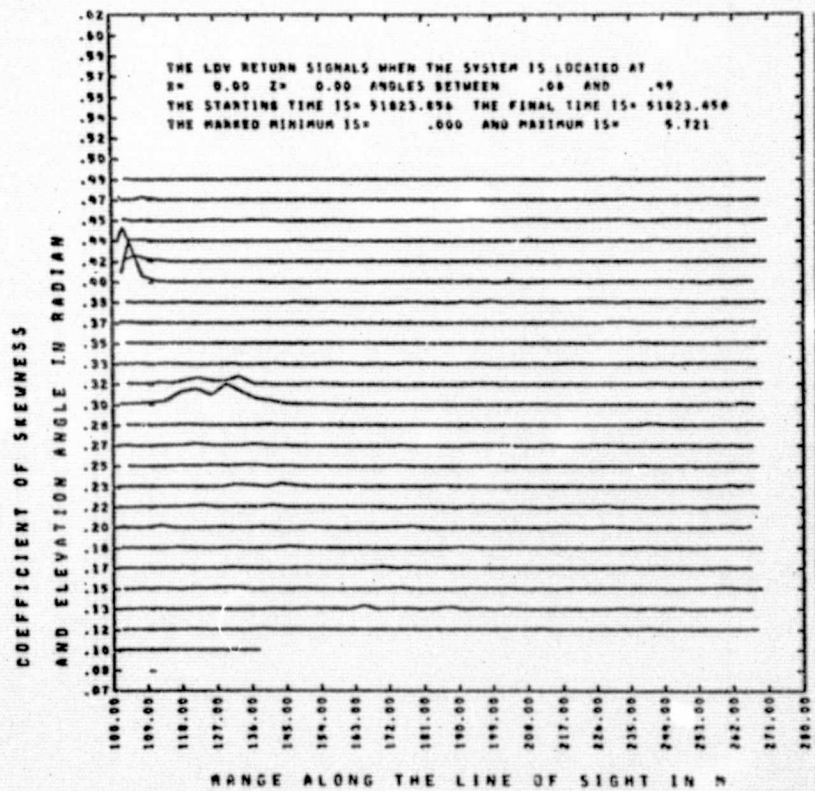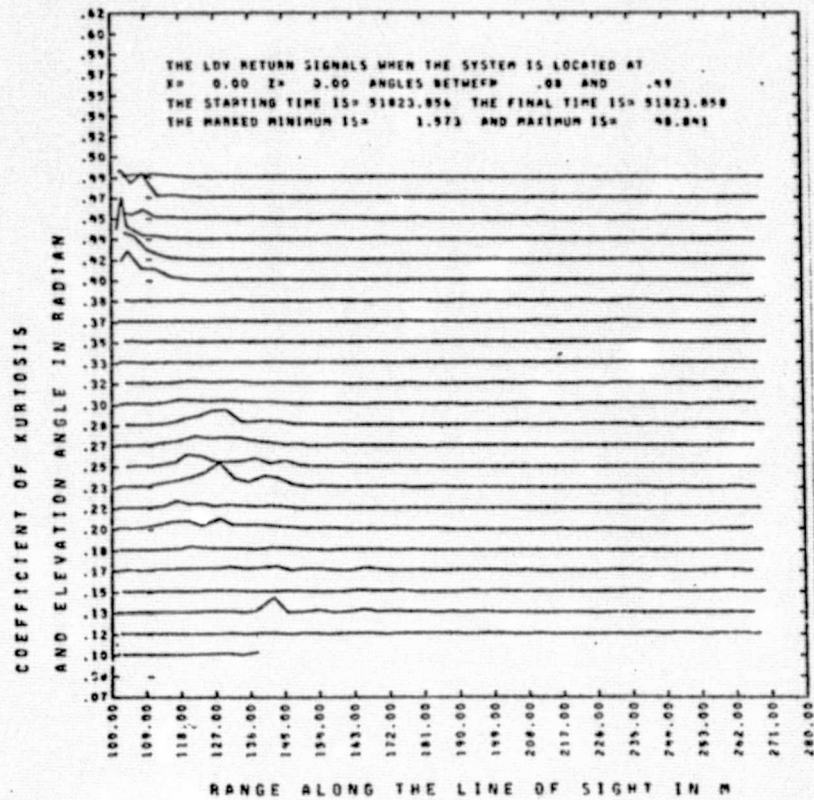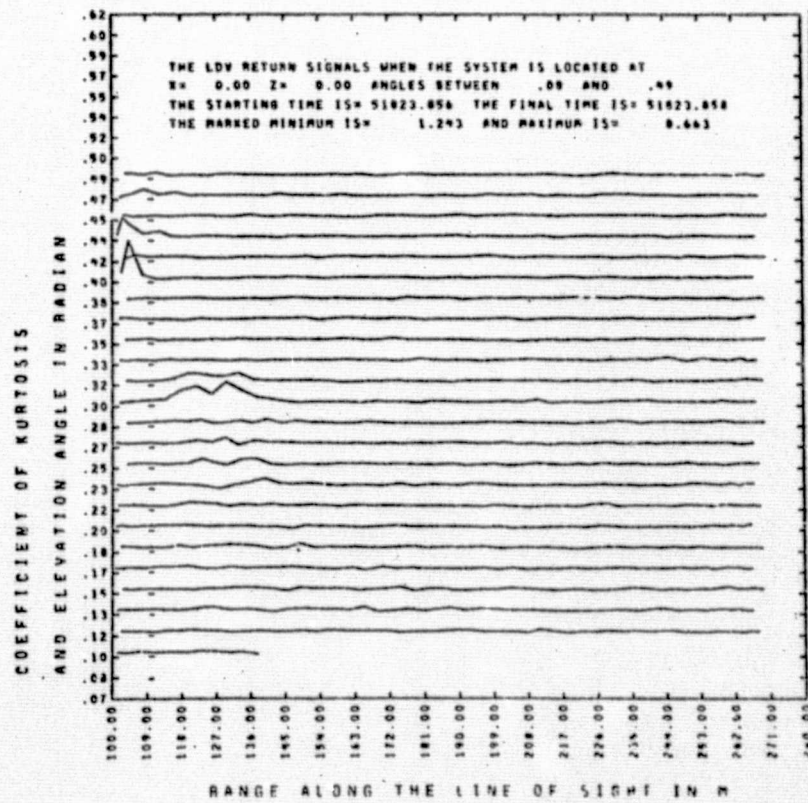FIGURE 17. EFFECT OF VELOCITY THRESHOLD ON I_{PEAK} AT LOW INTENSITY THRESHOLD   37

trend that the velocity threshold brought about in Figure 9
is again observed in Figure 13.

The coefficient of skewness now as

$$\beta = [\sum (v-\overline{v})^3 I(v)]^2 / \sigma^3$$

is shown in Figure 14. This quantity is always positive.
Its location of maxima coincides with the minima of σ.
Both Figures 14a and 14b show good vortex signatures, and
velocity threshold further improves the localization of
vortex signatures. The coefficient of kurtosis defined as

$$\kappa = [\sum (v-\overline{v})^4 I(v)] / \sigma^2$$

is shown in Figure 15. Both Figures 15a and 15b show good
signatures. The plots of skewness and kurtosis as defined
previously appear quite different from those shown in
Figures 14 and 15. Both skewness and kurtosis plots were
found to be similar to the variance shown in Figure 13, but
were quite noisy. The redefined coefficients of skewness
and kurtosis seem to yield clearer signatures.

Figure 16 shows that I_{sum} is maximum at the vortex
location, while the velocity threshold case in Figure 16b
shows the opposite trend. Finally, I_{peak} is shown in
Figure 17. The velocity threshold is seen to be able to
improve the angular resolution in I_{peak} significantly. The
V_{peak} versus angle plot for this low intensity threshold case
is not informative since V_{peak} is equal to the constant velo-
city at the highest channel for all angles.

Figure 18 shows the effects of different variable
intensity thresholds above the noise level, determined by
the second scheme. Figures 18a and 18d show the recorded
spectrum as the dotted line. The undotted line is the
threshold spectrum obtained by adding a constant value
(20 or 25) to the noise level derived from the minimum in-
tensity in each level. The threshold spectrum shown was used
in analyzing the data; although the data spectrum shown lies
mostly below the threshold spectrum, other spectra do not,
and these are responsible for the signals. One might expect
to find the same effect as was found in the first scheme.
However, the average velocity in Figure 18b shows a single
peak at a location totally unrelated to the vortex locations.
This was because of a very high intensity return at that
range point, which was obviously a noise return. Due to
that very high signal, all the rest of the variation is
suppressed. Figure 18e shows maxima in $\bar{V}$, but it is hard
to identify a localized vortex signature. Figures 18c and
18f, showing V_{width}, are almost identical, except for the
noise point which appeared in the $\bar{V}$ plot. Because of the
lower intensity threshold, Figure 19a shows several peaks
appearing in the plot of V_{peak}, while Figure 19d shows only
one peak. Figures 19b and 19e show V_{max}, and Figure 19e
appears to be similar to Figure 5e. Figures 19c and 19f,
together with 18b and 18e, show that plots of the variance

39
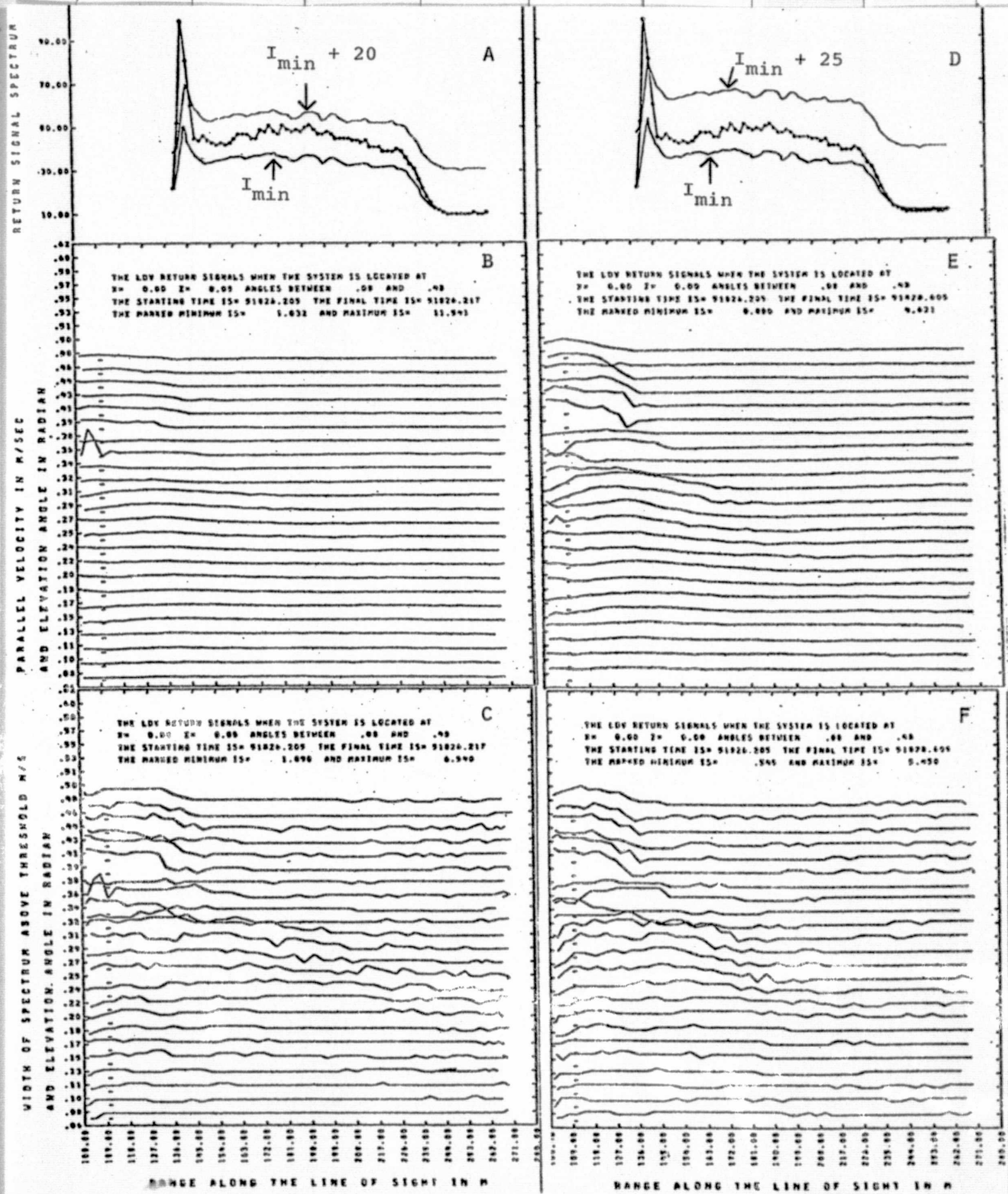
FIGURE 18. EFFECTS OF DIFFERENT INTENSITY THRESHOLDS ABOVE NOISE LEVEL
TO THE $\bar{V}$ AND V_{WIDTH}

THE LDV RETURN SIGNALS WHEN THE SYSTEM IS LOCATED AT
X= 0.00 Z= 0.00 ANGLES BETWEEN .00 AND .48
THE STARTING TIME IS= 91826.205 THE FINAL TIME IS= 91826.217
THE MARKED MINIMUM IS= 1.090 AND MAXIMUM IS= 17.990

THE LDV RETURN SIGNALS WHEN THE SYSTEM IS LOCATED AT
X= 0.00 Z= 0.00 ANGLES BETWEEN .00 AND .48
THE STARTING TIME IS= 91826.205 THE FINAL TIME IS= 91828.605
THE MARKED MINIMUM IS= 0.000 AND MAXIMUM IS= 5.450

THE LDV RETURN SIGNALS WHEN THE SYSTEM IS LOCATED AT
X= 0.00 Z= 0.00 ANGLES BETWEEN .00 AND .48
THE STARTING TIME IS= 91826.205 THE FINAL TIME IS= 91826.217
THE MARKED MINIMUM IS= .030 AND MAXIMUM IS= 47.056

THE LDV RETURN SIGNALS WHEN THE SYSTEM IS LOCATED AT
X= 0.00 Z= 0.00 ANGLES BETWEEN .00 AND .48
THE STARTING TIME IS= 91826.205 THE FINAL TIME IS= 91828.605
THE MARKED MINIMUM IS= 0.000 AND MAXIMUM IS= 3.477

FIGURE 19. EFFECTS OF DIFFERENT INTENSITY THRESHOLDS ABOVE NOISE LEVEL TO V_{PEAK}, V_{MAX}, σ

41

σ and of $\bar{V}$ depend in a similar fashion upon the intensity threshold. Figures 20a and 20c, and 20b and 20d, show that skewness and kurtosis also behave similarly. Figures 20e and 20f show the maximum V_{peak} versus elevation angle. Figure 20e has the higher maximum value of V_{peak} and shows three peaks at angles of .25, .35, and .45 radians. (These are also found in Figure 19a.) Figure 20f shows the highest V_{peak} at 17 m/sec, with three peaks at angles of .28, .34, and .40 radians.

Results from applying a higher intensity threshold are shown in the a, b, and c portions of Figures 21 through 24. These plots exhibit a behavior very similar to the series shown in the d, e, and f portions of Figures 4 through 7. The second noise determination scheme (minimum intensity) does not produce clear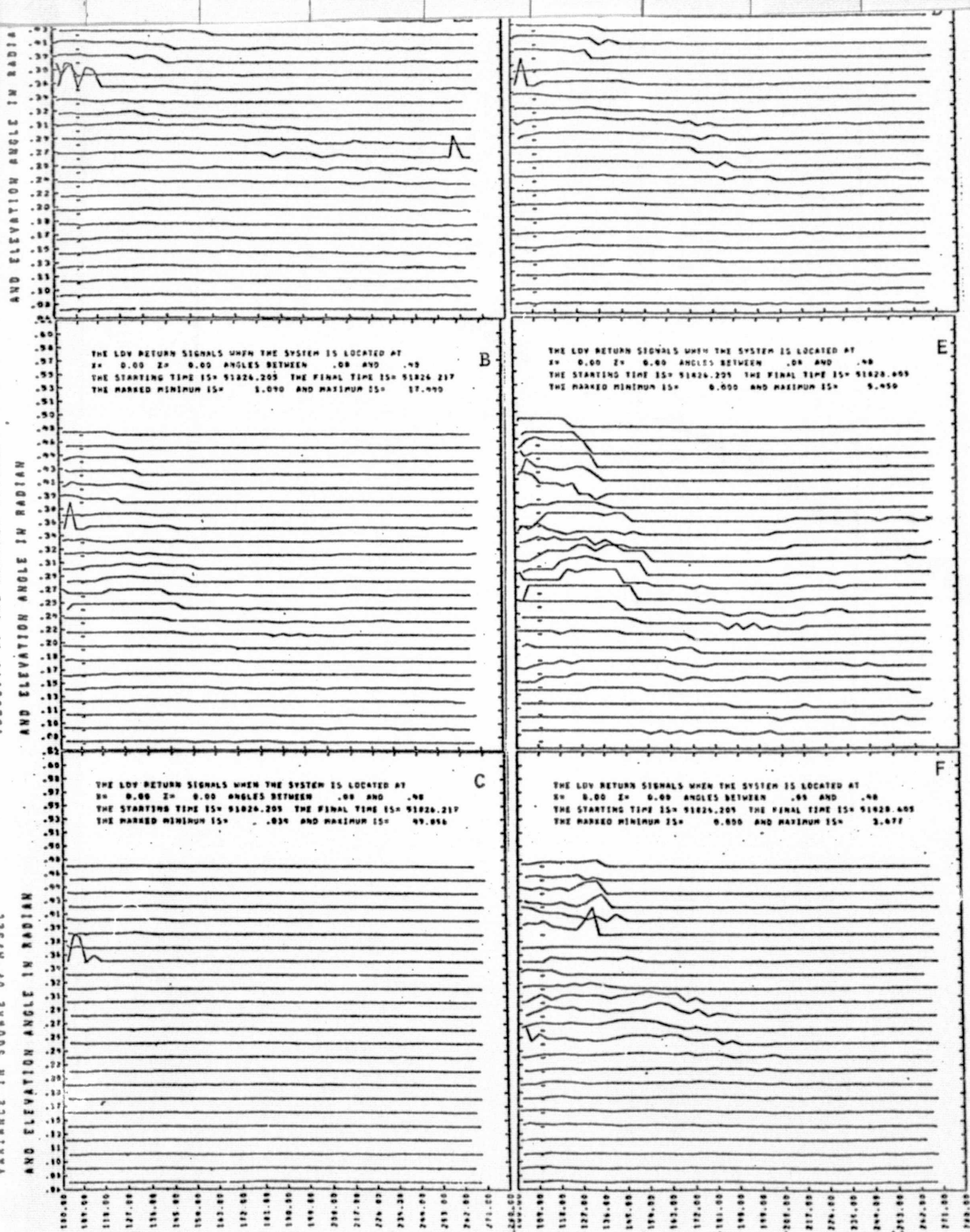er vortex signatures than the first scheme (constant noise level), and requires more effort to apply. However, the second scheme should be less sensitive to arbitrary assumptions in setting the intensity threshold.

Figures 21 through 24 show the effects of velocity thresholds. The vertical lines (at $V = 0$ in Figure 21a and $V = 7.3$ m/sec in Figure 21d) show the threshold values. A constant value of 30 is added to the minimum-signal noise level in all cases. All signals below the velocity threshold are dropped. This will subtract all wind information for the right column plots, so that signals will be due to the vortex only.

42

KURTOSIS IN QUADRATIC OF M/SEC AND ELEVATION ANGLE IN RADIAN

AND ELEVATION ANGLE IN RADIAN

A

C

THE LDV RETURN SIGNALS WHEN THE SYSTEM IS LOCATED AT
X= 0.00 Z= 0.00 ANGLES BETWEEN .00 AND .48
THE STARTING TIME IS= 91026.205 THE FINAL TIME IS= 91026.217
THE MARKED MINIMUM IS= .006 AND MAXIMUM IS= 3470.000

B

THE LDV RETURN SIGNALS WHEN THE SYSTEM IS LOCATED AT
X= 0.00 Z= 0.00 ANGLES BETWEEN .00 AND .48
THE STARTING TIME IS= 91026.205 THE FINAL TIME IS= 91026.605
THE MARKED MINIMUM IS= 0.000 AND MAXIMUM IS= 36.441

D

THE LDV RETURN SIGNALS WHEN THE SYSTEM IS LOCATED AT
X= 0.00 Z= 0.00 ANGLES BETWEEN .00 AND .48
THE STARTING TIME IS= 91026.205 THE FINAL TIME IS= 91026.217

E

THE LDV RETURN SIGNALS WHEN THE SYSTEM IS LOCATED AT
X= 0.00 Z= 0.00 ANGLES BETWEEN .00 AND .48
THE STARTING TIME IS= 91026.205 THE FINAL TIME IS= 91026.605

F

Angle in Radians

Angle in Radians

FIGURE 20. EFFECTS OF DIFFERENT INTENSITY THRESHOLDS ABOVE NOISE LEVEL TO β, κ
AND MAXIMUM V_{PEAK} VERSUS ANGLE
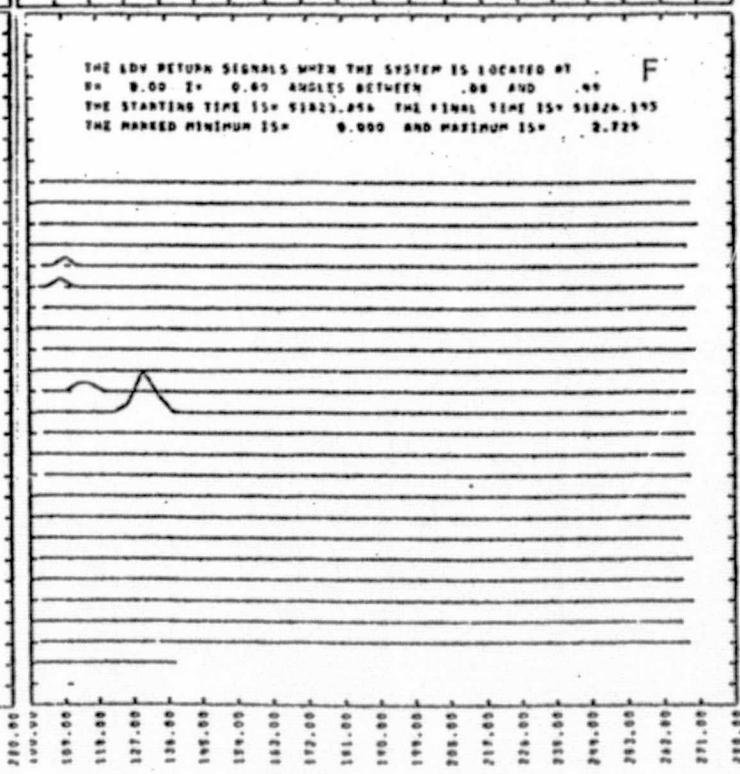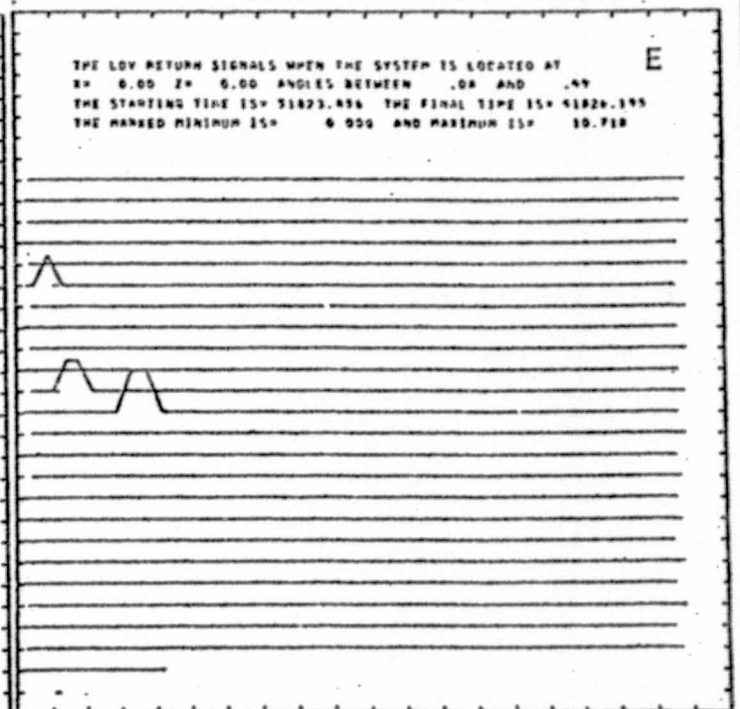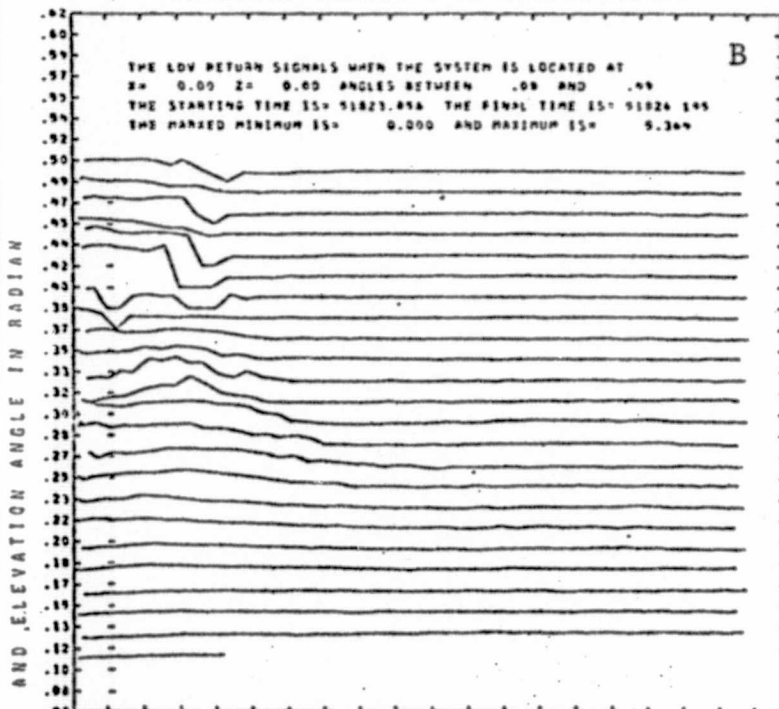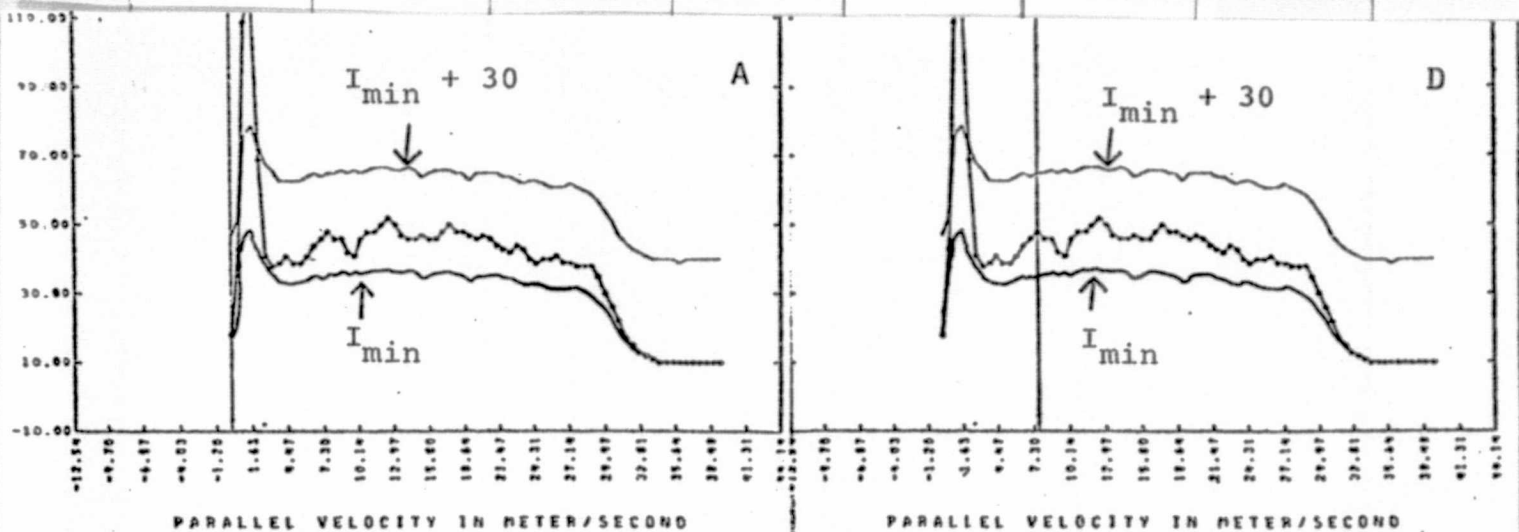
FIGURE 21. EFFECTS OF THE VELOCITY THRESHOLD ON $\overline{V}$, V_{WIDTH}
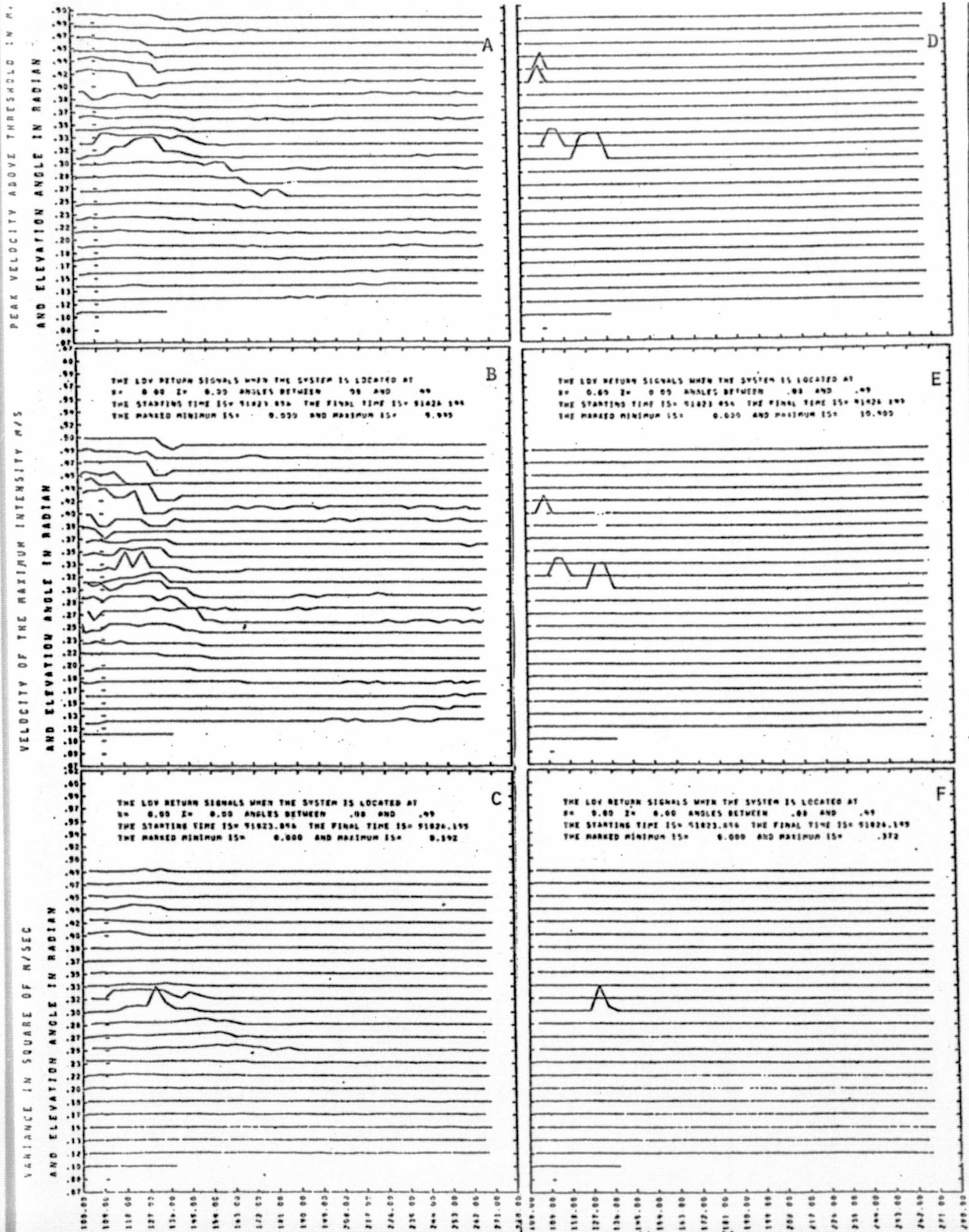
FIGURE 22.   EFFECTS OF THE VELOCITY THRESHOLD ON V_{PEAK}, V_{MAX}, σ
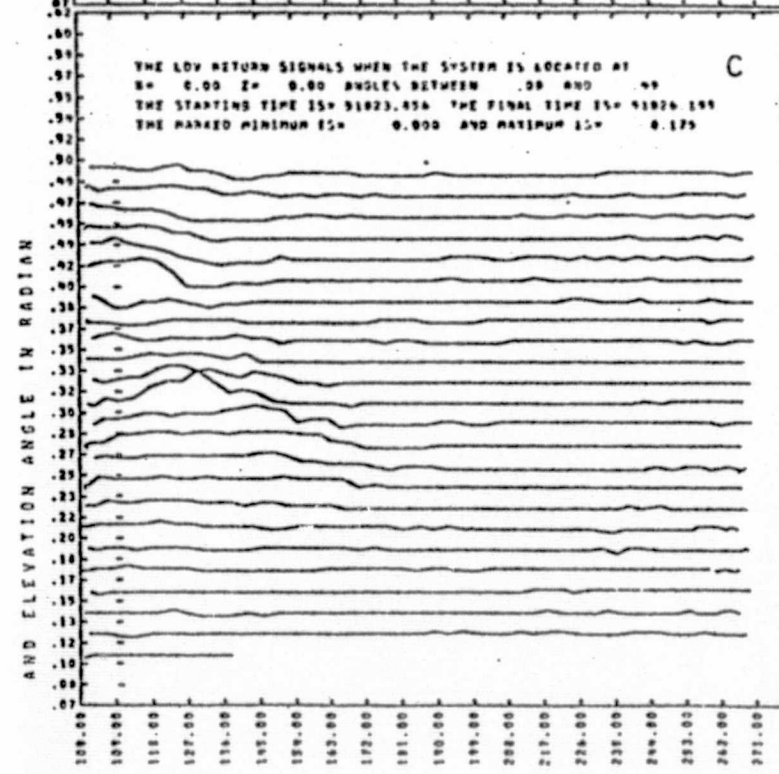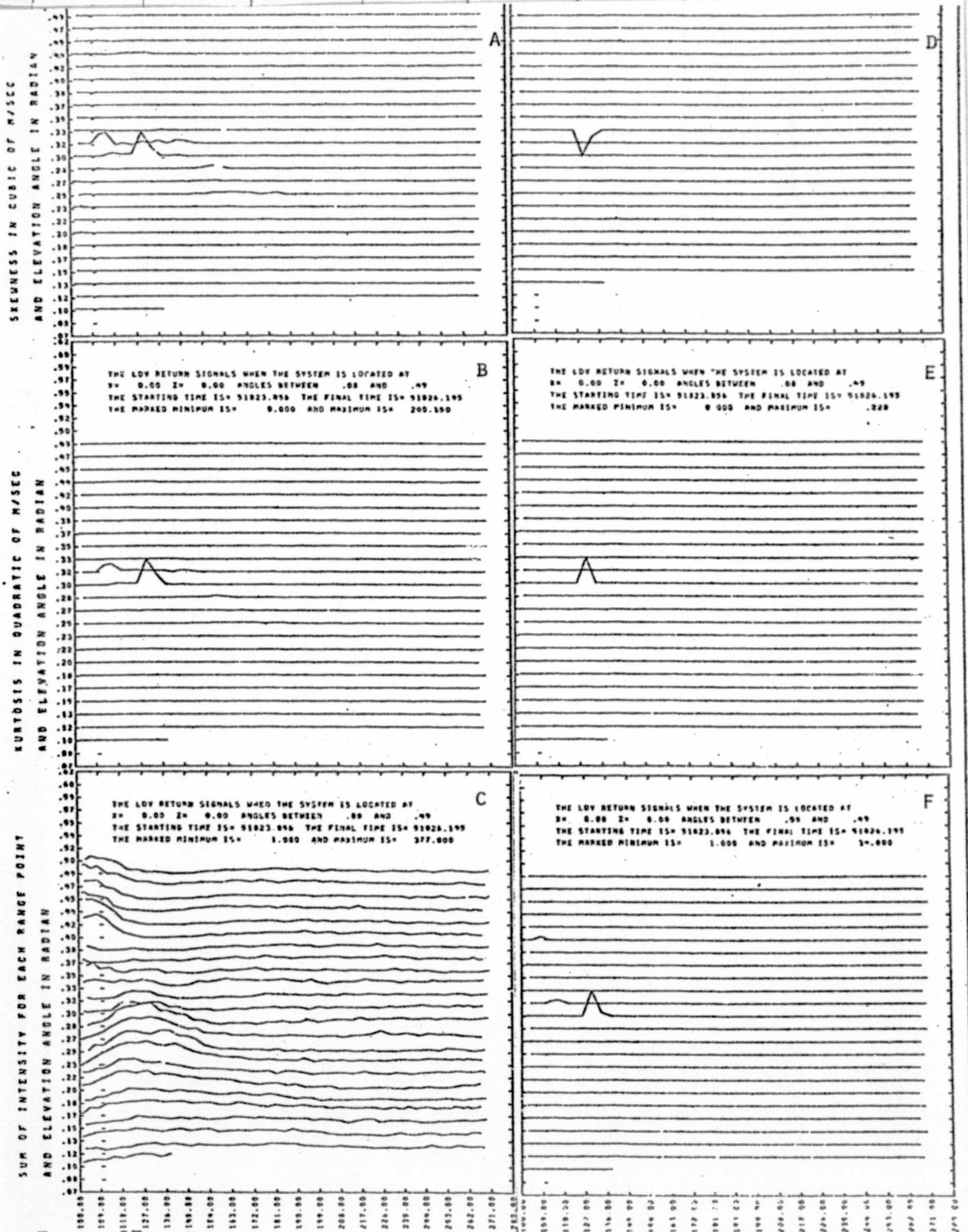
FIGURE 23.—EFFECTS OF THE VELOCITY THRESHOLD ON β, κ, I_SUM

46
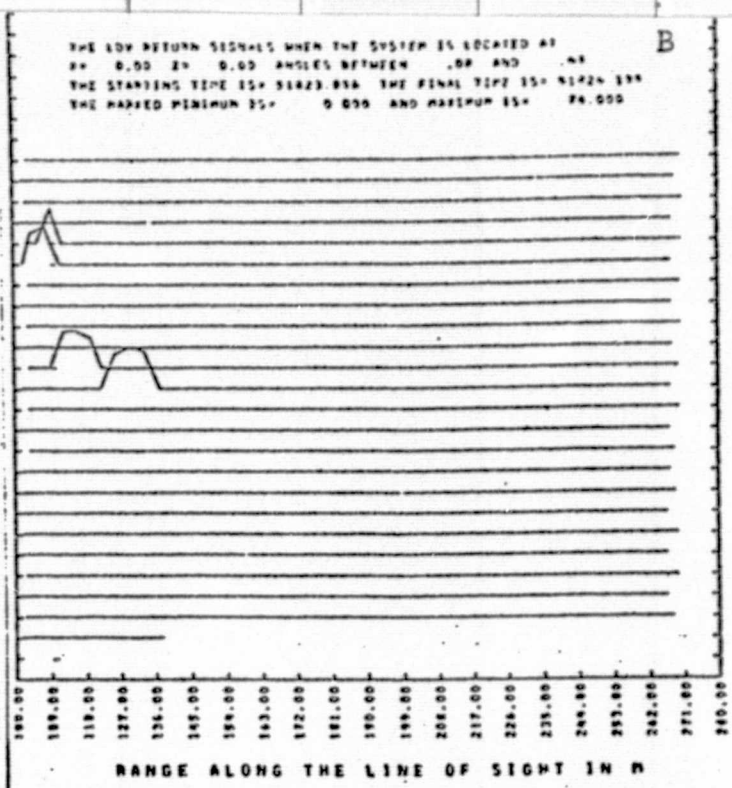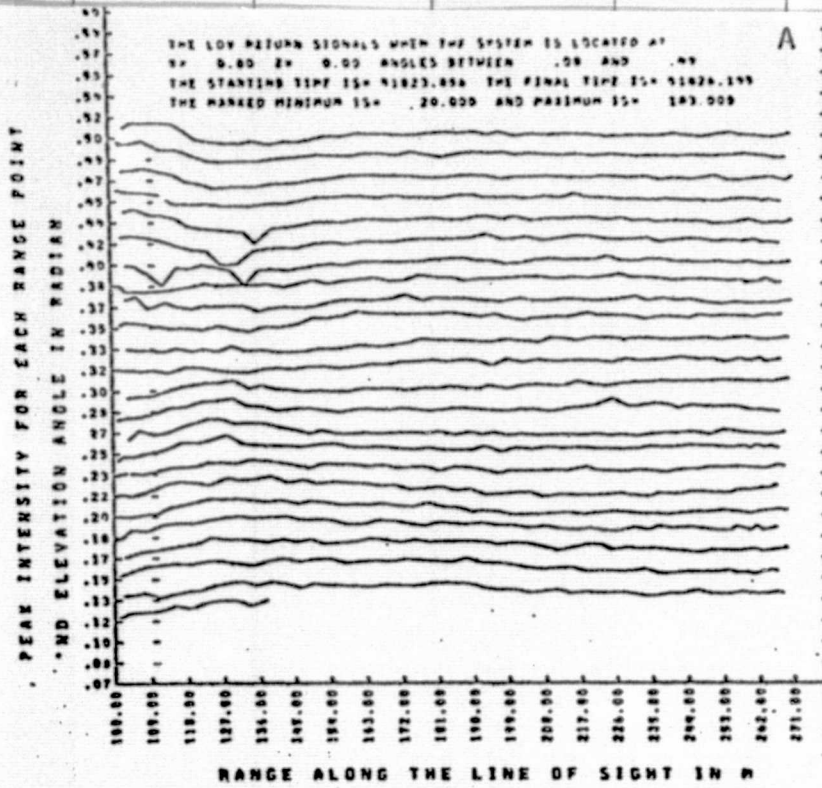
FIGURE 24. EFFECTS OF THE VELOCITY THRESHOLD ON I~PEAK~ AND THE MAXIMUM OF V~PEAK~ VERSUS ANGLE

47

Figures 21e and 21f show signals which are better isolated than those in Figures 21b and 21c. Figures 22d and 22e show almost identical results as those in Figures 21e and 21f. However, Figures 22f and 23 d,e,f reveal only one peak instead of the four peaks which appeared in the V_{peak} (Figure 22d) and V_{width} (Figure 21f) plots. The most remarkable effect of a velocity threshold is on I_{sum} (Figures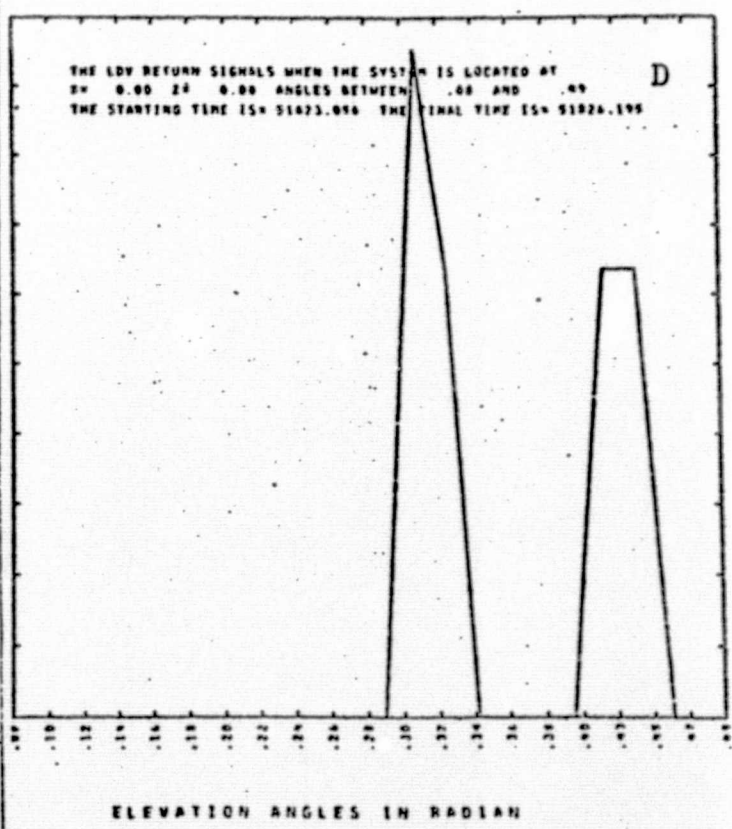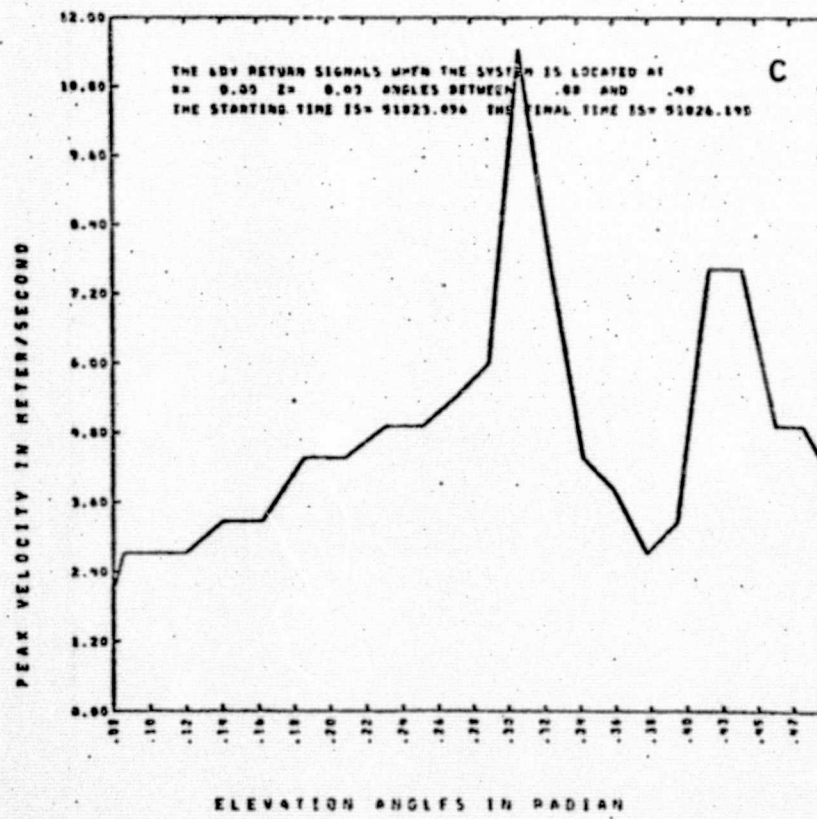 23c and f) and I_{peak} (Figures 24a and b); I_{peak} is a good indicator of vortex location if velocity thresholding is applied. Figures 24c and 24d both show two peaks at angles of .30 and .43, and the velocity magnitudes are the same. The gradual drop off on both sides of the peak shown in Figure 24c disappears when velocity thresholding is applied.

Figures 25 through 32 show a series of contour plots of $\bar{V}$, V_{max}, V_{peak}, σ, β, κ, I_{sum}, I_{peak}. A constant intensity threshold of 60 is applied and there is no velocity threshold.

The method of preparing the contour plots was discussed in Section III. The grid size is 200 m $\times$ 200 m. Values of the quantity on the contours are indicated near the top of each plot. An auxiliary cross-sectional plot is given below each contour plot to demonstrate the variation versus both x and y distances. The time of the scan is recorded on both the contour and the cross-sectional

48
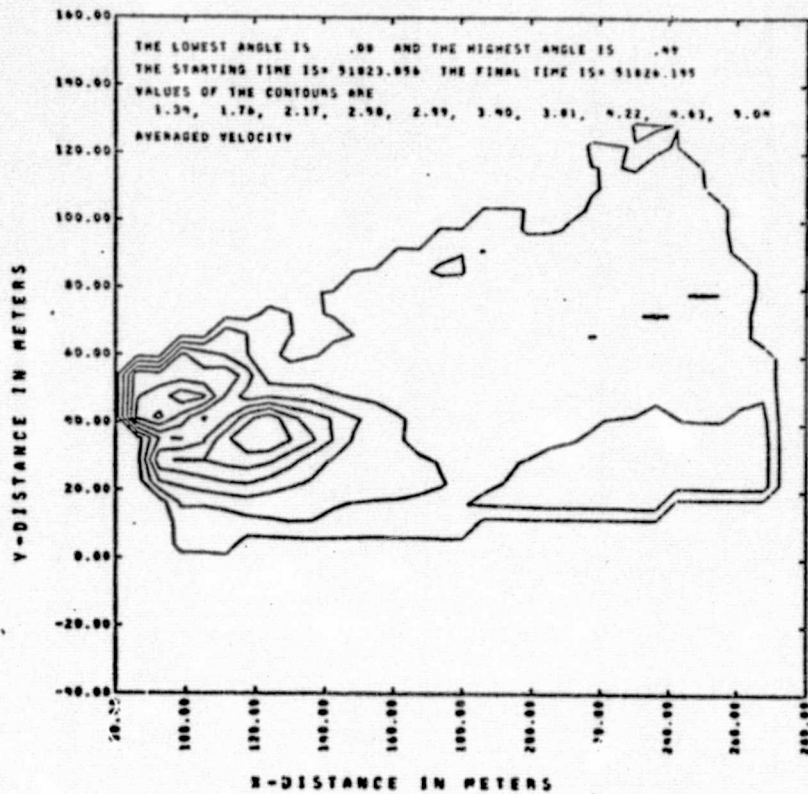
FIGURE 25. CONTOUR PLOT FOR $\bar{V}$

Top plot:

THE LOWEST ANGLE IS .00 AND THE HIGHEST ANGLE IS .49
THE STARTING TIME IS= 51823.856 THE FINAL TIME IS= 51826.195
VALUES OF THE CONTOURS ARE
1.35, 1.76, 2.17, 2.58, 2.99, 3.40, 3.81, 4.22, 4.63, 5.04
AVERAGED VELOCITY

Y-DISTANCE IN METERS

X-DISTANCE IN METERS

Bottom plot:

CROSSECTIONAL PROFILES
MINIMUM 1.353E-03 MAXIMUM 5.3?5E-00
TIME= 51833.856

Y DISTANCE

X DISTANCE
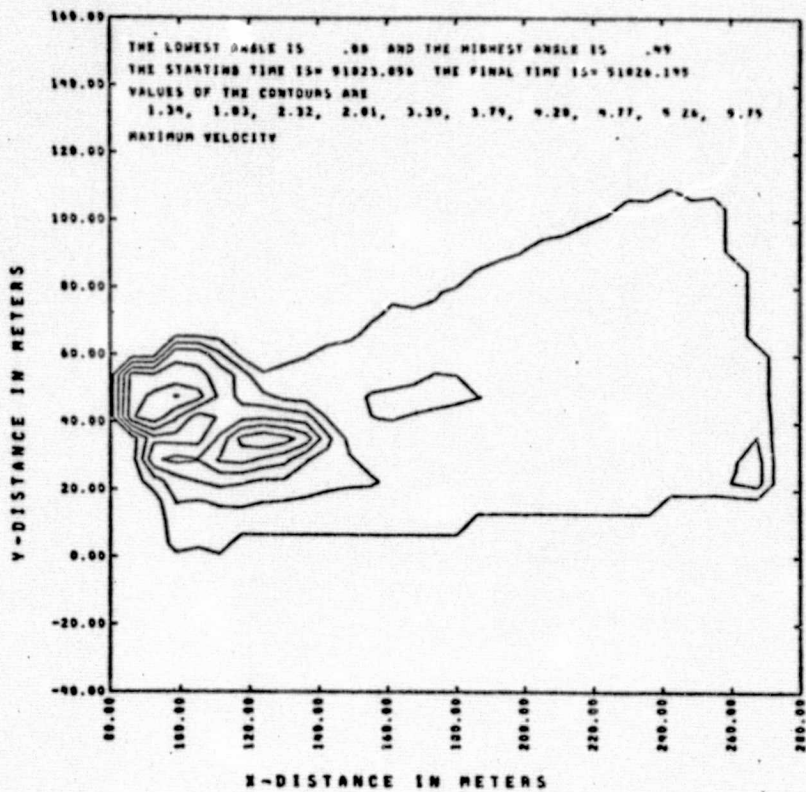
FIGURE 26. CONTOUR PLOT FOR V_{MAX}

50
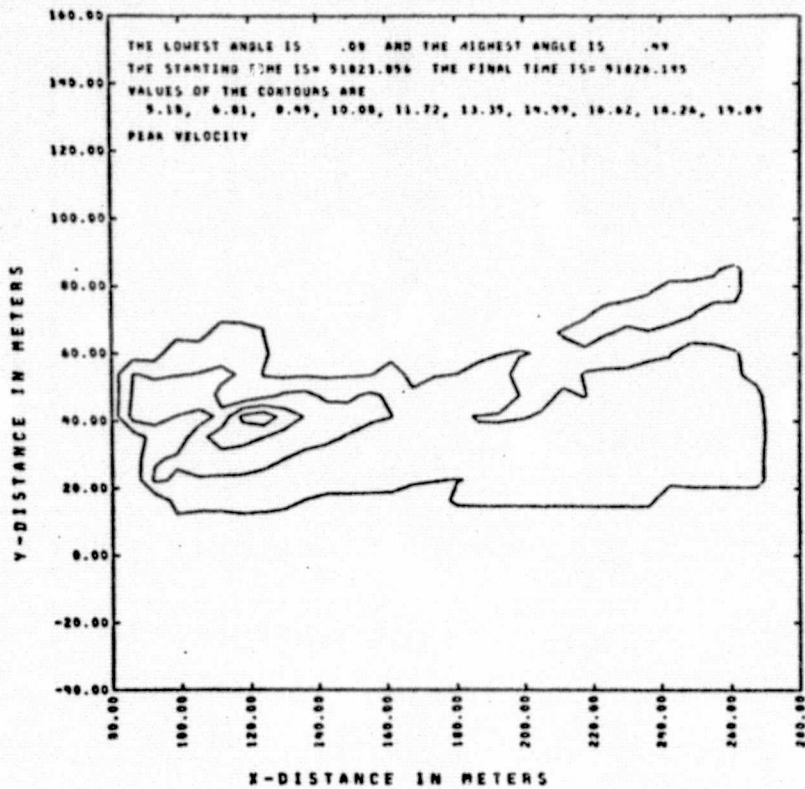
FIGURE 27. CONTOUR PLOT FOR V_{PEAK}

THE LOWEST ANGLE IS   .03 AND THE HIGHEST ANGLE IS   .49
THE STARTING TIME IS= 91823.096 THE FINAL TIME IS= 91826.195
VALUES OF THE CONTOURS ARE
   1.09, 2.11, 3.14, 4.16, 5.19, 6.22, 7.24, 8.27, 9.29, 10.32

NORMALIZED VARIANCE

Y-DISTANCE IN METERS

X-DISTANCE IN METERS

CROSSECTIONAL PROFILES

MINIMUM= 9.747E-01   MAXIMUM= 5.883E-01

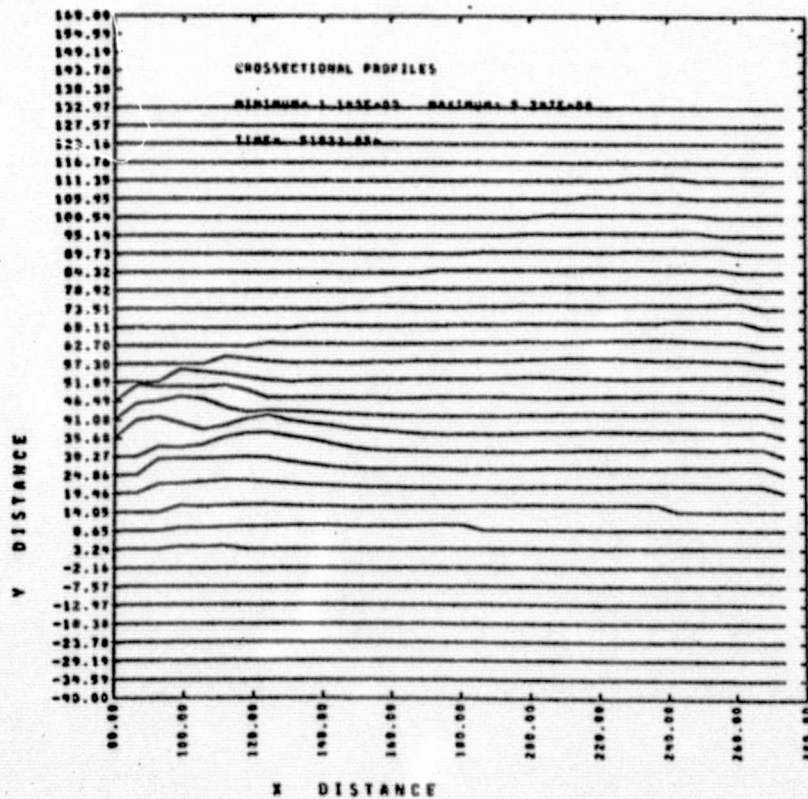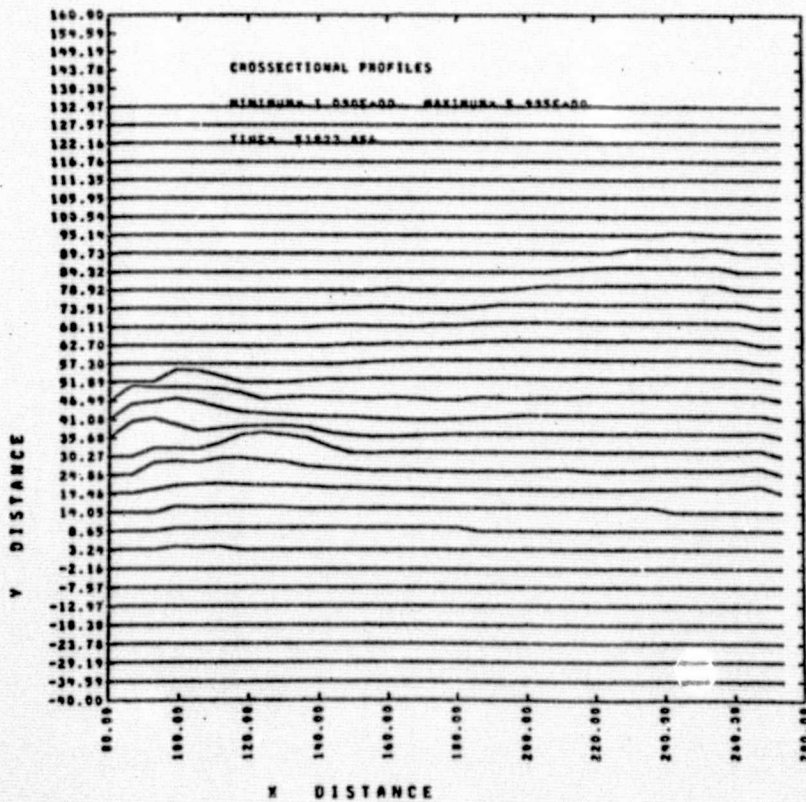TIME= 91823.454

Y DISTANCE

X   DISTANCE
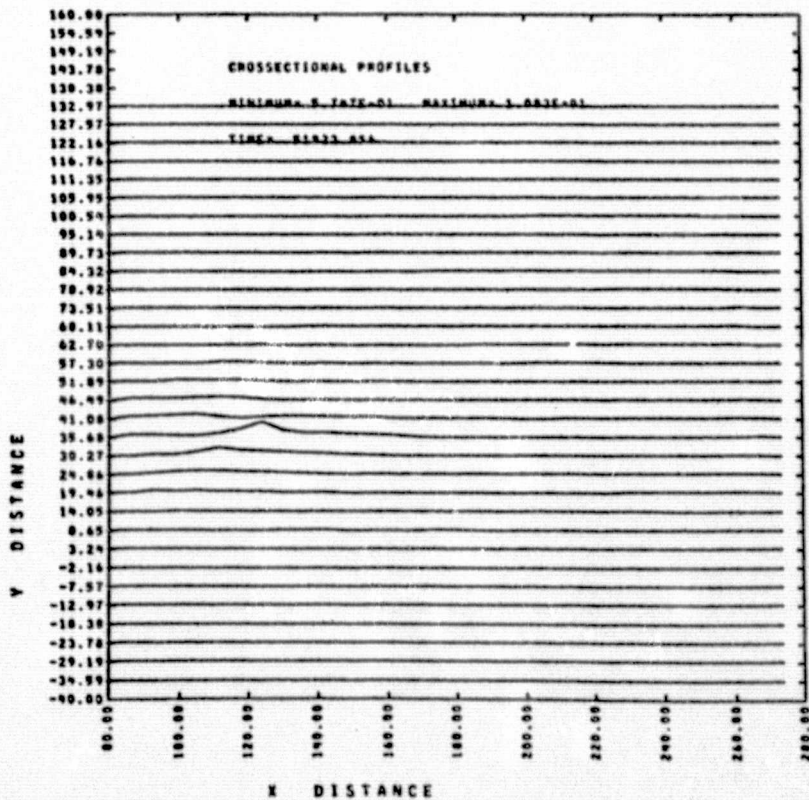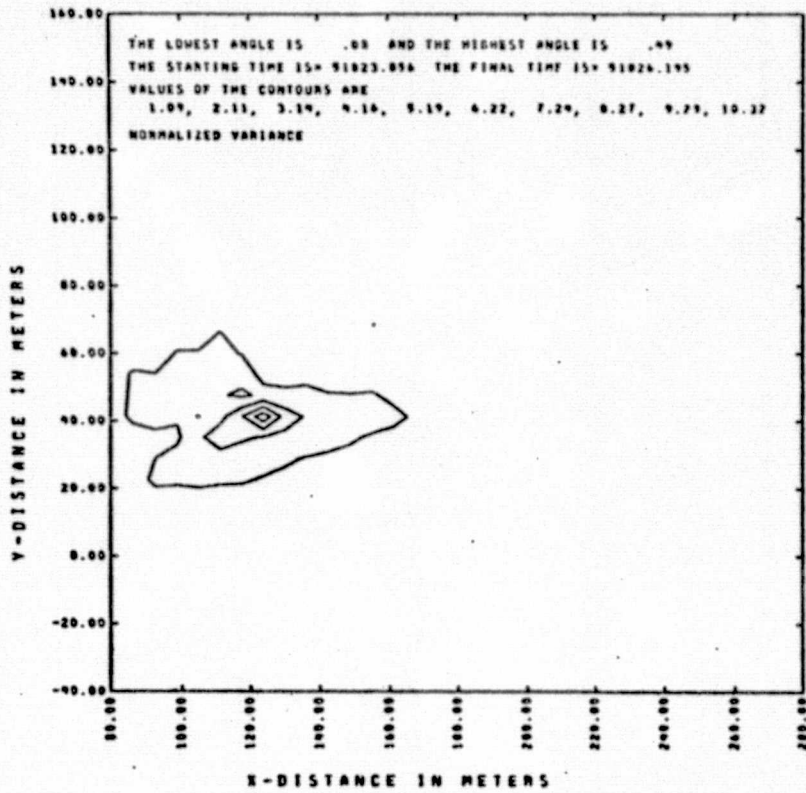
FIGURE 28. CONTOUR PLOT FOR σ

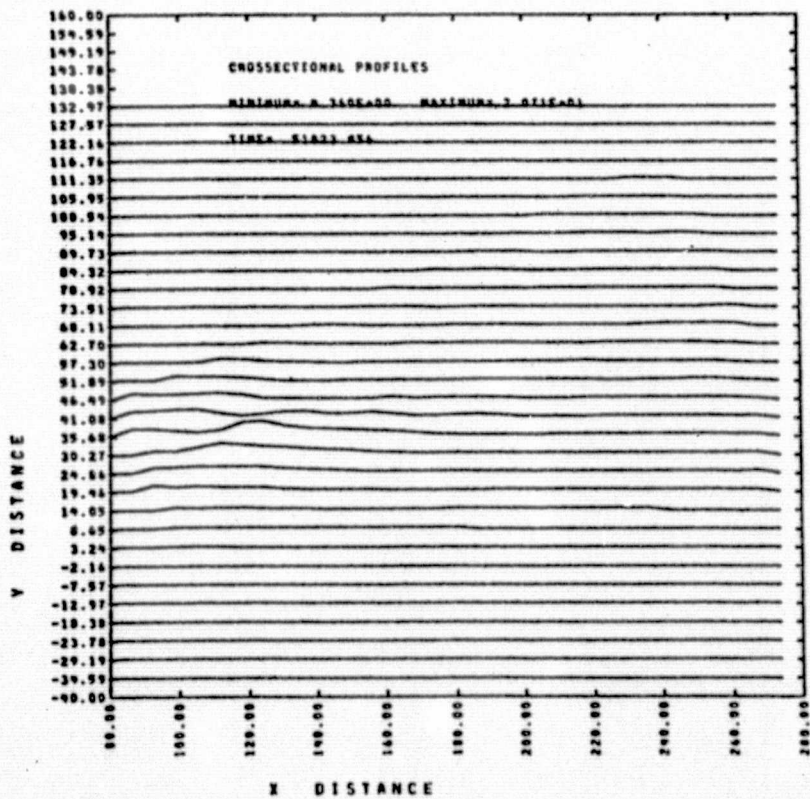52
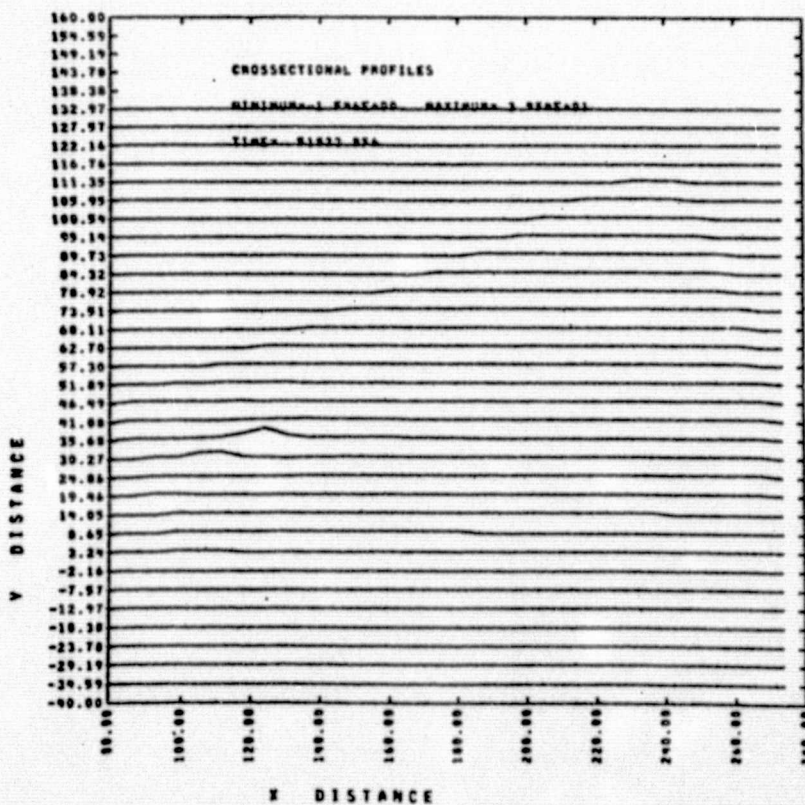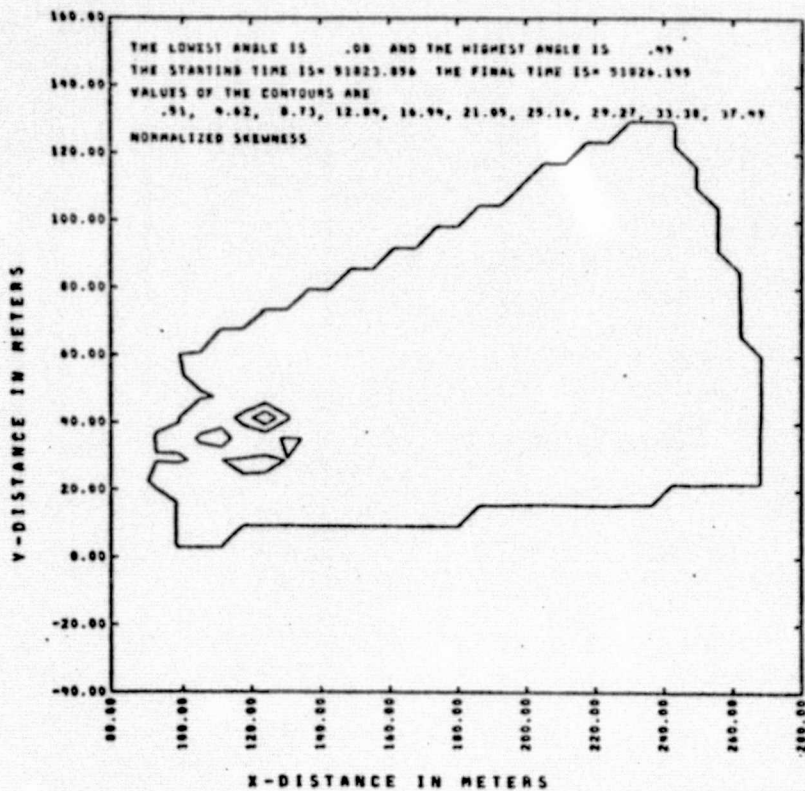
FIGURE 29. CONTOUR PLOT FOR β
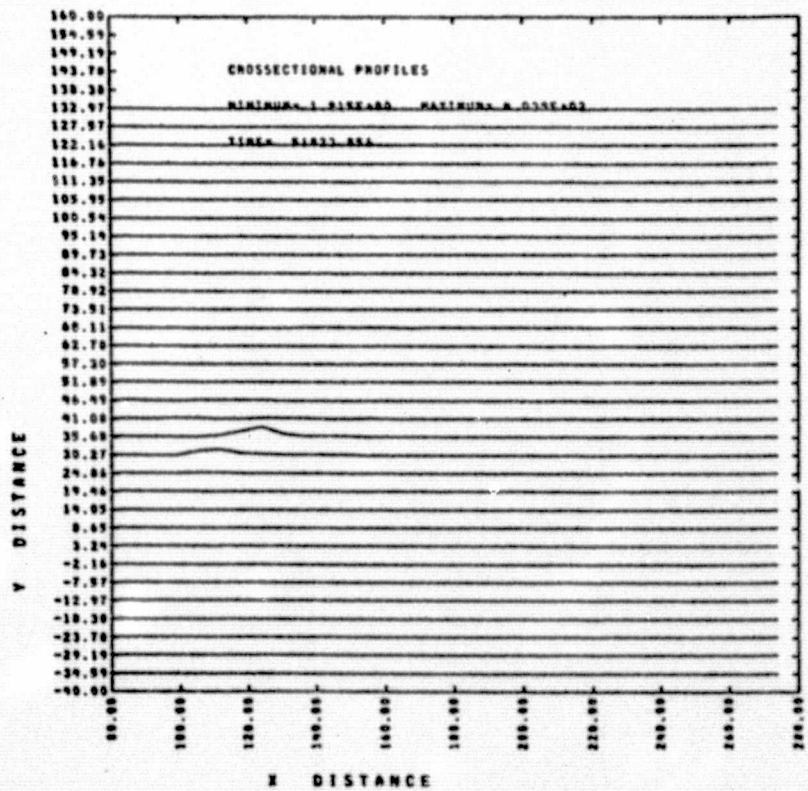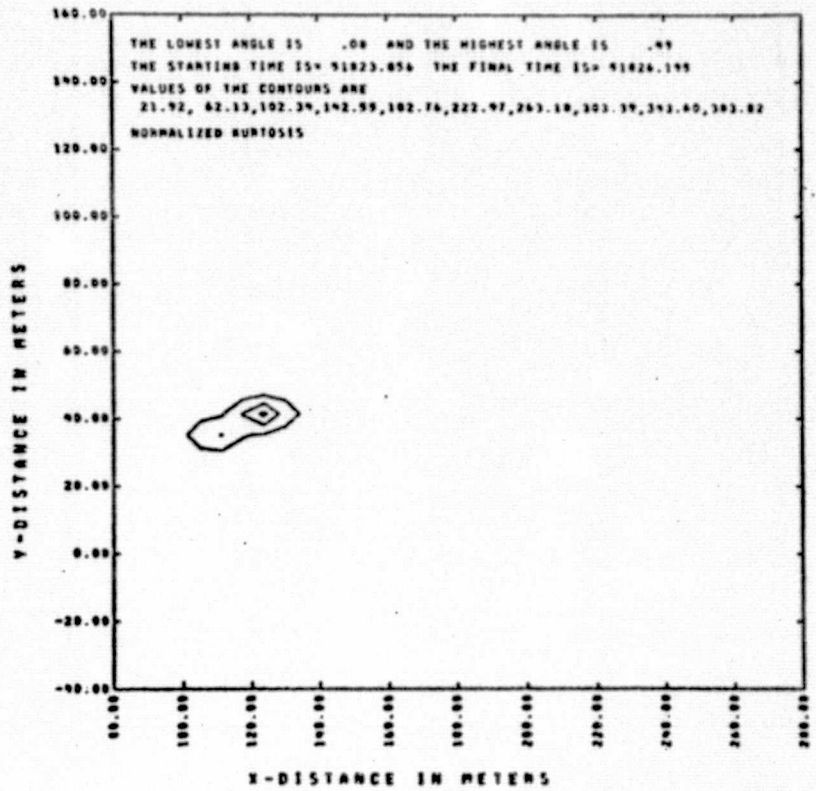
FIGURE 30. CONTOUR PLOT FOR κ
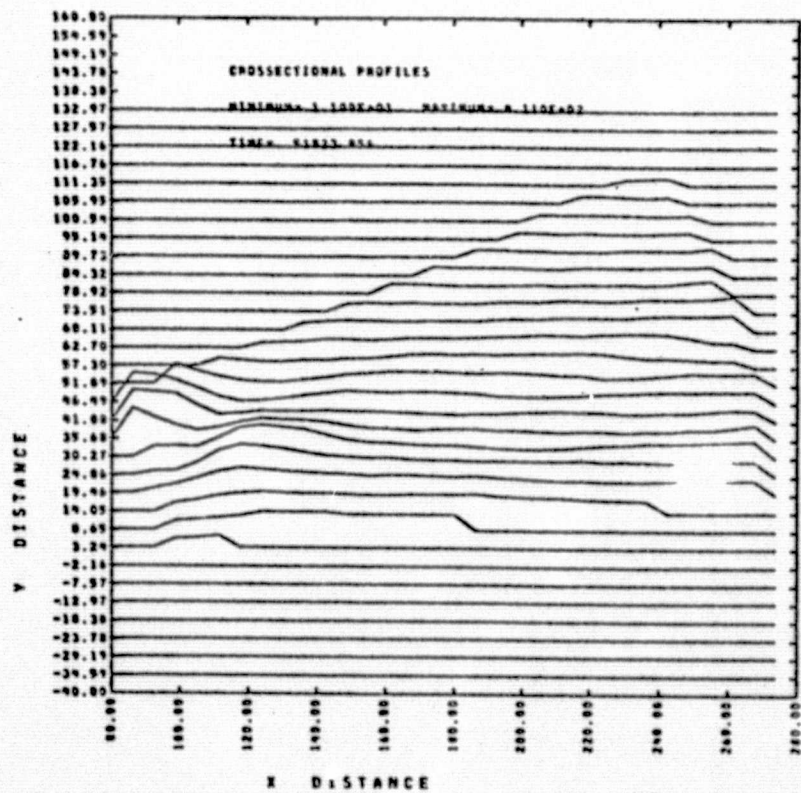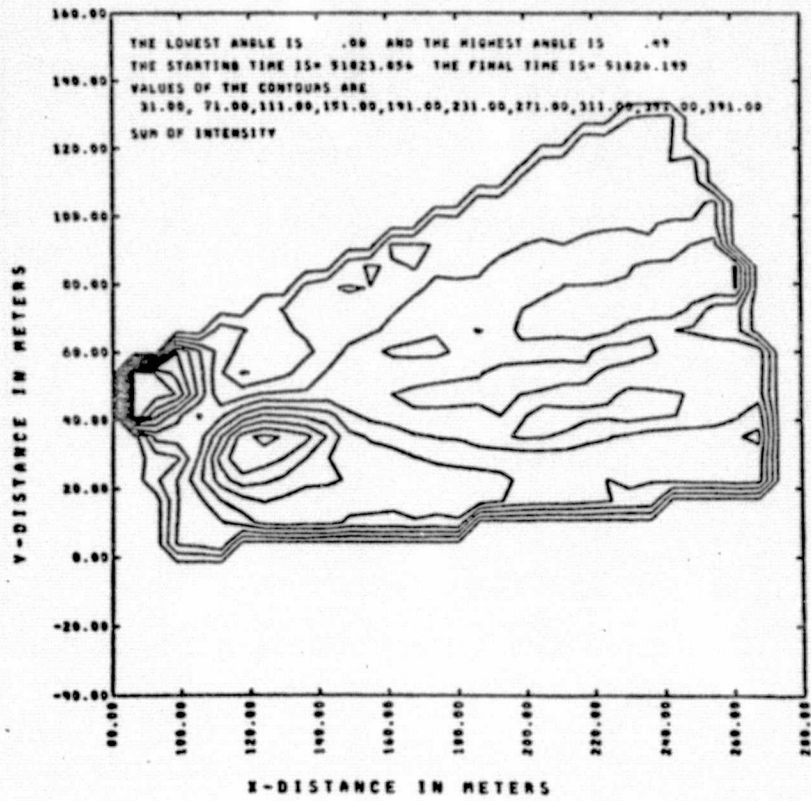
FIGURE 31. CONTOUR PLOT FOR I_SUM
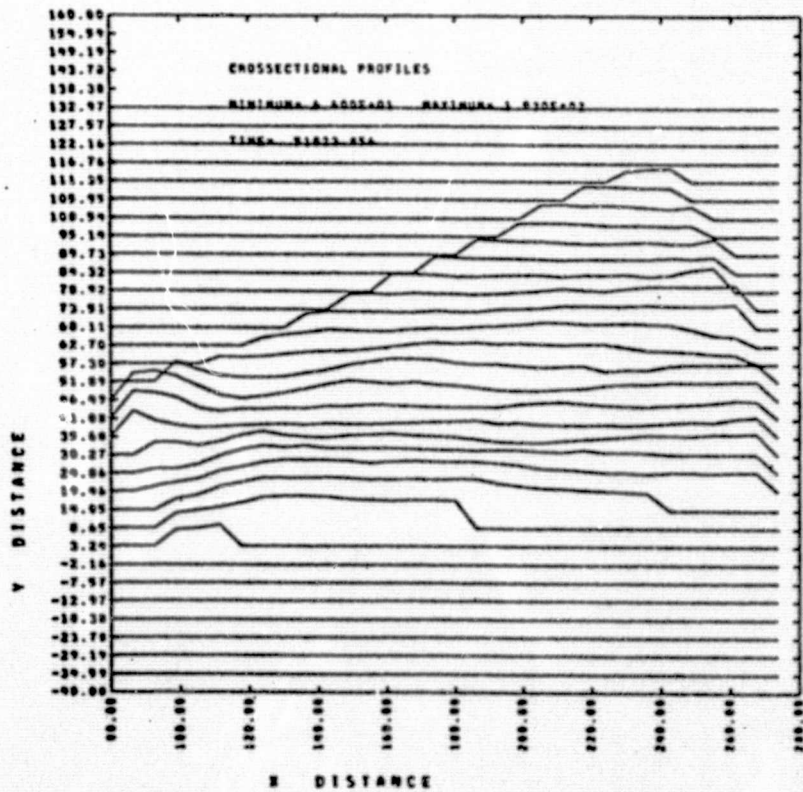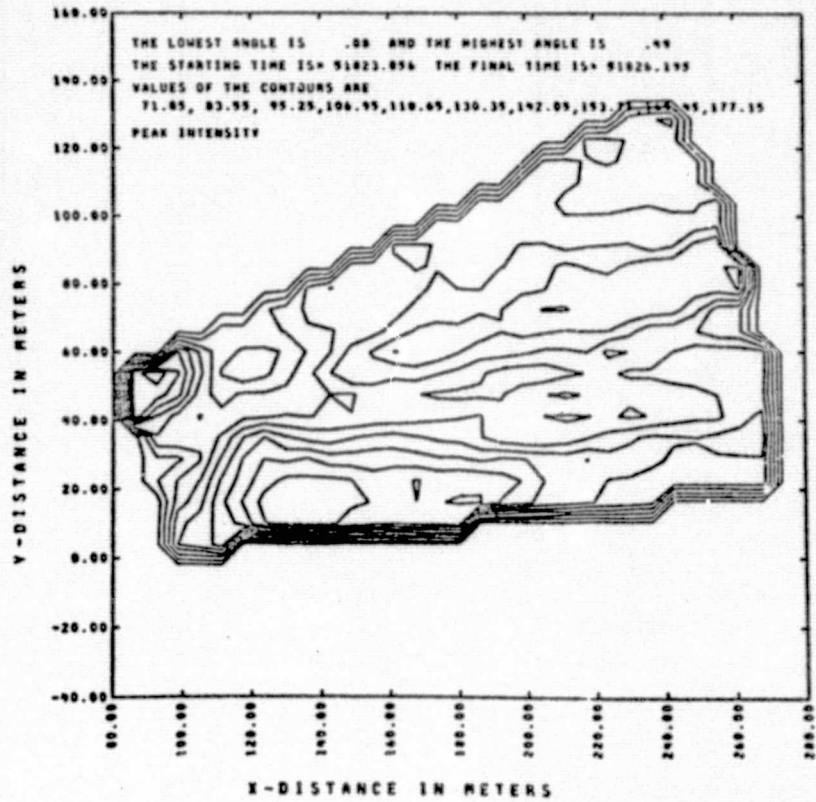
FIGURE 32. CONTOUR PLOT FOR I$_{PEAK}$

56

plots. The quantity being plotted is indicated near the upper left corner of each contour plot. The highest and lowest value of the quantity are written out in the cross-sectional plots.

Figure 25 shows contours of $\bar{V}$ in meters/sec. The separation distance between the two maxima in the contour plot is approximately 25 meters, which is quite close to the theoretical prediction of 28 meters. The vertical dimension of each maximum is about 25 meters, which is also reasonable when compared to the simulation results. Figure 26 shows the contour plot for V_{max}. It is quite similar to that of $\bar{V}$, and the maxima are closely correlated to those of $\bar{V}$. Figure 27 shows the contour plot for V_{peak}. Due to the high intensity threshold, it seems that the left vortex signature has been lost in this plot. All higher moments of the spectrum seem to give well localized signatures, but they also lose the weaker signature at high intensity thresholds.

Figure 28 shows the variance σ in $(m/sec)^2$. It shows only one peak at (125, 40); the other peak is almost completely lost. Similarly, in Figures 29 and 30, the contours for β and κ are shown to have one peak only. Finally, Figures 31 and 32 show the contours of I_{sum} and I_{peak}. I_{sum} shows well-defined maxima which correlate with those in $\bar{V}$ and V_{max} but disagree with the position of the maxima of

all other quantities. The reason for the discrepancy is unknown and deserves further study. Locations of the maxima in I_{peak} (Figure 32) are difficult to determine unambiguously; they become fewer and more sharply defined when a velocity threshold is applied.

Summarizing the discussion so far, we can conclude that the results from both noise level determination schemes appear to be similar. The choice of the intensity thresholds is very important for all variables, but it is less critical for I_{sum} and I_{peak}. I_{sum} is a good vortex locator; I_{peak} is a good vortex locator if a velocity threshold is applied. At high intensity thresholds, the low order velocity moments yield spatially-distributed, but smooth, contours. The high order velocity moments are very localized but lose the weaker signals completely.

A series of contours for I_{sum} are shown in Figure 33abcd. It is known from simulation studies that maxima of $\bar{V}$, σ, β, and κ are identified with the vortex location if range is above 100 meters. On the other hand, the data output shows the locations of maxima in $\bar{V}$ are closely correlated to those for I_{sum}. Therefore, one could identify a maximum in I_{sum} as the vortex core. Plotting the maxima of I_{sum} as functions of time, we can obtain the vortex tracks depicted in Figure 34. It can be seen that there are two vortices moving from left to right at a rate of about 1.84 m/sec

THE LOWEST ANGLE IS   .09 AND THE HIGHEST ANGLE IS   .99
THE STARTING TIME IS= 51823.885   THE FINAL TIME IS= 51826.199
VALUES OF THE CONTOURS ARE
23.50, 68.50,113.50,158.50,203.50,248.50,293.50,338.50,383.50,428.50

SUM OF INTENSITY

THE LOWEST ANGLE IS   .08 AND THE HIGHEST ANGLE IS   .98
THE STARTING TIME IS= 51830.996   THE FINAL TIME IS= 51833.346
VALUES OF THE CONTOURS ARE
19.30, 55.90, 92.50,129.10,165.70,202.30,238.90,275.50,312.10,348.70

SUM OF INTENSITY

FIGURE 33AB.   TIME SEQUENCE OF I$_{SUM}$

59

A
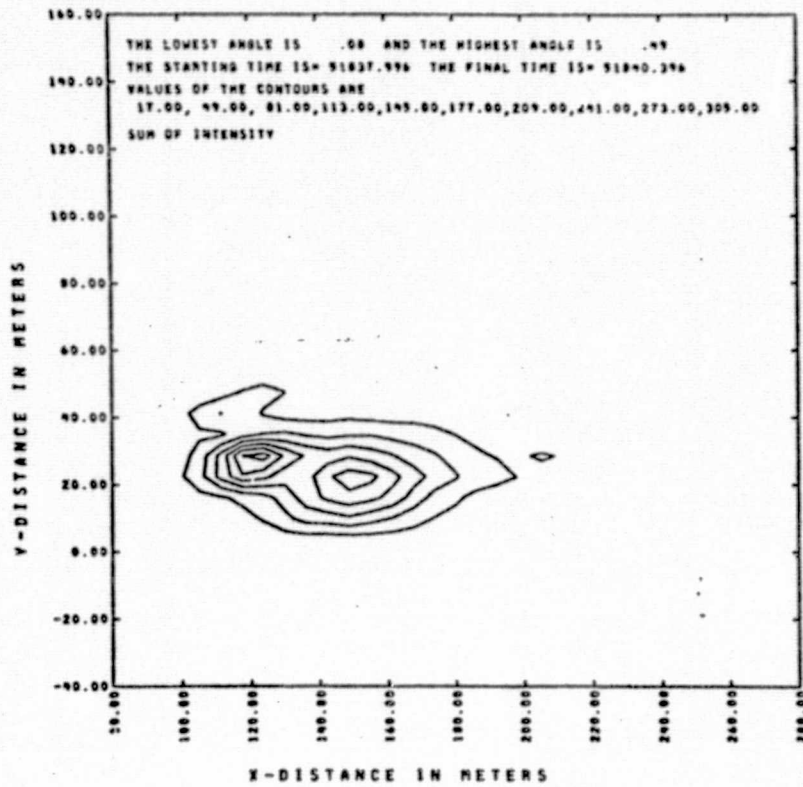
B
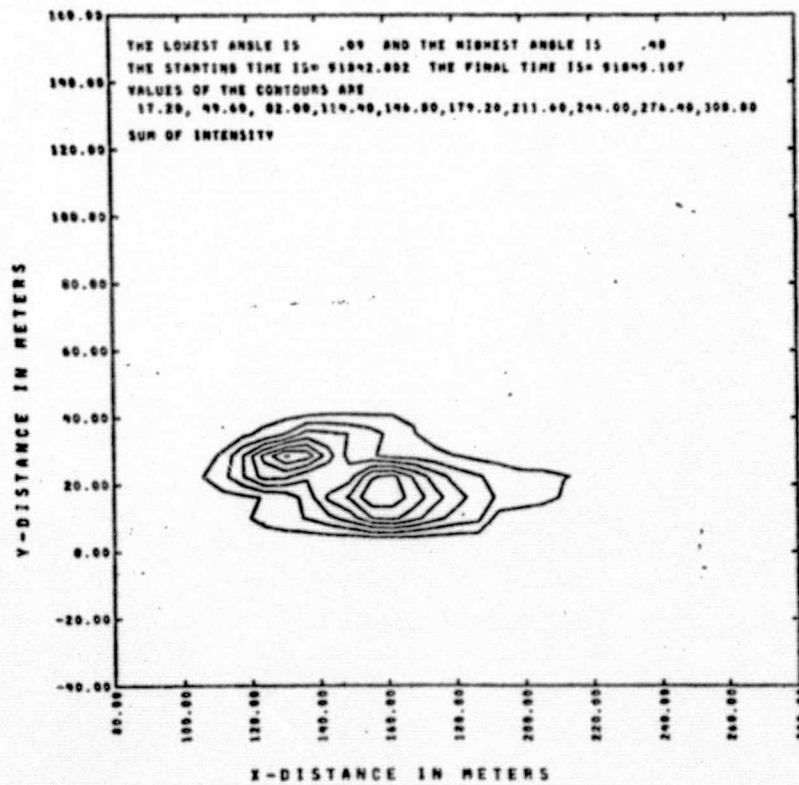
FIGURE 33CD. THE SEQUENCE OF I$_{\text{SUM}}$

60

RUN 1023 – time difference between con-
secutive data points = 2.3 seconds.
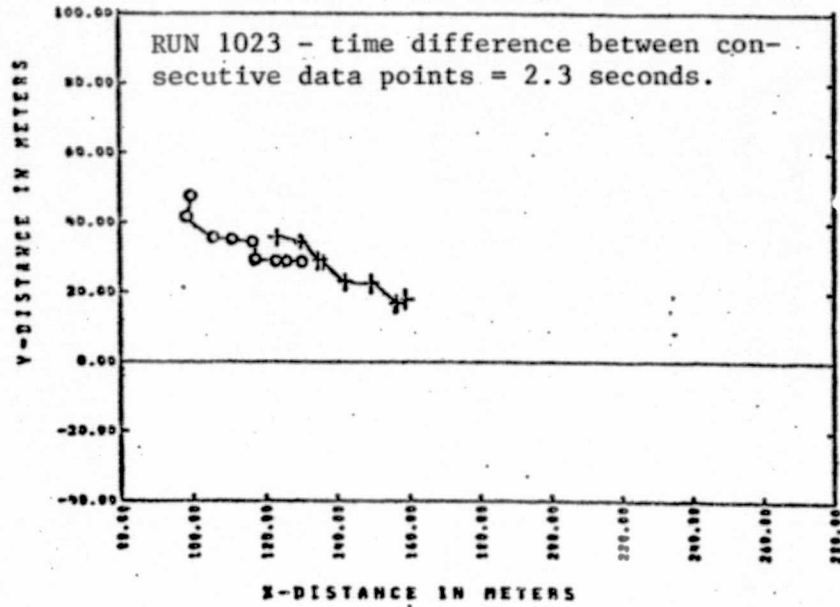
FIGURE 34. VORTEX TRACK OBTAINED FROM I_{SUM}

61

and descending at ∿1.08 m/sec. The average vortex separation is about 30 meters, so that the total circulation contained in the vortex is about 204 m^2/sec (2205 ft^2/sec), which is also close to the theoretical prediction of 2360 ft^2/sec. The entire content of a seven track data tape can be represented by these nine points.

The actual range resolution of the LDV system can also be assessed from the contour plots of I_{sum} in Figure 33. If we define the range resolution Δs as the half width of I_{sum} along the beam, we can determine the dependence of Δs upon range s. Figure 35 shows Δs (meters) versus range (meters) obtained this way. Also shown is the predicted value $\Delta s = 2f \frac{\lambda}{\pi} (\frac{s}{R})^2$, where $f = 2.1$, $\lambda = 10.6\mu$ and $R = 15.24$ cm. The range resolution is poorer than predicted value.

Vortex tracks can also be obtained by analyzing data from two LDV systems scanning simultaneously over generally the same area. One procedure is to multiply the variable defining the vortex track (say $\bar{V}$) from one system by its value given by the other system, and to then plot contours of this product. The positions of the maxima are then identified as the vortex positions. A second procedure is to apply triangulation, as discussed in Section II.

Figure 36 shows an overlapped fan beam configuration. The first system (left) is located at -61.11 meters; the second system (right) is at 240.33 meters. The contour

The plot contains:

o I_{sum} data of run 1023

— $4.2 \dfrac{\lambda}{\pi} \left(\dfrac{s}{R}\right)^2$, $\lambda = 10.6\ \mu$

$R = 15.24$ cm

Axis labels: Range Resolution in Meters (vertical), Range s in Meters (horizontal)
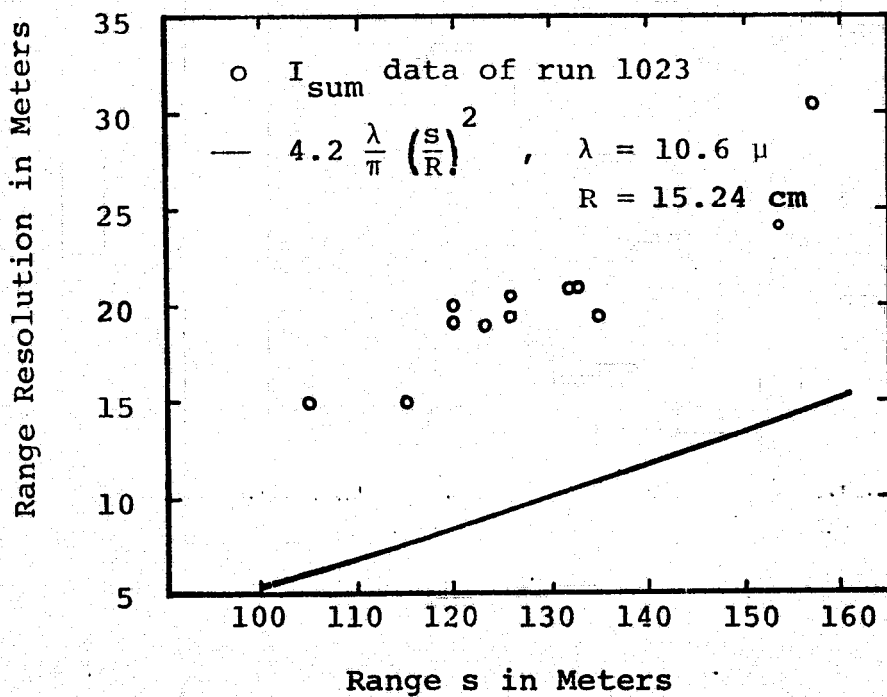
FIGURE 35. RANGE RESOLUTION AS A FUNCTION OF RANGE

THE LOWEST ANGLE IS   .18   AND THE HIGHEST ANGLE IS   .42
THE STARTING TIME IS= 51021.794   THE FINAL TIME IS= 51023.706
THE LINES OF SIGHT FOR THE LASER DOPPLER VELOCIMETER SYSTEM
THE RUN NUMBER IS 1023
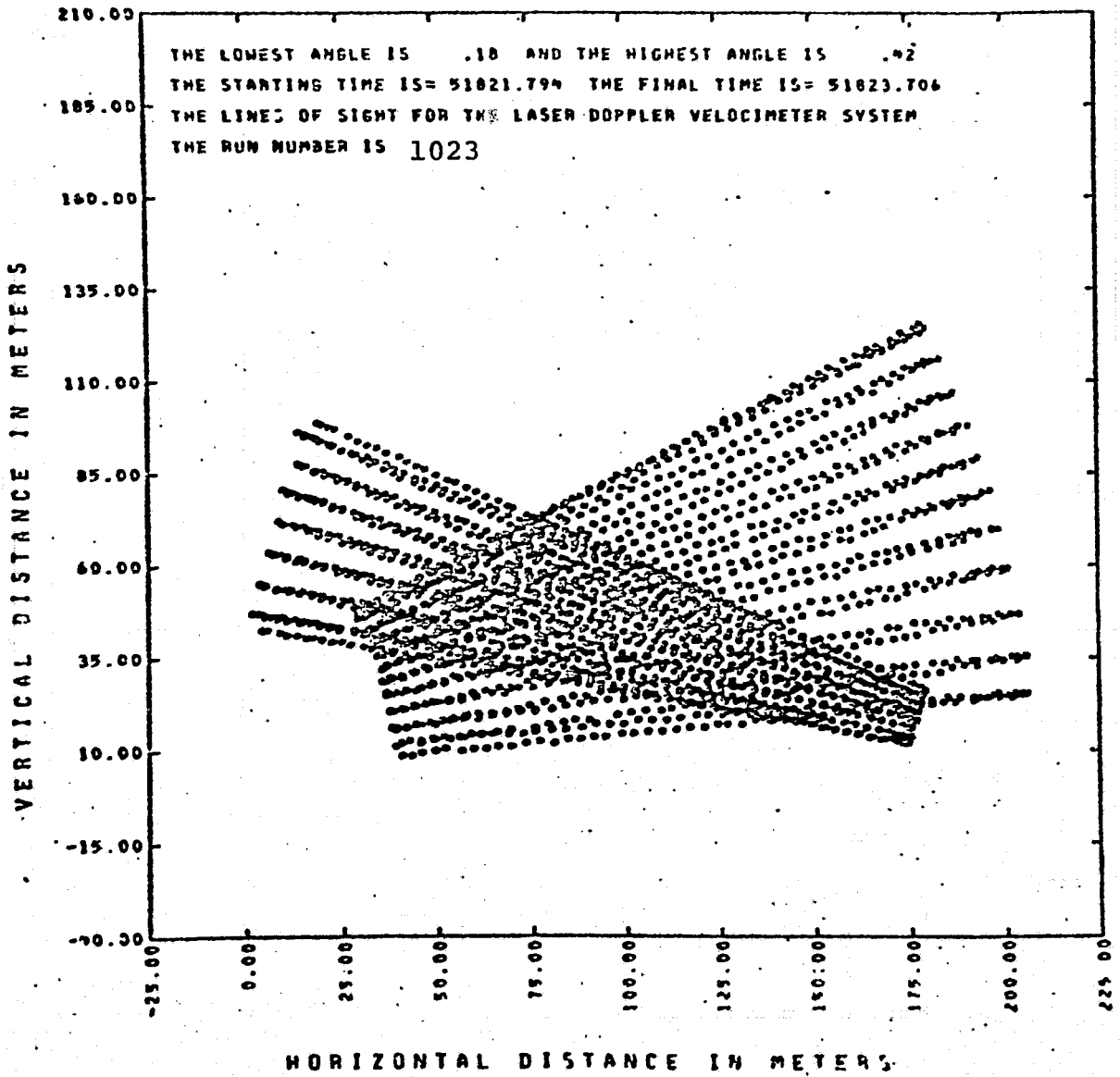
FIGURE 36. FAN BEAM CONFIGURATIONS FROM TWO LDV SYSTEMS

plots for $\bar{V}$ from both systems are plotted separately in Figure 37a and b. Both show elongation characteristic of the LDV system. The contour for their product is given in Figure 37c, which is well defined over a reasonable dimension, and the noisy contours elongated along the range appearing in Figure 37a and b are eliminated. Doing this for each time step will produce the desired vortex track.

If the same process as described above is repeated for the quantity I_{sum}, smoother and clearer vortex tracks can be expected. This was not done, but simple comparisons of I_{sum} from outputs of these LDV systems were performed. The contour plots of I_{sum} from both Runs 1023 and 2023 at approximately the same time are shown in Figures 38 and 39. The intensity threshold was set at 50 in Figures 38a and 39a, and at 25 in Figures 38b and 39b. The run numbers are indicated in each plot; ground level is marked in Figures 38a and 39a. The cross symbols are used to identify the maxima in each plot. Range in meters is measured from each LDV system and can be converted to a common frame. Figure 38a shows two maxima, while Figure 38b shows only one. The location of maxima when converted to the common frame are not closely correlated. Figure 39a shows the maxima at (53,35) and (76,25), while Figure 39b shows the maxima at (70,25) and (88,27) when converted to

Contour plot of $\bar{v}$ for LDV van 1

Contour plot of $\bar{v}$ for LDV van 2

Contour plot of product of $\bar{v}$ from vans 1 & 2

X-DISTANCE IN METERS
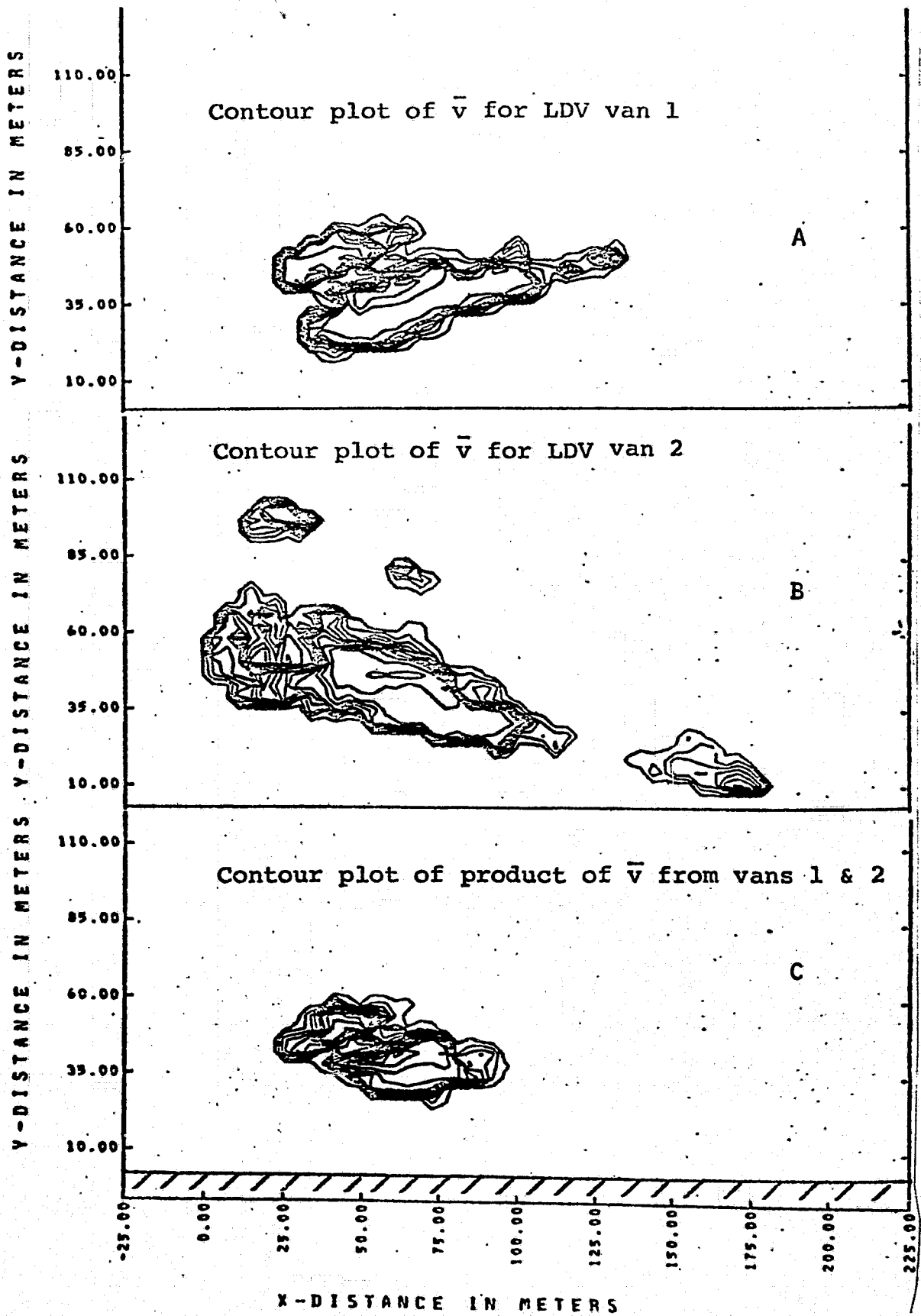
FIGURE 37. CROSS CORRELATION OF $\bar{V}$ FROM TWO LDV SYSTEMS

66
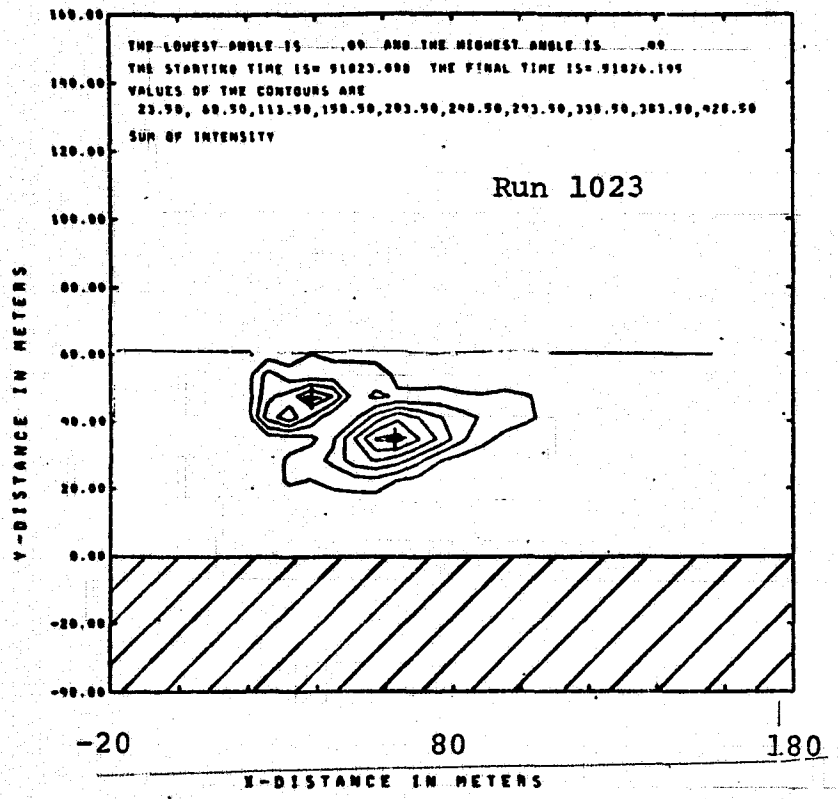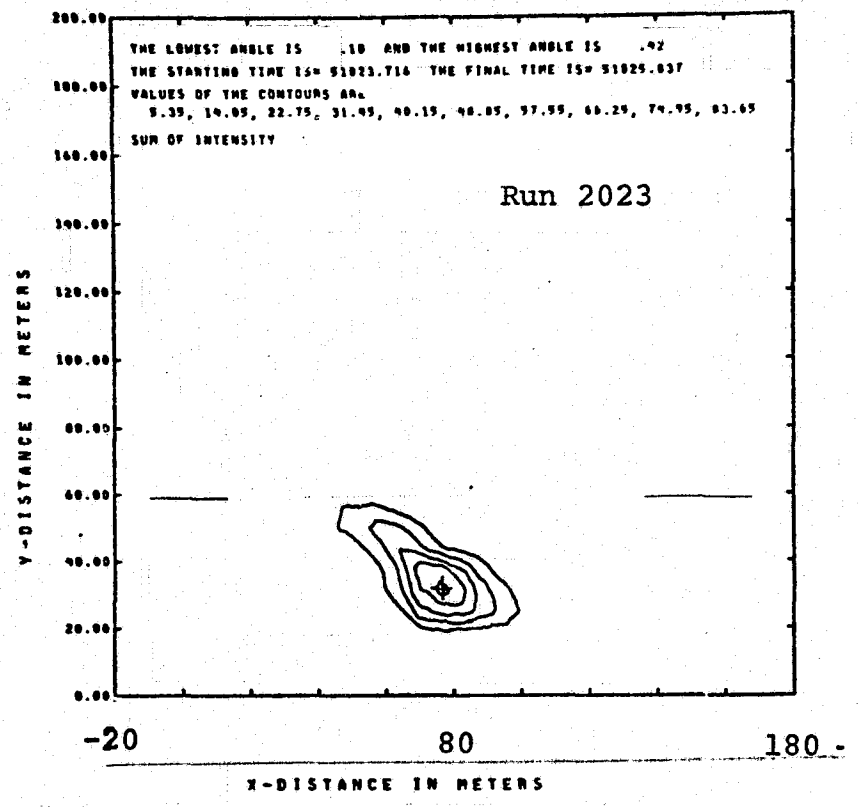
FIGURE 38. COMPARISONS OF I_{SUM} CONTOURS FROM TWO LDV SYSTEMS

A (Run 1023)

THE LOWEST ANGLE IS   .08   AND THE HIGHEST ANGLE IS   .40
THE STARTING TIME IS= 91030.996   THE FINAL TIME IS= 91033.396
VALUES OF THE CONTOURS ARE
  19.30, 55.90, 92.50,129.10,165.70,202.30,238.90,279.30,312.10,348.70

SUM OF INTENSITY

Run 1023

Y-DISTANCE IN METERS

X-DISTANCE IN METERS

B (Run 2023)

THE LOWEST ANGLE IS   .10   AND THE HIGHEST ANGLE IS   .41
THE STARTING TIME IS= 91031.041   THE FINAL TIME IS= 91033.700
VALUES OF THE CONTOURS ARE
  4.85, 12.55, 20.25, 27.95, 35.65, 43.35, 51.05, 58.75, 66.45, 74.15

SUM OF INTENSITY

Run 2023

Y-DISTANCE IN METERS

X-DISTANCE IN METERS

FIGURE 39. COMPARISONS OF I_{SUM} CONTOURS FROM TWO LDV SYSTEMS

a common frame. There are considerable deviations. The discrepancy could be attributed to range resolution and different thresholding conditions.

A series of plots of V_{peak} vs. angle for both LDV systems are given in Figures 40 through 42. The 'a' series is from the first system; the 'b' series is from the second system. From each of these plots, the angle at which the V_{peak} is a maximum can be read. Then a ray can be drawn at that angle from the location of the corresponding system. Intersection of the rays will determine the vortex locations. The accuracy of the vortex track determined this way in Figure 43 is not very clear. The only guidance is to compare the simulation results of V_{peak} versus angle to actual vortex location. It appears difficult to determine the vortex track from V_{peak} information alone.
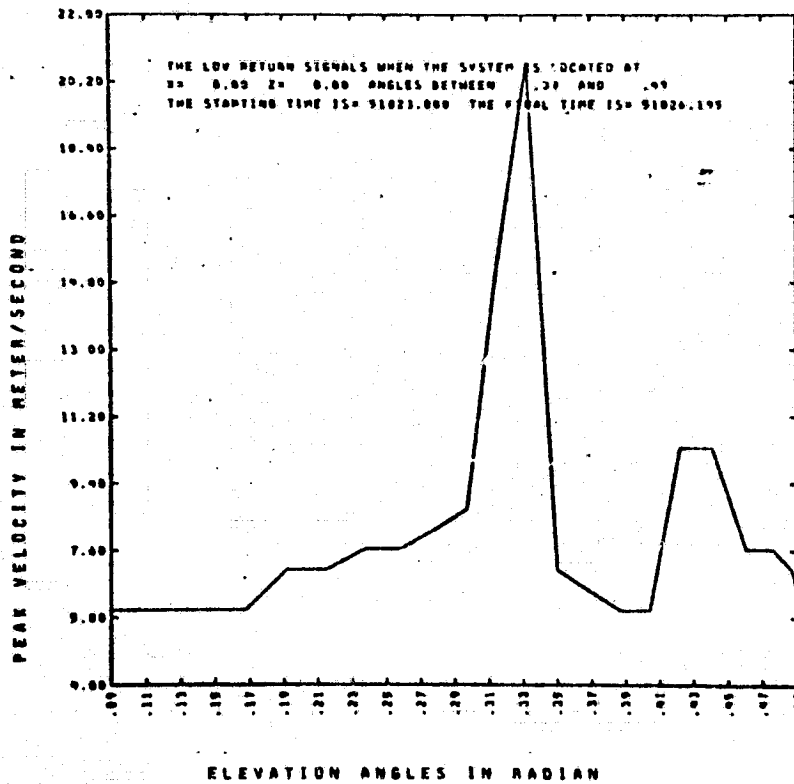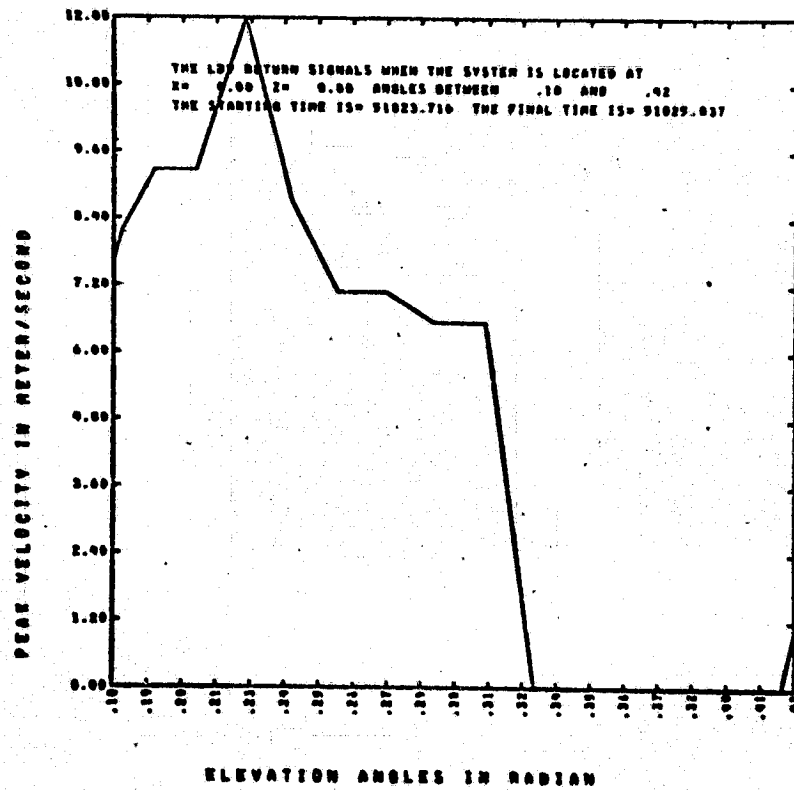
FIGURE 40. V_{PEAK} VERSUS ANGLE FROM TWO LDV SYSTEMS AT $T \stackrel{\sim}{=} 51823$
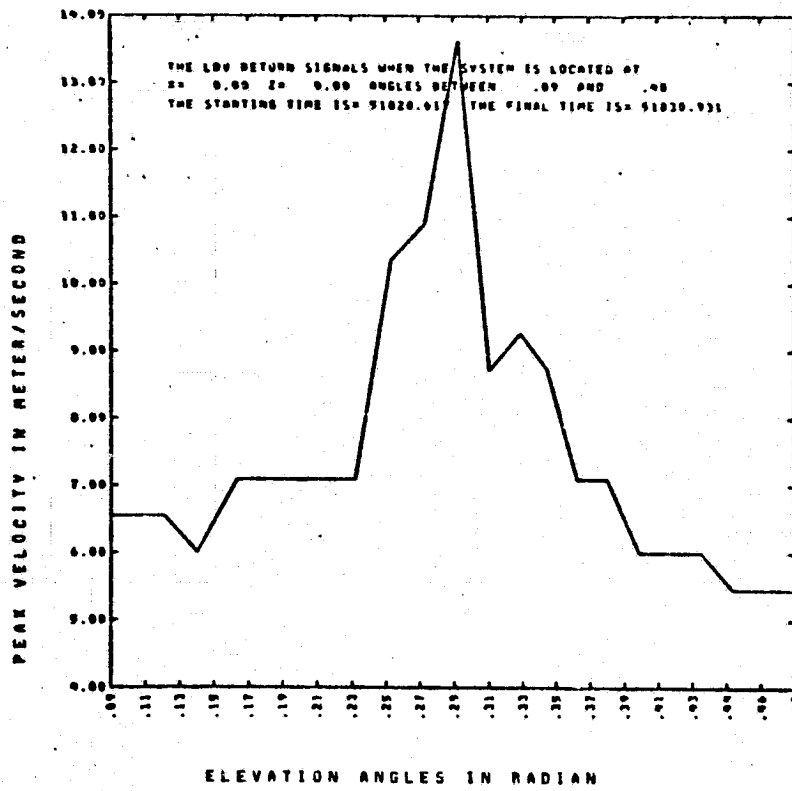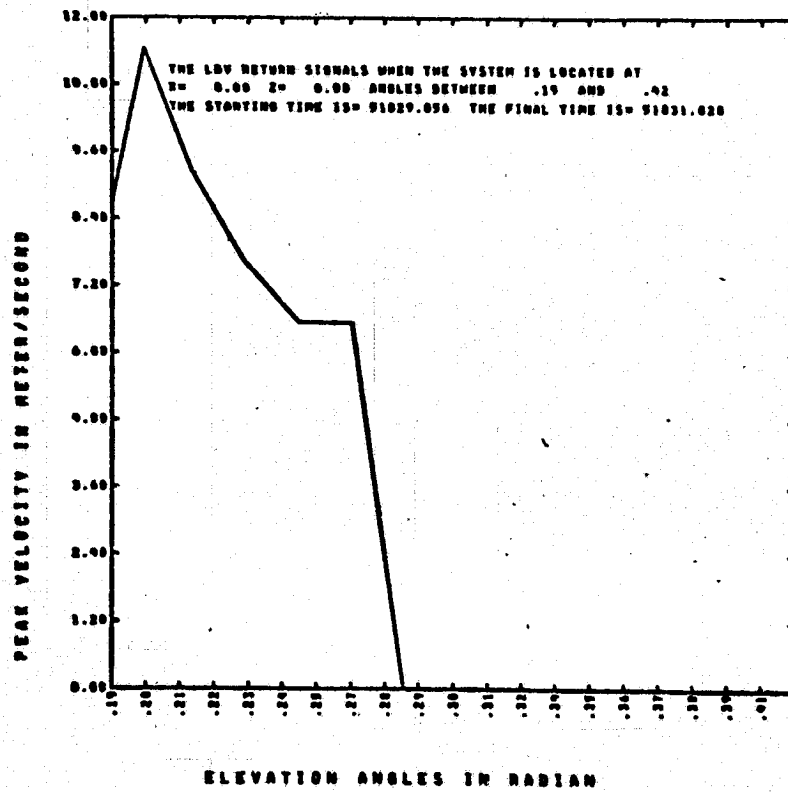
FIGURE 41. V_{PEAK} VERSUS ANGLE FROM TWO LDV SYSTEMS AT $T \cong 51828$

71
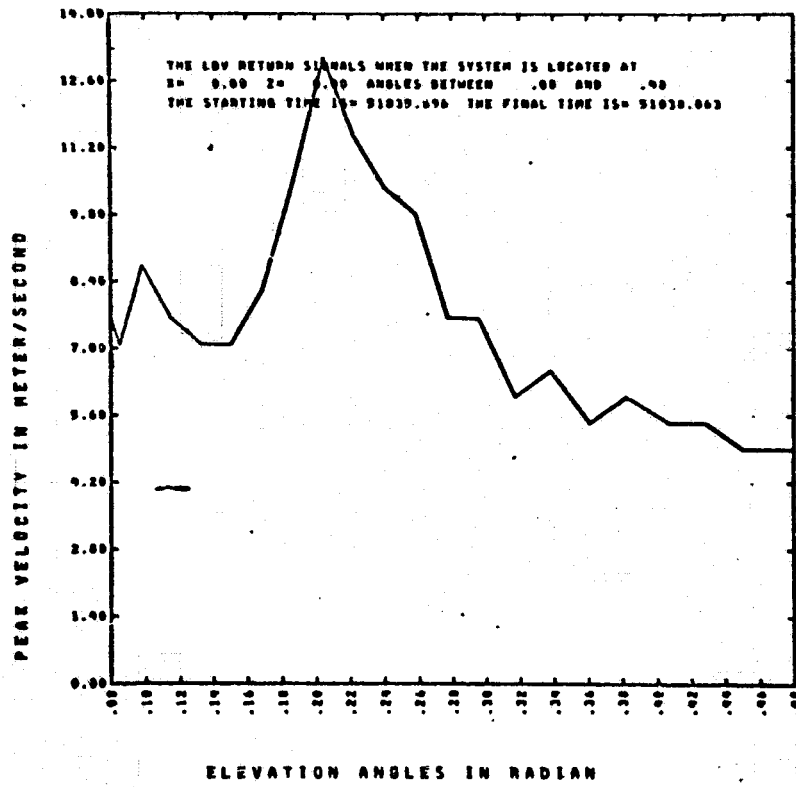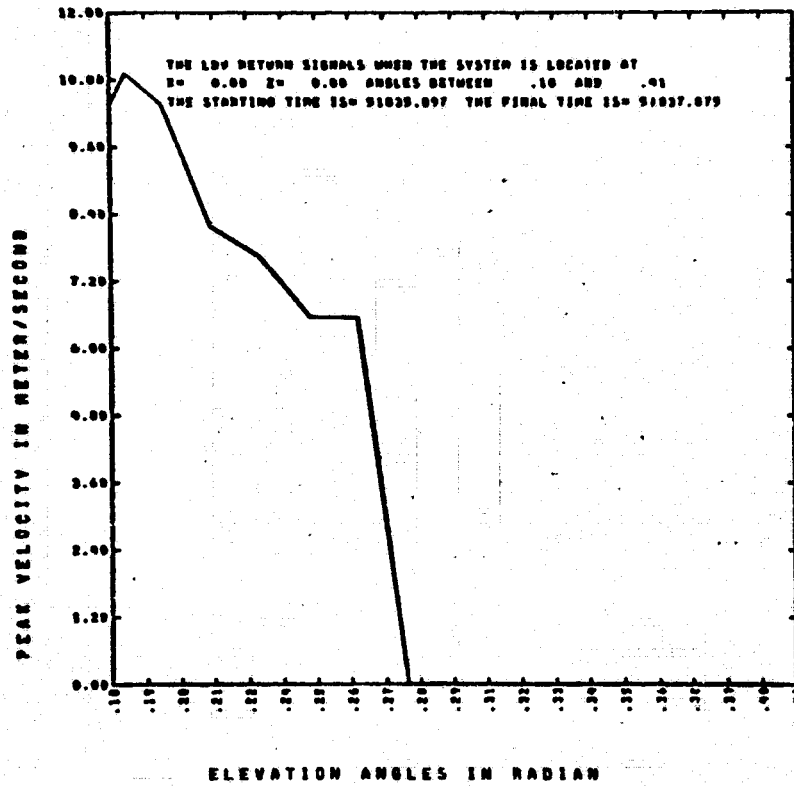
FIGURE 42. V_{PEAK} VERSUS ANGLE FROM TWO LDV SYSTEMS
AT T $\cong$ 51835

72
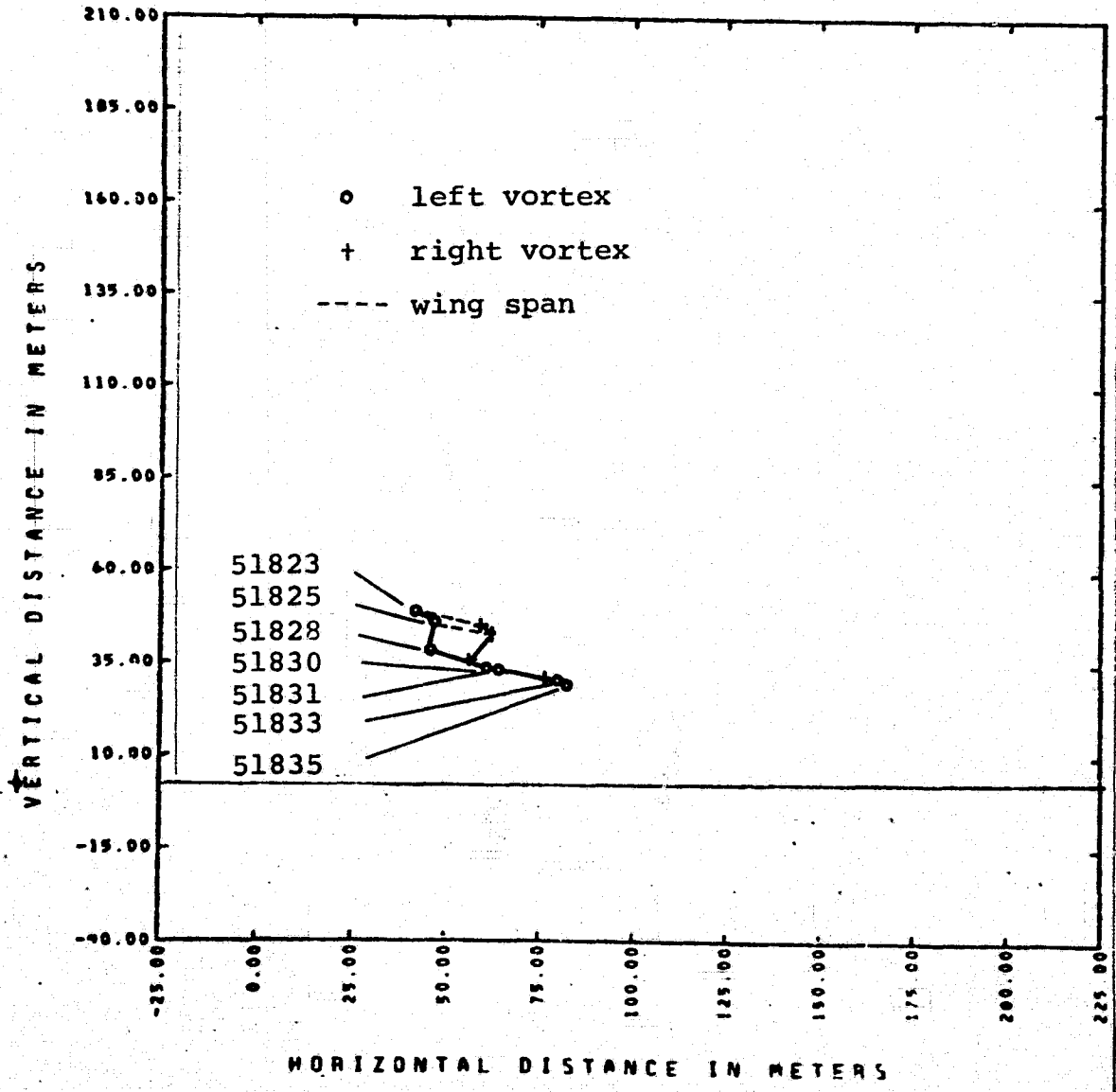
FIGURE 43. VORTEX TRACK DETERMINED BY TRIANGULATION METHOD

73

V. CONCLUSIONS AND RECOMMENDATIONS

Two vortex detection modes were considered: a "soft target" mode which deduces the vortex track by assuming the vortex is located at the maxima of a well-defined, smoothly varying quantity such as I_{sum}; a "hard target" mode in which a triangulation method was applied to locate the center of the peak velocity for both LDV systems. Several conclusions and recommendations were drawn from examination of the data:

1) The two noise-determining schemes are successful and both produce clear vortex signatures; the best value of I_{th} must be evaluated by trial and error.

2) The vortex wake appears as a spatially-distributed target; the clarity of the signature depends critically on the chosen thresholds, either I_{th} or V_{th}.

3) The spatial dimensions of $\bar{V}$, V_{max}, V_{peak} appear to be larger than those for σ, β, and κ. However, the utility of these variables in locating the vortex core deserves further study.

4) The variable which has the least dependence upon the value selected for I_{th} is I_{sum}, and the maxima of its contour appear to define the vortex center satisfactorily.

5) Range resolution based on I_{sum} of the LDV system appears to be poorer than theoretical prediction.

6) The best V_{peak} versus angle plot is generated by the data analysis code when no velocity threshold is applied and only medium I_{th} is applied. Too high an I_{th} will eliminate the weaker vortex signal and too low an I_{th} will yield unrealistically high V_{peak}. If a velocity threshold is applied, the angle dependence near a vortex may be lost.

7) Certain ambiguities must be cleared up before the triangulation method can produce reliable vortex tracks. This is mainly because the V_{peak} versus angle plot is range dependent; that is, it appears very different at long range from that at close range. In addition, it requires better coordination between the two LDV systems to maximize the overlap in scanning.

8) The contour plot of the cross correlation of I_{sum} from two LDV systems should be a good vortex track generator. Evaluation of I_{sum} should also be easily adaptable in the present on-line system to yield the vortex track.

9) The noise level as a function of time should be recorded on the high speed tape to eliminate the trial-and-error procedure.

10) A translator should be included in the LDV system to obtain the sense of velocity. The velocity vector obtained from the existing data is not meaningful.

75

REFERENCES

Skolnik, M., editor, RADAR HANDBOOK, McGraw-Hill (1970).

Thomson, J.A.L. and J.C.S. Meng, "Laser Doppler Velocimeter
    System Simulation for Sensing Aircraft Wake Vortices.
    Part I: Simulation Model," Physical Dynamics report
    PD-74-058 (1974).

Appendix: FLOW CHART FOR THE LDV DATA ANALYSIS PROGRAM

The basic program setup is described in the flow chart. The data tapes are first converted into 60-bit binary words in order to be analyzed on the CDC 7600 computer. The data reduction program LDVDA is then applied to study these tapes.

Since the recording of the data does not always start at the range maximum or minimum, the first range maximum or minimum is used as the first point for data processing. This is done in the subroutine RESET. Then the stored data points are fetched and the spectrum plotted for several space points. All the variables $\bar{v}$, v_{width}, v_{peak}, v_{max}, σ, β, κ, I_{sum}, I_{peak} are then computed as a function of range and elevation angle.

After one complete scan is obtained, the subroutine DISPLAY is called to present various plots. The spatial pattern of data points is first displayed. The subroutine 3DPRØFL is called to produce the r, θ plots for all the variables: $\bar{v}$, v_{width}, v_{peak}, v_{max}, σ, β, κ, I_{sum}, I_{peak}. The highest velocity for each angle is also plotted versus angle.

The filtering procedures are then applied to analyze the data. First of all, the fan beam configuration is mapped into a rectangular mesh. This is done by calling the sub-routine SETUP; then CONMAP is called to generate the contour

plots for the array on the rectangular mesh. This is valuable for comparing to the plots after the filtering is applied. Subroutine MATCH then performs one of three different filtering operations: matched filter, smoothing or deconvolution.

Subroutine CONMAP is again called to plot the contours of the filtered data and all the variables $\bar{v}$, v_{peak}, v_{max}, v_{width}, σ, β, κ, I_{sum}, I_{peak} are again processed through the same contour plotting procedure.

II. Flow Chart for the LDV Data Analysis Program

The basic program setup is described in the flow chart. The data tapes are first converted into 60-bit binary words in order to be analyzed on the CDC 7600 computer. The data reduction program LDVDA is then applied to study these tapes.

Since the recording of the data does not always start at the range maximum or minimum, the first range maximum or minimum is used as the first point for data processing. This is done in the subroutine RESET. Then the stored data points are fetched and the spectrum plotted for several space points. All the variables $\bar{v}$, v_{width}, v_{peak}, v_{max}, σ, β, κ, I_{sum}, I_{peak} are then computed as a function of range and elevation angle.

After one complete scan is obtained, the subroutine DISPLAY is called to present various plots. The spatial pattern of data points is first displayed. The subroutine 3DPRØFL is called to produce the r,θ plots for all the variables: $\bar{v}$, v_{width}, v_{peak}, v_{max}, σ, β, κ, I_{sum}, I_{peak}. The highest velocity for each angle is also plotted versus angle.

The filtering procedures are then applied to analyze the data. First of all, the fan beam configuration is mapped into a rectangular mesh. This is done by calling the subroutine SETUP; then CONMAP is called to generate the contour

plots for the array on the rectangular mesh. This is valuable for comparing to the plots after the filtering is applied. Subroutine MATCH then performs one of three different filtering operations: matched filter, smoothing or deconvolution.

Subroutine CONMAP is again called to plot the contours of the filtered data and all the variables $\bar{v}$, v_{peak}, v_{max}, v_{width}, σ, β, κ, I_{sum}, I_{peak} are again processed through the same contour plotting procedure.

LDVDA (MAIN PROGRAM)

Read data tape up to 1295 points and store in the large core memory

Set noise level for each channel

Data tapes from the NASA fly-bys

CALL RESET to find the beginning of the range scan

RESET

Set up flags for both range and elevation angle scans

Fetch the data from the large core memory

Program CONV

to convert the tape to a 60-bit word tape to be analyzed on the CDC 7600

SPTRUM

plot the spectrum versus the velocity or the channel number

CALL SPTRUM

Compute the variables $\overline{v}$, v_{peak}, v_{max}, σ, β, κ, sum intensity, peak intensity

DISPLAY

generate the fan beam configuration

Test: Is this the end of the range scan?

Program LDVDA

to analyze the data tape

CALL 3DPROFL

for R,θ plots for the $v_{\shortparallel}$, v_{peak}, v_{max}, σ, β, γ, sum of intensity peak intensity

No

Yes

Test: Is this the end of the angle scan?

3DPROFL

generate R,θ plots

No

Yes

generate the peak velocity versus angle plots

CALL DISPLAY

for TV plots

CALL SETUP

set up a rectangular mesh from the (r,θ) fan beam configuration

SETUP

to seed the fan beam focal points on a fixed x,y-plane mesh

CONMAP

generate contour plots

CALL CONMAP

CALL MATCH

apply the matched filter techniques

MATCH

CALL CONMAP

PUSHUP

discard used data points and read additional data to fill up 1295-point LCM storage

CALL PUSHUP

push out used data and continue to read data